SISSA - SCUOLA
INTERNAZIONALE
SUPERIORE
STUDI AVANZATI
TRIESTE
Strada Costiera 11

ISAS - INTERNATIONAL SCHOOL FOR ADVANCED STUDIES

T E S I

DIPLOMA DI PERFEZIONAMENTO

"DOCTOR PHILOSOPHIAE"

POLYMORPHIC TRANSITIONS IN ALKALI HALIDES

CANDIDATO:

Dott. Chen Chuan hong

RELATORE:

Prof. M. Parrinello

Anno Accademico 1982/1983

TRIESTE

T E S I

DIPLOMA DI PERFEZIONAMENTO

"DOCTOR PHILOSOPHIAE"

POLYMORPHIC TRANSITIONS IN ALKALI HALIDES

CANDIDATO:

Dott. Chen Chuan hong

RELATORE:

Prof. M. Parrinello

Anno Accademico 1982/1983

POLYMORPHIC TRANSITIONS IN ALKALI HALIDES

Chen Chuan hong

Department of Physics, Xiamen University

Xiamen, Fujian, China

September 1983

This thesis is submitted for the degree of Philosophiae Doctor at the International School for Advanced Studies in Trieste, Italy.

CONTENTS

CHAPTER I - INTRODUCTION

An essential aspect of solid state physics concerns the explanation of the absolute and relative stability of different crystal structures of a substance and the interpretation of transition between different structures. The understading of this subject implies a profound insight into the mechanism which governs the interactions between atoms, ions and molecules in solids.

The transition from rocksalt(as B1) to cesium chloride structure (as B2) in alkali halides has been studied both experimentally and theoretically by a large number of investigators since the discovery of this transition by Slater [1]. A summary of the subject was given by Born and Huang [2]. A more detailed survey is to be found in the review by Tosi [3], Tosi and Arai [4], and by Tosi and Fumi [5]. The theoretical approaches to treat alkali halide crystals can roughly be divided into two classes: the a priori quantum mechanical approach and the Born-Mayer approach.

The a priori quantum-mechanical Hartree Fock approach was initiated by Hylleraas [6] and by Landshoff [7]. It was firmly formulated later by Löwdin [8] who has shown that a quantum mechanical model which considers the effects of the overlap between the ground state electronic configurations of the free ions, but neglects the effects of the crystal field, reproduces reasonably well the lattice energy, the lattice parameter, the elastic constants and the critical pressure of the B1 to B2 transition for several alkali halides, and leads to a many body contribution to the lattice energy. Löwdins approach is based on a full study of the solution of the many body Schrödinger equation and gives a more correct physical picture. The major difficulty of this approach is that it involves lengthy and tedious numerical computations which introduce different degrees of approximation at different stages of the calculation. Because of this limitation the calculation of even the static properties of a crystal in all its entirety has not been done. The more serious limitation however

is the difficulty of extending the method to calculate the lattice dynamics. More recently the so-called "local density functional scheme" [9,10] has become a useful technique for computation of the properties of solids. The use of the local density functional scheme for the description of many-electron interactions in solids has led to considerable progress in the theoretical understanding of the structural properties of solids. This was aided by the introduction of the first principles pseudopotentials [11] in the local density functional scheme. Very accurate results have been obtained for a number of semiconductors[12] and metals [13] . Recently, this scheme has been extended by Andreoni, Maschke and Schlüter to a study of pressure induced structural transition in partially ionic semiconductors [14], and by Andreoni and Maschke to a study of cohesion in NaCl [15] . While this appears to be the most rigorous approach to the problem of polymorphic transition, its implementation is very costly and the extension of the method to incorporate dynamical properties is at present prohibitively expensive.

On the other hand a totally empirical approach was introduced by Born and Mayer [16-18] . In the Born model, the lattice energy is expressed as a sum of central, two body energies, namely the attractive interactions which are dominated by the so-called Madelung energy and are balanced by the so-called Born repulsive forces. The Born-like semiempirical theory models the repulsive energy as a simple functions of the interionic distance and determines the intervening parameters from experimental data. Many later extensions were concentrated on the best possible representation of the interionic potentials in order to reproduce better agreement with experiments on cohesive properties of alkali halides. The potential of Tosi and Fumi [19-20] represents a culmination of the earlier efforts of many, including Born, Mayer, Huggins and Pauling. Among the most recent approaches along this phenomenological line, it is worth while considering the empirical potential proposed by Narayan and Ramasechan [21] which deviated somewhat from the standard Born model in that it includes many body forces. The application of the Narayan-Ramasechan potential to the polymorphic transition

in alkali halides is very successful, but no basic justification has so far been given for its validity. A critical review on the more recent phenomenological potentials has been given by Eggenhoffner, Fumi and Murthy [22, 23]. It is a common feature that the Born-type approach requires some of the parameters to be determined only from the experimental data on the crystals of interest, thereby ruling out predictions on new systems. The resulting potential usually only partly reproduces perfect crystal data and the limitations of this approach when it is applied to the calculations of the transition pressure have been underlined by Tosi and Fumi [5].

A middle of the way approach has been taken by Gordon and Kim [24-25] , who have developed a theory for calculation of interaction forces between closed shell systems. It enables one to follow the Born-type approach by using a first principle pair potential instead of the empirically obtained one, so that no empirical parameter is introduced into the model. It has been applied to a number of simple ionic crystals, such as alkali halides [26-27] and alkaline earth oxides [28] and appeared to be quite successful. This study was extended by Boyer [29] who included the effects of harmonic vibration in the calculation of the free energy; this however did not materially affect the conclusions based on the static calculations. The GK model has the advantages of giving an inexpensive and widely usable way of performing parameter free calculations of crystal binding and structural properties. Such a first principle, though simple theory, predicted cohesive properties of alkali halides which are, in general, less accurate in comparison with that of semiempirical theories. The predicted structural stability is in poorer agreement with the experiments [29] . However there is still room for further improvements [29,30] . We also notice that some of the assumptions in the GK model are still open to criticism [31-32].

In summary, in spite of the enormous body of literature, the question of the polymorphic transition in alkali halides still presents many open questions. In this thesis we shall concentrate mainly on two different

aspects of the B1 to B2 transition. The first one is a study of the role of many body forces in the B1 to B2 transitions. As has been often underlined in the literature, many body forces, being highly structure sensitive, are expected to play an important role in the transition. This may, at first, appears rather surprising since many body forces are rather small. However, since the energy differences involved are also small, their effect is rather significant as we shall demonstrate later. As a theoretical framework for the calculation of the forces we have chosen the Gordon-Kim scheme, which is free of parameters and can easily be extended to the calculation of three body forces [33] . While certainly the GK scheme is open to criticism, its a priori nature and its simplicity make it a very convenient scheme for the present calculation.

The other aspect of polymorphic transformations in alkali halides we shall focus onto, is the kinetics of the transition. Experimental and theoretical progress has been made in this direction only recently.

Different microscopic mechanisms for the tranformation from the B1 to B2 structure have been postulated by many authors [34-37] . The most recent experimental progress in the field has been made by Blaschko et al. [38-41] . In their neutron scattering studies of the B1 to B2 transformation in RbI [41] , they investigated the changes in the mosaic structure (due to the nucleation of the B2 structure included in the B1 matrix) below and near the actual transition point and obtained some insight into the mechanisms involved in the transformation. Based on their experimental investigations (particularly the orientational relation between the B1 and B2 phases), a model for initial stages of the B1 to B2 transition in Rbl was put forward [41] . The main idea of the model is centered around the fact that the B1 structure can transform to the B2 structure by a collective translation of the B1 (100) alternative planes. This qualitative mechanism describes an inhomogeneous transformation, which starts in regions of high dislocation densities. Furthermore, it was shown that a transformation hysteresis depending on the previous thermal and me-

chanical treatments of the sample, implies an actual transformation pressure different from the thermodynamic equilibrium point. However many aspects of this phenomenon have not yet been theoretically understood.

Recently Parrinello and Rahman [42] have developed a new molecular dynamic (MD) method, which allows one to study the structural change of a crystal by computer simulation. They applied their new computational method to the polymorphic transition of KCl using a parametrized form of the GK potential [43]. The calcualtion showed the dynamical history of the occurrence of the B1 to the B2 transition. The microscopic mechanism proposed for the B1 to B2 transition is described as a phonon softening associated with a spontaneous uniaxial deformation of the B1 structure. When analysed in detail, this mechanism is equivalent to the one proposed by Blaschko et al. However the pressures and temperatures needed to accomplish the transformation on computer simulation were much larger than those experimentally observed and in disagreement with the predictions made by Boyer [29] on the basis of a harmonic free energy calculation that used the same GK potential. This leads us to believe that a correct description of the transitions requires not only an accurate evalaution of the free energy differnece between the two phases but also a reasonable estimate of the energy barriers that hinder the transition. The knowledge of the path followed by the system in going from the B1 to B2 structure allows now the possibility of evaluating the free energy barrier and the effect on them of various choices of the potential, of external stress and of the presence of defects that can help in nucleating the different phases. In this thesis some of these aspects will be elucidated.

The layout of the thesis is as follows. First, in chapter II we shall give a brief survey of work on polymorphic transition in alkali halides. Of course, it is not the purpose of this chapter to give a full account of the subject. An excellent summary of earlier work has been given by Tosi [3]. We shall pay more attention on some aspects of recent advances in this field, especially the first principle calculations. A

detailed discussion of the GK model will be given. It will be shown that using the GK model for the description of polymorphic transition in alkali halides, the pair potential approxiamtion needs to be abandoned.

The problem that we shall tackle in chapter III are then to discuss the nonadditive three body interactions (TBI) in alkali halides and their effects on the B1 to B2 transition. The TBI will be calculated for nine crystals using the GK model [33]. It will be shown that TBI plays an important role in improving the GK model for the description of cohesive and structural properties in the alkali halides.

In chapter IV we shall discuss the microscopic mechanism of the polymorphic transition in alkali halides. As alluded to before, the microscopic mechanism of the B1 to B2 transition was described by Parrinello and Rahman as a phonon softening associated with a spontaneous uniaxial deformation of the crystal. We will achieve the effect of the deformation by a convenient uniaxial tensile load and discuss its effects on the crystal stability. We shall evaluate the energy barrier along the path in which crystal evolves its configurations to accomplish the transition and investigate the dependence of the height of the energy barrier on the generally applied stresses. In order to include zero point energy in the calculation of free energies, the special point method of summation over the B.2. will be used. For the deformed structures of interest here these special points are not available in the literature and will be explicitely evaluated in the appendix A [44].

Finally some conclusions and discussions will be given at the end of this thesis. Our main contribution to the thesis will mostly be included in chapter III and chapter IV.

Chapter II. BRIEF SURVEY OF WORK ON POLYMORPHIC TRANSITIONS IN ALKALI HALIDES

2.1 Polymorphic Transitions in Alkali Halides

Before looking at the problems of polymorphic transitions in alkali halides, it is convenient to give a short description on the crystal structures of rocksalt (as B1) and cesium chloride (as B2).

The B1 (or B2) structure is composed of two interpenetrating face-centered cubic (or simple cubic) Bravais lattices. With reference to the cube axes the B1 (or B2) structure is composed of two fcc (or sc) lattice, one for each species of ions, shifted by (½,½,½) relative to one another, as illustrated in Fig. 2.1. The fundamental translations vectors of the fcc lattice are

$$\vec{a}_1 = a(0, \tfrac{1}{2}, \tfrac{1}{2}), \quad \vec{a}_2 = a(\tfrac{1}{2}, 0, \tfrac{1}{2}), \quad \vec{a}_3 = a(\tfrac{1}{2}, \tfrac{1}{2}, 0) \tag{2.1}$$

and those of the sc lattice are

$$\vec{a}_1 = a(1, 0, 0), \quad \vec{a}_2 = a(0, 1, 0), \quad \vec{a}_3 = a(0, 0, 1) \tag{2.2}$$

The reciprocal lattice of the fcc and sc Bravais lattices are body-centered cubic and simple cubic lattice respectively. With reference to the cube axes, their fundamental translation vectors are given by

$$\vec{a}_1^* = \frac{2\pi}{a}(-1, 1, 1), \quad \vec{a}_2^* = \frac{2\pi}{a}(1, -1, 1), \quad \vec{a}_3^* = \frac{2\pi}{a}(1, 1, -1) \tag{2.3}$$

and by

$$\vec{a}_1^* = \frac{2\pi}{a}(1, 0, 0), \quad \vec{a}_2^* = \frac{2\pi}{a}(0, 1, 0), \quad \vec{a}_3^* = \frac{2\pi}{a}(0, 0, 1) \tag{2.4}$$

respectively. Fig. 2.2 shows the associated first Brillouin Zones. We have indicated on these figures the various symmetry points and symmetry axes. The notation follows that of Bonckaerdt, Smoluchwski and Wigner [45] .

Parrinello and Rahman [43] pointed out that it is important to understand the following geometrical fact when studying the structure transformations in alkali halides. A body central tetragonal lattice with edges 1,1, $\sqrt{2}$ is a fcc lattice and inversely a faced central tetragonal lattice with edges $\sqrt{2}$, $\sqrt{2}$,1 is a bcc lattice. Moreover, a based central tetragonal lattice with edges $\sqrt{2}$, $\sqrt{2}$,1 is a sc lattice, if the square face is specified as the base. As shown in Fig. 2.3, the B1 (or B2) structure can be identified as composed of the two above mentioned body-central tetragonal lattice (or based-central tetragonal lattice), one for each species of ions, shifted by an appropriate vector relative to one another.

There is conclusive evidence that all of the alkali halides crystallize at normal pressures and temperatures in the B1 structure expect for cesium chloride, cesium bromide and cesium iodide which exhibit the B2 structure. Since the discovery of the polymorphic transition in the alkali halides by Slater [1] and the pioneering work of Bridgman [46] there have been many high-pressure experiments to study the polymorphic transitions of the alkali halide crystals. The two principle experimental techniques which have been used to induce the B1 to the B2 transition are dynamic shock wave compression [47] and diamond-anvil high pressure cell [48] The transitions which have been most extensively studied are the B1 to B2 transitions of KCl, KBr, KI, RbCl, RbBr and RbI in the range of 4 to 25 Kbar [49] . The B1 to B2 transition in NaCl occurs experimentally at 300 Kbar [50] . The B2 to B1 transition of CsCl occurs at 450 C and atmospheric pressure with a heat of transition of about 1.4 Kcal/mole. The transformations have been found to be first order and reversible [51] . The transitions on the other twelve alkali halide crystals have not been experimentally observed.

A phase transition is marked by the equality of the Gibbs free energies of the two phases

$$G_{B1} = G_{B2} \quad \text{at the transition} \qquad (2.5)$$

and

$$G = W_L + F_{vib} + PV \tag{2.6}$$

where P, V, W_L and F_{vib} are the pressure, volume, static lattice energy and harmonic vibration energy of a phase respectively. The difference in lattice energy of the two phases of each salt at the transition is given by the equation:

$$\Delta W_L = - P \cdot \Delta V \; - \Delta F_{vib} \tag{2.7}$$

For the pressure transition, the change in vibration free energy ΔF_{vib} is expected to be negligible, since the transition pressure is almost independent of temperature [52]. Therefore ΔW_l is very close to the mechanical work involved in the transition.

Experimentally one usually studies the relative volume changes $-\Delta V/V_{ol}$ associated with compressions. These are defined as the negative of the differences between the volume of the more stable phase at a given pressure and the volume of the B1 phase at zero applied pressure V_{ol} divided by V_{ol} [48]. It is useful to define $-\Delta V_t/V_{ol}$ by

$$- \Delta V_t/V_{ol} = (V_{t1} - V_{t2})/V_{ol} \tag{2.8}$$

where V_{ti} is the volume of phase B_i at the transition pressure, and $-\Delta V_t/V_{ol}$ is , of course, the magnitude of the discontinuity in $\Delta V/V_{ol}$ in the first order phase diagrams. Table 2.1 gives the observed B1 to B2 transition pressure P_c, ΔW_l and the relative volume changes at transition for some alkali halides.

The transition pressures of KCl, KBr, KI, RbCl, RbBr and RbI are rather low. In addition relative large volume changes are observed for these salts. The low-transition pressures for the crystals can in part be understood by the low-lattice-energy differences between the two phases.

In addition, kinetic effects have been observed in these experiments [41], [46] so that there is no exact value of experimental transition pressures in these crystals. For example, Bassett et al. [48] have observed a B1 to B2 polymorphic transition in KCl near 21 Kbar, rather than near 19 Kbar as observed by Bridgman [46] . In contrast to the polymorphic transitions described above the B1 to B2 phase transformation in NaCl which occurs experimentally at 300 Kbar is rapid, reversible and exhibits little hysteresis effects [48] .

We have given above a short review of the experimental work on the macroscopic properties of the polymorphic transition in alkali halides. The experimental work on the microscopic mechanism of the polymorphic transition will be discussed later on. In the next section we will review the theoretical work of the polymorphic transition in alkali halides.

2.2 A priori quantum mechanical theory

The importance of a priori quantum mechanical theory for the description of cohesive and structural properties in solid is its predictive capability. There have been two distinct approaches for the study of ionic crystals, i.e. Hartree-Fock approach and the local density functional scheme. In this section we only concentrate on discussion of a few models, such as Löwdin's Hartree-Fock approach, the Gordon-Kim model and the theory of Muhlhausen and Gordon.

2.2.1 Löwdin's theory

Löwdin [8] has investigated the cohesive property of alkali halide crystal by a quantum mechanical model which considers the effects of the overlap between the ground state electronic configurations of the free ions, but neglects the effects of crystal field.

On this treatment the cohesive energy of a ionic crystal is defined as the difference between its total energy and the energy of its free constituents

$$E_{coh} = E_{tot} - E_{free} \tag{2.9}$$

He uses Hartree-Fock approximation which gives for the total energy in terms of the density matrix ρ. The density matrix can be constructed from a knowledge of its free constituents. Löwdin starts from the free ion Hartree-Fock wave function $\varphi_{i\tau}$, from which he constructs a set of Bloch functions

$$\Phi^{\kappa}_{i\tau}(\vec{r}) = \left(\frac{\Omega}{V}\right)^{-\frac{1}{2}} \sum_{\ell} \varphi_{i\tau}(\vec{r}-\vec{R}_{\ell}-\vec{\tau}) \exp(i\vec{\kappa}\cdot\vec{R}_{\ell}) \tag{2.10}$$

where V and Ω are the volume of unit cell and crystal respectively and $\Omega/V = N^3$; $\vec{R}_1$ and $\vec{\tau}$ denote translation and basis vector respectively, i is the atomic quantum numbers. The Bloch functions corresponding to the occupied state of the free ions are then used to construct a Slater determinant

$$\Psi(x_1, x_2, \cdots, x_N) = (N!)^{-\frac{1}{2}} \det\{\Phi^{\kappa}_{i\tau}(x_j)\} \tag{2.11}$$

where x_j is the combination of a space coordiante $\vec{r}_j$ and a spin coordiante s_j. Note that the Bloch functions defined in eq. (2.10) are not orthogonal with respect to the index τ. This has important consequences for the evaluation of the density matrix ρ. Following Löwdin we define the matrix

$$\Delta_{\kappa}(i\vec{\tau}, j\vec{\tau}') = \langle \Phi^{\kappa}_{i\tau} | \Phi^{\kappa}_{j\tau'} \rangle \tag{2.12}$$

The functions

$$\Psi^{\kappa}_{i\tau}(x) = \sum_{j,\tau'} \Delta^{-\frac{1}{2}}_{\kappa}(i\vec{\tau}, j\vec{\tau}') \Phi^{\kappa}_{j\tau'}(x) \tag{2.13}$$

form the orthonormal set. The density matrix corresponding to the Slater determinant (2.11) is given by

$$\rho(x_1,x_2)=\sum_{\kappa}\sum_{i\tau}\bar{\Psi}^{\kappa *}_{i\tau}(x_1)\Psi^{\kappa}_{i\tau}(x_2)$$

$$=\sum_{\kappa}\sum_{i\tau,j\tau'}\bar{\Phi}^{\kappa *}_{i\tau}(x_1)\Phi^{\kappa}_{j\tau'}(x_2)\Delta^{-1}_{\kappa}(i\vec{\tau},j\vec{\tau}') \qquad (2.14)$$

Together with eq.(2.10) one obtains

$$\rho(x_1,x_2)=\sum_{\ell\ell',\tau\tau',ij}\varphi^{*}_{i\tau}(x_1-\vec{R}_{\ell}-\vec{\tau})\varphi_{j\tau'}(x_2-\vec{R}_{\ell'}-\vec{\tau}')\cdot$$
$$\cdot\Delta^{-1}(i\vec{\tau}\vec{R}_{\ell},j\vec{\tau}'\vec{R}_{\ell'}) \qquad (2.15)$$

where

$$\Delta(i\vec{\tau}\vec{R}_{\ell},j\vec{\tau}'\vec{R}_{\ell'})=\int dx\,\varphi^{*}_{i\tau}(x-\vec{R}_{\ell}-\vec{\tau})\varphi_{j\tau'}(x-\vec{R}_{\ell'}-\vec{\tau}') \qquad (2.16)$$

is called the total overlap matrix, whose elements describe the various overlap integral in the solid. Löwdin assigned the various part of the electron charge cloud in a solid to its nuclei in such a way that

$$\rho(x_1,x_2)=\sum_{g}\rho_g(x_1,x_2) \qquad (2.17)$$

He then separates out the contribution from the undistorted ionic charge distribution ρ_g^{free} by introducing the formal difference

$$\Delta\rho_g(x_1,x_2)=\rho_g(x_1,x_2)-\rho_g^{free}(x_1,x_2) \qquad (2.18)$$

The deformation density matrix $\Delta\rho_g$ can be written as

$$\Delta\rho_g(x_1,x_2)=-\sum_{\ell}^{all}\sum_{i\tau,j\tau'}^{g}\varphi^{*}_{i\tau}(x_1-\vec{R}_{\ell}-\vec{\tau})\varphi_{j\tau'}(x_2-\vec{R}_{\ell'}-\vec{\tau}')\cdot$$
$$\cdot P(i\vec{\tau}\vec{R}_{\ell},j\vec{\tau}'\vec{R}_{\ell'}) \qquad (2.19)$$

where

$$P=1-\Delta^{-1}=S-S^2+S^3-\cdots+\cdots \qquad (2.20)$$

In the frame of first order perturbation theory he only takes first term in the r.h.s. of eq.(2.20) for P. It is apparent from eq.(2.19) and (2.20) that the overlap matrix are strongly connected to the charge density distortion induced by the crystalline arrangement of the ions.

Finally the cohesive energy can be expressed in terms of the free constituents placed together in the solids and deformations $\Delta\rho_g$. The expression is given in the form

$$E_{coh} = E_{elstat} + E_{exch} + E_S \tag{2.21}$$

where

$$E_{elstat} = \frac{e^2}{2}\sum_{gk}{}' \frac{Z_g Z_k}{r_{gk}} - e^2 \sum_{gk}{}' Z_g \int \frac{\rho_k(1,1)}{r_{1g}} dx_1 + \frac{e^2}{2}\sum_{gk}{}' \int \frac{\rho_g(1,1)\,\rho_k(2,2)}{r_{12}} dx_1 dx_2 \tag{2.22}_1$$

$$E_{exch} = -\frac{e^2}{2}\sum_{gk}{}' \int \frac{\rho_g(1,2)\,\rho_k(2,1)}{r_{12}} dx_1 dx_2 \tag{2.22}_2$$

$$E_S = -e^2 \sum_{gk}{}' Z_g \int \frac{\Delta\rho_k(1,1)}{r_{1g}} dx_1 + e^2 \sum_{gk}{}' \int \frac{\Delta\rho_g(1,1)\Delta\rho_k(2,2) - \Delta\rho_g(1,2)\Delta\rho_k(2,1)}{r_{12}} dx_1 dx_2 + \frac{e^2}{2}\int \frac{\Delta\rho(1,1)\Delta\rho(2,2) - \Delta\rho(1,2)\Delta\rho(2,1)}{r_{12}} dx_1 dx_2 \tag{2.22}_3$$

where we denote $\rho_k(x_1, x_2)$ by $\rho_k(1,2)$ etc. and

$$\Delta\rho(1,2) = \sum_g \Delta\rho_g(1,2) \tag{2.23}$$

The first 2 terms give the HF energy of the undistorted ions while E_s represents the energy associated with the change in the electronic distribution. The S-energy is of essential importance in the whole theory since all the repulsive force between the ions arise from the overlapping.

This approach has often been used [53, 54] to obtain the lattice properties of alkali halide crystals. The results for the lattice constant, cohesive energy and bulk modules are in tolerably good agreement with experiment. Löwdin's approach was also applied to a calculation of transition

pressure for some alkali halides. Some results are listed in table 2.2. The inclusion of many body interactions in the result is one of the main features of Löwdin's theory.

To summarise, Löwdin's formalism is of theoretical importance. He starts from the free ion Hartree-Fock wave functions and considers the many electron interaction by taking into account their overlapping and nonorthogonality. The main mathematical difficulties involved in the orthonormalization procedures and the approximation introduced to overcome these difficulties have so far limited the practical value of the theory. In view of the fact that most of the HF wave functions of the free ions for alkali halides are now available [55] and considering the progress in computational method, it would be highly desirable if one could make a comprehensive calculation of the static and dynamic properties of alkali halides following the Löwdin's a priori quantum mehcnaical approach. However the implementation of Löwdin's theory when the perfect crystalline order is lost appears rather difficult.

2.2.2 Models based on local density functional scheme

1. Gordon-Kim (GK) model

Several years ago Gordon and Kim [24] developed a model for evaluating the interaction between two closed-shell systems (*) based on the local density functional scheme. The electron density is approximated as the sum of the densities of individual ions, component densities being taken from Hartree calculations. If ρ_a and ρ_b are component densities, the total density is

$$\rho_{ab}(r_a, r_b) = \rho_a(r_a) + \rho_b(r_b) \qquad (2.24)$$

(*) hereafter we shall simply write the "closed shell systems" as "ions".

and

$$\rho_a(r) = \sum_i |\varphi_{ai}(\vec{r})|^2 \qquad (2.25)$$

where i denotes the atomic quantum numbers, φ_{ai} is the Hartree-Fock wave function of a component. The interaction potential between two ions is then evaluated as the sum of the Coulomb interaction energy and the rest:

$$V = V_c + V_{eg} \qquad (2.26)$$

The Coulomb interaction is

$$V_c = \frac{Z_a Z_b}{R} + \iint \frac{\rho_a(r_1)\rho_b(r_2)}{r_{12}} dr_1 dr_2 - Z_b \int \frac{\rho_a(r_1)}{r_{1b}} dr_1 - Z_a \int \frac{\rho_b(r_2)}{r_{2a}} dr_2 \qquad (2.27)$$

where Z_a and Z_b are atomic numbers of ion A and B respectively; R is the distance between the nuclei, r_{12} is the distance between two electrons; and r_{1a} and r_{1b} are the electron nuclear distances. Making use of the Hohenberg and Kohn [9] theorem they write the remaining part of the energy as

$$V_{eg} = \int d^3r \left(\rho_{ab} E_G(\rho_{ab}) - \rho_a E_G(\rho_a) - \rho_b E_G(\rho_b)\right) \qquad (2.28)$$

furthermore the energy density functional is evaluated in the local density approximation. This consists in taking for E_G the uniform electron gas expression and evaluating it for the local value of the density. As usual the uniform electron gas density functional is written in the form [56]

$$E_G(\rho) = C_k \rho^{2/3} + C_e \rho^{1/3} + E_{corr}(\rho) \qquad (2.29)$$

where

$$C_k = \frac{3}{10}(3\pi^2)^{2/3} \qquad (2.30)_1$$

and

$$C_e = -\frac{3}{4}\left(\frac{3}{\pi}\right)^{1/3} \qquad (2.30)_2$$

The first and second term in eq. (2.29) are the kinetic and exchange energy functional and denoted by E_{kin} and E_{ex} respectively; the third term is correlation functional, which is given by [57]

$$E_{corr}(\rho) = \begin{cases} 0.0311 \ln r_s - 0.048 + 0.009 r_s \ln r_s - 0.018 r_s, & r_s \leq 0.7 \\ -0.0615 + 0.01898 \ln r_s, & 0.7 \leq r_s \leq 10 \\ -0.438 r_s^{-1} + 1.325 r_s^{-3/2} - 1.47 r_s^{-2} - 0.4 r_s^{-5/2}, & r_s \geq 10 \end{cases} \qquad (2.31)$$

where $r_s = \left(\frac{3}{4\pi\rho}\right)^{1/3}$.

The GK model has the advantage of giving an inexpensive way of calculating reliable potentials between two closed-shell species. It is superior to many earlier similar models [58] stemmed from the Thomas-fermi and Thomas-Fermi-Dirac theories, whose validity was only restricted to the repulsive region. The GK model has been applied to many closed shell systems, such as rare gas atoms and alkali halides ions, rather good agreements have been obtained with experiments [24,25] . However, the GK model is not without its problems: (1). the reasons for the success of such a simplistic model and the limitations of its accuracy are not well understood; (2). it does not give the van der Waals tails of the potential and; (3). the potential well for most of the rare gas systems tended to be too deep by about 15% - 20% and much too deep for the helium systems. This is not surprising since the method is expected to fail when applied to system with a small number of electrons.

The main two distinct approximations made in the GK model are that (1). the total density of the system can be written as the superposition of

the charge density of the free ions, thus the charge density of the total system was allowed to change only because of the mutual overlap of the rigid free ions; (2). the interaction energy can be calculated from the density functionals in eq.(2.29). This means that the energy of the real system may be approximated by the simple energy functional of the uniform electron gas. Improvement to the model can be made by using more exact density functionals and by using a better description of the density in the interacting system.

Some steps along this direction were taken by Waldman, Gordon and Cohen [27,59].

Kim and Gordon have revealed systematic errors in each of the energy terms in the electron gas formulas when applied to single atoms and concluded that the error in each interaction electron gas energy term is greater than in the total energy. In order to reduce some of the errors made by the original GK theory, Waldman, Gordon and Cohen [27,59] proposed a modified electron gas model (MEG) in which GK model is modified by multiplicative scaling factors to the kinetic, exchange and correlation terms in the energy functional. The scale factors are determined uniquely by the condition that the energy functional yield correct results for the corresponding terms in an atom isoelectronic to the molecular system of interest. Thus MEG replaces electron gas functional in eq.(2.29) by

$$E_q^{MEG} = R(N) C_x \rho^{2/3} + X(N) C_e \rho^{1/3} + C(N) E_{corr}(\rho) \qquad (2.32)$$

where R(N), X(N) and C(N) are appropriate constants that depend on the N, the number of electrons in the molecular system of interest. Note that the kinetic term gives repulsive and exchange and correlation term gives attractive force to interaction potential, thus the introduction of the scale factors gives more repulsion to the interionic forces than that of the original GK model. This effect increases progressively from ion pairs which involve more electrons to those that have less electrons. The MEG predicts intermolecular

forces that are in better agreement with experiment for light rare gas atoms, such as helium. However, results for the alkali halide molecules are in considerbly poorer agreement than that based on the original GK model [27] .

Waldman and Gordon [60] have modified the GK model by use of a Drude model [61] . This modification corrects somewhat for rigid ion approximation by allowing harmonic distortion to occur. But one of the ingredients of this model is to determine the effective electron number from reliable Van der Waals coefficient whose value for alkali halide ion pairs is not presently available, so that those calcualtion using Drude model for ion pairs of alkali halides have never been performed.

Finally, we mention that some researchers [62] have tried to improve energy density functional by including gradient corrections. This causes the electron gas approximation to loose much of its simplicity and leads only to a marginal improvement.

The GK model and some of its modifications can be used for evaluating the ionic pair potentials that subsequently are used in a Born-Mayer type of calculation for the properties of alkali halides. Some of these calculation will be described in the following section.

2. Theory of Muhlhausen and Gordon [MG][63]

Another and more sophisticated approach has recently been developed by MG, who extended the GK model to include some many body interactions.

MG write the crystal charge density as a sum of the electron density $\rho_\tau^F(\vec{r})$ of the free ions

$$\rho(\vec{r}) = \sum_{\ell\tau} \rho_\tau^F(\vec{r} - \vec{R}_\ell - \vec{\tau}) \qquad (2.33)$$

with

$$\rho_\tau^F(\vec{r}) = \sum_i \left|\varphi_{i\tau}(\vec{r})\right|^2 \qquad (2.34)$$

whose notations in eq.(2.33) and (2.34) has been explained in section 2.2.1. Furthermore MG write the binding energy W_b as

$$W_b = (W_c + W_{Eg})/n \qquad (2.35)$$

where W_c is the electrostatic interaction energy per unit cell, W_{eg} is the electron gas interaction energy per unit cell and n is the number of formula units in the unit cell. W_c can be calculated using Ewald method [64]. W_{eg} is written as follows:

$$W_{Eg} = \int_v d\vec{x}\left[E_G^{MEG}(\rho(x))\rho(x) - \sum_\tau \sum_\ell E_G^{MEG}(\rho_\tau^F(x-\vec{R}_\ell-\vec{\tau})) \cdot \rho_\tau^F(x-\vec{R}_\ell-\vec{\tau})\right] \qquad (2.36)$$

where MG used MEG model, i.e; the electron energy density functional is given by eq.(2.32). The subscript v indicates an integration over a single unit cell of volume V. Thus the MG theory also include nonadditive many body interactions arising from the simultaneous overlap of the densities of several free ions.

MG have also extended this model to take account for changes of charge densities when free ion was placed into solid, introducing an additional empirical stabilizing potential [65]

$$V_\tau(r) = \begin{cases} -N_\tau/r_0, & r \le r_0 \\ -N_\tau/r, & r > r_0 \end{cases} \qquad (2.37)$$

The potential $V_\tau(r)$ is produced by Watson's sphere of total charge $-N_\tau$ and of radius r_0. The value of r_0 is obtained after a selfconsistent minimization of the expression for the total energy. By this procedure MG got ion density (i.e. ss density) which differes from free ion density mainly in effect of contraction of charge density around the anion. MG then replaced the free ion density by ss density and used eq.(2.36) and

(2.35) to calculate the binding energy. The theory has applied to some alkali halides and oxide crystals. The predictions of lattice constant and energies agree with expt. to a typical accuracy of 2%. The results for NaF and LiF are listed in table 2.3.

The nonadditive many body interaction in MG theory produces a small amount of repulsion thus to increase lattice constant and decrease lattice energy in better agreement with the experiments. A very recent work of Gygi, Maschke and Andreoni [32] has pointed out some of the deficiencies of MG approach which make their conclusions unreliable. Thus it appears that there are not compelling reasons to prefer the modifications of the G.K. scheme to its first version. In fact the original GK scheme has the great merit over its more sophisticated developements of being very simple to use.

Finally we mention that recently the first principle pseudopotential method has been introduced in the local density functional scheme. The success of this method in semiconductors are very impressive. We notice that this method has great methodological importance in the description of cohesive and structural properties of solids. This method has selfconsistent treatment between electron density of crystal and potential thus gives correct descritpion of the charge density distribution of the crystal. This is essential in the use of local density functional method. Also this method can be used to determine the phonon frequency with high accuracy [66] . Even though only some initial steps [15] have recently been taken for the study of cohesive properties of alkali halides, one can expect that this method may become more important in this field.

However at present it does not appear to be feasible to derive effective potentials from this highly sophisticated schemes.

2.3 The Born-Mayer approach

In the previous section we have discussed the a priori quantum mechanical approach for the binding and structural properties of alkali halides. This approach gives more sophisticated description of many electron interactions in ionic crystals and it is endowed with predictive capabilities to the theory. However the mathematical complexities involved have limited its practical use. On the other hand, to-date, the most widely applied approaches have been of semi-empirical Born-Mayer type, in which the many body interactions are neglected, the binding in solids is described as sums of the effective pair interactions. This can be constructed a priori as in the GK scheme that we have described above or more empirically the forces between pairs are written in terms of an interaction potential with variable parameters to be determined by empirical fitting to experimental data. With a careful selection of a flexible pair potential, the Born-Mayer approach can give good agreement with a large variety of experimental results. Due to the simplified treatment of interionic interactions in solid and an essentially empirical nature of the theory the range of applicability of Born-Mayer model is severely limited by the experimental data available.

In the Born-Mayer approach, ionic crystal is regarded as composed of spherical non overlapping ions bearing net charges of integral amount. The lattice energy of the crystal is written as a sum of the Madelung energy plus the short range interaction energy

$$W_L(R) = -\alpha_R/R + W_{rep}(R) \qquad (2.38)$$

where the structure dependent constant α_R is called the Madelung constant. It is referred to the characteristic length R (i.e. here we denote R as the nearest neighbour distance). α_R can be obtained using standard technique of lattice sums [64] for a given structure. The Madelung energy is the dominant part which is about 90% of the total lattice energy for alkali halides.

This attractive energy is often supplemented by the total Van der Waals attractive energy W_{van}, which is the sum of two body Van der Waals energy corresponding to dipole-dipole and dipole-quadrupole interaction energy between two ions at a distance r_{ij}. it is of the form

$$W_{van}(r_{ij}) = -C_{ij}/r_{ij}^{6} - d_{ij}/r_{ij}^{8} \tag{2.39}$$

where the Van der Waals coefficients C_{ij} and d_{ij} can be expressed in terms of polarizabilities and excitation energies. Then the total Van der Waals energy of the crystal can be expressed as

$$W_{vdw} = -C/r^{6} - D/r^{8} \tag{2.40}$$

and

$$C = C_{+-} S_1^{(6)} + \frac{1}{2}(C_{++} + C_{--}) S_2^{(6)} \tag{2.41}$$

$$D = d_{+-} S_1^{(8)} + \frac{1}{2}(d_{++} + d_{--}) S_2^{(8)} \tag{2.42}$$

where the quantities $S_1^{(n)}$ and $S_2^{(n)}$ are structure-dependent factors, representing appropriate sums over the Bravais lattice of the structure. Their value for B1 and B2 structure are given in Table 2.4. The Van der Waals coefficients are hard to determine with accuracy [3,67]. However in calculation of the lattice energy of the crystals the uncertainties in these coefficients are fairly unimportant since the Van der Waals contribution to the lattice energy is only about 1%.

The Born model makes no attempt to evalaute the repulsive energy from first principles. Instead it assumes a simple functional dependence of the repulsive energy on the interionic distance and determines the intervening parameters from experimental data. The most common procedure to determine the repulsive parameters for a cubic crystal involves a use of the

equation of state and its volume derivative at constant temperature in the Hildebrand form [68] :

$$\frac{dW_L}{dV} = -P + \frac{T\beta}{K} \tag{2.43}$$

$$V\frac{d^2W_L}{dV^2} = K^{-1} + \frac{T}{K^2}\left[\left(\frac{\partial K}{\partial T}\right)_P + \frac{\beta}{K}\left(\frac{\partial K}{\partial P}\right)_T\right] \tag{2.44}$$

where P is pressure, K and ß are the isothermal compressibility and the coefficient of volume thermal expansion of the crystal respectively.

The requirements of equilibrium of a crystal has led to the adoption of either the inverse power potentials (A/R^n) or exponentive decaying potentials $be^{-R/\rho}$. Fumi and Tosi have found the latter form to be more satisfactory than the former [20].

If one considers explicitly the Born repulsion of the first nearest neighbours, the repulsive energy can be written [18] in the Born-Mayer form:

$$W_{rep} = Mb\exp(-R/\rho) \tag{2.45}$$

If one includes explicitly the Born repulsions of the second neighbours, one has the Huggins-Mayer form of repulsive energy [69]

$$W_{rep} = Mb_{+-}\exp(-R/\rho) + \frac{1}{2}M'(b_{++}+b_{--})\exp(-aR/\rho) \tag{2.46}$$

Here the structure dependent constants M, M' and a are given in Table 2.4. The expression (2.45) contains two parameters, b and ρ , which are determined directly for each crystal from the equation of state and the compressibility. In the alkali halides, the average value of ρ is 0.320 Å, with a root-mean-square deviation of 7%. On the other hand, the parameter ρ entering the expression (2.46) is assumed to be independent of the ionic species in a given crystal. The evaluation of the repulsive energy of an ionic crystal by means of eq.(2.46) still requires the determination

of three repulsive parameters namely Mb_{+-}, $M'(b_{++} + b_{--})$ and ρ. Fumi and Tosi [19,20] have shown that the number of independent parameters in a family of salts of a given structure can be reduced by imposing the condition that the model yields the empirical law of approximate additivity of the interionic distance in a family of crystals. Tosi and Fumi [19,20] have also shown that the variation of ρ from crystal to crystal can be determined from the compressibility. This yields the Fumi-Tosi potentials, which represent a culmination of earlier efforts of many, including Born, Mayer, Huggins and Pauling.

The general form of Fumi-Tosi potentials can be written as:

$$\Phi_{ij}(r) = Z_i Z_j e^2/r + b_{ij} \exp(-r/\rho_{ij}) - C_{ij}/r^6 - d_{ij}/r^8, \qquad i,j = +- \tag{2.47}$$

Fumi and Tosi take the full ionic value ± 1 for the charge and use the Mayer [70] values for the Van der Waals coefficients c_{ij} and d_{ij}. For the short range repulsive terms they make the following assumptions: (1). for any crystal $\rho_{++} = \rho_{--} = \rho_{+-} = \rho$, but the value of ρ varies from crystal to crystal; (2). the constants b_{ij} are written in the form

$$b_{ij} = \beta_{ij} b \exp[(r_i + r_j)/\rho] \tag{2.48}$$

with b a constant for all crystals and for all interaction types, r_i and r_j the ionic radii, which depend only on the ions involved and β_{ij} the Pauling factors which are defined by

$$\beta_{ij} = 1 + Z_i/n_i + Z_j/n_j \tag{2.49}$$

with n_i, n_j the number of electrons in the outer shell (usually 8, but for Li^+, 2). Thus for the 17 salts considered the parameters required are 17 values of ρ; 5 values of r_+, 4 values of r_- and 1 value of b. The parameters are obtained by a least squares fit to the equation of state and

its volume derivative at constant temperature. The experimental data required for each salt are the lattice parameter, the thermal expansion coefficient and the compressibility and its temperature and pressure derivatives.

The prediction of the B1 to B2 transition pressures by traditional Born model are in quantitatively good agreement with experimentally observed values, but they are usually too high. This is due to the fact that the traditional Born model consistently over-estimate the lattice energy in the B1 structure relative to the B2 structure and systematically somewhat underestimated the compressibilities of the B1 structure. Tosi and Fumi [5] concluded that the only possible phenomenological approach to the stability of alkali halides must involve the assumption that the parameters b and ρ of the Born-Mayer potential are structure dependent, i.e. that they have different values for the B1 and B2 structures. With this modification they showed that consistent agreement can be obtained with the experimental value for the work involved in the observed pressure transition and thermal transition.

We shall not examine the limitations involved in the above Born-type potentials individually. We note that a basic assumption involved in the Born model is that the lattice energy is expressed as a sum of central, two body energies of point like charges; furthermore, by fitting the repulsive parameters to experimental data, the Born approach depends heavily on those experimental quantities. They reproduce the perfect-crystal data only in part. The assumed forms of potential may also be too restrictive for wide practical uses. It is known that the point-like charge assumption cannot give a good representation of the optic branches of the phonon dispersion curve [71] : the splitting between the LO and TO branches will be too great and the high frequency dielectric constants calculated from this model differ from the actual values which would be in the range 2-3 for the most alkali halides. Furthermore the violation of the Cauchy relation $C_{12} = C_{44}$ of elastic constants shows that central, two body interactions are not exact. To incorporate many body interactions one should resort to

the first principle calculations.

It has been noticed that in the Born model, the determination of the Born repulsive parameters through the fitting of the isothermal compressibility or the static dielectric constant (in both cases together with the equilibrium interionic distance) leads to rather different values for the repulsive parameters. Although the functional forms of a/r^n or $b\exp(-r/\rho)$ have been typically chosen for repulsive energy but some arbitrary variants [72] have been explored may be adjusted to give the correct compressibility and lattice constant at equilibrium.

Various phenomenological potentials have been proposed in recent years by Catlow, Diller and Norgett [73] , by Corish, Parker and Jacobs [74], by Sangster et al. [75] and by Hardy and Karo [76] . These authors have tried to combine in various ways the Born model with models of deformable ions, such as the shell models, in an attempt to reproduce simultaneously both the elastic and the dielectric properties of the alkali halide crystals. Based on their detailed studies, Eggengoffner, Fumi and Murthy [22,23] have concluded that it is difficult to say whether these new potentials, taken as a whole, have truly improved our knowledge of the effective short range pair interaction potentials in the alkali halides.

Recently Narayan and Ramaseshan NR [21] have proposed a new empirical potential for ionic crystals. NR view an ionic crystal as a collection of compressible ions in polyhadral, space filling cells. Repulsion arises solely from the increased compression energy at the cell faces. The main feature is that they use two parameters for each ion which, once obtained from one set of crystal data, can be used in any other crystal in which it occurs. This may lead predictive power to the theory to some extent, but it still needs to be tested. This theory in their newly revised form has been used to study the B1 to B2 transition in alkali halides, the results appeared to be in very good agreement with experiments. But their procedure seems to be rather ad hoc and no basic justification has so far been given [33] . Furthermore the NR potential cannot be used either in MD simulations or in Phonon calculations.

2.4 Polymorphic transition in terms of the GK model

So far, we have described two types of theoretical approaches to treat the alkali halides: the a priori quantum mechanical approach and the semiempirical Born-Mayer approach. Both the approaches have been fairly successful in their predictions of the binding and structural properties in alkali halides. A middle of the way approach has been taken by Gordon and Kim, who have developed a theory for the calculation of interaction forces between closed shell systems, as discussed in section 2.2.2. The GK treatment is parallel to the Born-Mayer theory in that it writes lattice energy as a sum of pair interactions and neglects many body interaction energies. However, since it uses the a priori GK potential instead of the empirically obtianed one so that no empirical parameters are introduced. It thus eliminates some difficulties which the empirical Born-Mayer theory often encounters, and gives some predictive power to the theory. The GK treatment is similar to the Löwdin's theory in that it has the nature of first principle calculation. However, contrary to Löwdin's theory, it neglects the lattice induced modification of the electronic charge density.

Gordon and Kim [GK] [25,26] first applied their ion pair potential to a preliminary study of the cohesive energy of the B1 and B2 phase and the transition pressure of some alkali halides. In their treatment they assumed: (1). Crystals are composed of the free ions; (2). The interactions of ions are pair-wise additive, many body interactions are neglected; (3). Neglecting thermal effect, either harmonic vibration energy or zero point energy; (4). For short range interactions only the first nearest neighbour interactions are included. Generally good agreement is obtained for the lattice energy of B1 phase and the B1 to B2 transition pressure with available experimental data. But there are some discrepancies, for example (1). for most crystals they overestimate lattice energy by about 10% and the equilibrium lattice constants are too small; (2). the calculated transition pressures are rather good, but if one includes second neighbour interaction,

then the predicted value becomes much lower. From table 2.5 one can conclude that the contribution of second nearest neighbour interaction to lattice energy is clearly not negligible. Thus GK result only has qualitative meaning. As we shall show in the following, we also found that for those salts for which the calculations have not been done, namely the iodine compounds, the transition pressures are negative. this implies that for a whole class of alkali halides the original GK model predicts the wrong structure.

Successively, Cohen and Gordon [CG][27] have tried to improve this by using a modified electron gas treatment and extending short range interactions up to second and third nearest enighbour for the B1 and B2 structure respectively. The average magnitude of the deviation between the predicted and observed lattice constants and lattice energies are about 2%. This scaled electron gas results give a modest improvement over GK results for the transition pressures but still large discrepancies remain. Furthermore Boyer [29] has also shown that using scaled GK model one obtaines worsened results for some other properties. Thus one must look to other approximations to correct the larger discrepancies between theory and experiments. Boyer [29] has presented full first principle equation-of-state calculations for all alkali halides except for cesium compounds, since the Hartree-Fock wave function for Cs^+ has not been computed. His treatment includes thermal vibrations in the harmonic approximation and the effect of as well as zero point motion. He uses a parametrized version of the original GK potential [GK(B)] and includes short range force to second nearest neighbours for B1 structure, to third nearest neighbours for B2 structure. A number of pro - perties are treated within this framework: lattice dynamics, elastic behaviour, structure determination, thermal expansion, compressibility and the overall stability of the lattice as a function of temeprature and pressure. It is shown that including the effect of harmonic vibrations in evaluating the free energy did not materially affect the conclusions on polymorphic transitions based on the static calculations. The results of the above

various treatment for equilibrium lattice constant, lattice energies and predicted the B1 to B2 transition pressure are listed in table 2.6. to - gether with the experimental data for comparison. In this Table we also include the results from our calculation [Present] , which follows Boyer's treatment but omits effects of harmonic vibrations.

An attempt was made by Boyer to ascribe trends in the discrepancies between theory and experiment to particular approximation of the theory. From this analysis it appears that the pair-potential approximation (PPA) is in greatest need of improvement.

The breakdown of PPA can be seen by noting that the magnitude of the errors are found for those compounds with a big difference between the size of the consituent ions. This is most evident in the thermal exapansion coef- ficient α (see Table 2.7), for example, the predicted values of α for the iodides are in all cases considerably too small with progressively worse agreement going from Rb to Li . The generally poorer agreement between theory and experiment for the polymorphic critical pressure is also an indication of a breakdown in the PPA (see table 2.8). The reason of these big errors in the PPA can be understood from a simple geometrical argument. In the calculation of a pair potential, the largest contribution comes from the region where there is greatest overlap of the two charge densities. However, in a solid substantial portion of the total charge density in the overlap region of a given ion pair can come from enighbouring ions as well. This is especially true if one ion is much smaller than the other.

As mentioned before within the PPA the calculated equilibrium lat- tice constants are too small and the lattice energies are too great for most compounds , and if one includes the Van der Waals energy into the lattice energy the situation will become even worse. it is then not surprising that the calculated transition pressures come out to be too low. To bring the theoretical results in closer agreement with the experiment, one thus need a supplement of repulsive force in the B2 structure that should be

larger than that in the B1 structure. In the next chapter we will show that this supplement can be achieved by including the nonadditive three body interactions.

CHAPTER III - MANY BODY INTERACTIONS AND ITS EFFECTS ON POLYMORPHIC TRANSITIONS

3.1 Introduction

In the previous chapter we have shown that while pair-wise additive forces have played a very important role in the theory of ionic crystals, there are indications that many body forces though comparatively small, cannot be neglected in the study of polymorphic transitions. This conclusion is, for instance, supported by the phenomenological analysis of Tosi and Fumi [5]. However, a semi-empirical treatment does not allow one to clearly separate the small many body terms from the two body terms, because it involves the use of experimental data pertinent to the transition the accuracy of which is often not sufficient. For this purpose one has to resort to quantum mechanical treatments.

Much work has been done to evaluate the non-additive contributions to many body force [77] for rare gas atoms. At large inter-nuclear separation, the dominant contribution to the non-additive three body forces comes from triple dipole interaction which has been calculated by Axilord and Tellor [78] using third order perturbation theory. It is a straightforward extension of the London-vander Waals R^{-6} dipole-dipole interaction between two atoms at large distances. If we denote the angles of the triangle formed by the triplets (a.b.c) by γ_1, γ_2 and γ_3 and the distances between the atoms by R_{ab}, R_{ac} and R_{bc}, then the triple-dipole interaction, ΔE_3, for three identical atoms is

$$\Delta E_3 = \frac{9}{16} \frac{E_{av} \alpha^3 (3 \cos\gamma_1 \cos\gamma_2 \cos\gamma_3 + 1)}{R_{ab}^3 R_{bc}^3 R_{ca}^3} \qquad (3.1)$$

where α is the atomic polarizability and E_{av} and "average excitation energy" per atom ; E_{av} is usually taken to be the first ionization potential. However, at smaller inter-nuclear separations, the triple dipole interaction ceases to be dominant, and its description in the conventional manner becomes inadequate as a result of the neglected effect of electronic overlap. In principle, one can use fully quantum mechanical methods to evaluate non-addivite three body forces. However, the actual calculation becomes very

complicated with increasing number of electrons, so that only hydrogen or helium atoms have been treated so far by this method [79] and this only to a limited extent. Present [80] has calculated the non-additive three body forces for Kr_3 and He_3 using the Thomas-Fermi-Dirac model and obtained results valid only for very small distances. At these small distances, the non-distorsion assumption which he used for the separate atomic densities is not valid. In addition the region of inter-nuclear distances covered by his calculations falls outside that of many physically interesting problems. Review of work on calculations of non-additive three body interaction can be found in ref. [77] and ref. [81].

The first explicit analysis of many ion interaction in alkali halide crystal was given by Löwdin [8], who undertook a calculation of the total cohesive energy for a number of alkali halides using first order perturbation theory. The lattice energy was found to contain a considerable amount of many-ion exchange contribution, which can be written as

$$E_s^* = -e^2 \sum_g \int V_{Mad,g}(1)\, \Delta\rho_g(1,1)\, dx_1 \qquad (3.2)$$

where

$$V_{Mad,g}(1) = \sum_{h \neq g} \frac{Z_h - n_h}{r_{1h}} \qquad (3.3)$$

is the Madelung potential of the ionic lattice of point charges at point r_1; Z_h and n_h are atomic number and number of electrons of ion h respectively; $\Delta\rho_g$ in expression (3.2) is defined in eq. (2.18). Thus the many ion interaction term is essentially proportional to the Madelung constant and is found to be dominated by three body interactions. This implies that the structure sensitivity of the many ion interaction as calculated by Löwdin, is too low, since the Madelung constants of the B1 and B2 phases differ by only 1%; the maximum difference in three ion interactions between these two structures is only of the order of 0.1 kcal/mole; and the magnitude of this three body interaction decreases rapidly as the cation and the anion approach equal

size. Later attempts to introduce many-ion interactions in the lattice energy of alkali halide crystal have been directed towards an interpretation of Löwdins results on a simpler basis, for example, the so-called "shell" model developed by Dick and Overhauser [82].

In shell model the ion is modelled by a charged massless shell through which short range forces act. The shell is coupled through a harmonic spring to a charged core which has the mass of the ion it belongs to. In order to reproduce the experimental dispersion curves for the lattice vibrations as close as possible an extra degree of freedom allowing the deformation of the shell has been introduced [83]. This takes into account the polarization effects in ionic crystals. All the models explain the breakdown of the Cauchy relation and include some of the many body interactions. Few attempts so far have been made to apply these models to the study of static properties such as cohesive energy, relative stability, phase transition pressure, etc. [84]. One difficulty common to all those theories is that the mathematical equations are too complicated and unless drastic approximations are made, numerical calculations become impossible. In addition, it is difficult to discern explicitly the many ion contribution to the crystal energy. Furthermore the use of potentials obtained from the shell model, in a context different from that of the harmonic approximation, say in molecular dynamics calculations, though feasible [85] it is very costly.

Jansen and co-workers [81, 86] treated the three body interaction by perturbation theory using single effective electron charge distributions of a Gaussian form for the unperturbed atomic densities. This semi-empirical method has been used extensively by these authors mainly to explain the relative stabilities of rare gas and alkali halide crystals. Although they succeeded in predicting correctly the relative stabilities of the crystal by using this model, the method has been criticized as having ambiguities both in its theoretical formulation [87] and in the actual choice of the range parameters of the Gaussian electron charges [88].

As discussed before, recently Muhlhausen and Gordon [63] have developed a modified electron gas theory of ionic crystal including some many body effects. The calculations have been done only for some alkali halide crystals, namely LiF, NaF and alkali chlorides. We also note that there is no conclusive evidence that the MEG theory is to be preferred over the original GK model.

As we discussed in the previous chapter, some descrepancies between predictions of the experiment and the GK model have been ascribed to the pair potential approximation (PPA). The original GK model can be extended to the calculation of the non-additive three body interactions (TBI) among triplets of closed shell systems [33]. The TBI are expected to dominate the non-additive many body interactions. The calculation of TBI can be more easily and explicitly carried out. It is a first principle calculation and it is done once and for all, and there is no additional assumption introduced. Thus a study of the effects of TBI on the cohesive and structural properties in alkali halides can quantitatively give evidence that the GK model can be improved along these lines. In section 3.2 of this chapter we shall calculate TBI for NaCl, NaBr, NaI, KCl, KBr, KI, RbCl, RbBr and RbI. The properties of the TBI will be discussed in section 3.3. In section 3.4 we shall apply these results to the study of polymorphic transitions for the above-mentioned nine crystals. It will be shown that incorporating TBI in the evaluation of lattice energy will to a great extent correct the systematical errors involved in the PPA of the GK model for a family of alkali halides and give an improvement in the prediction of the structural stabilities. As a primilinary study, we will not consider the change of ion size and polarization effects. To correct the rigid free ion picture of the GK model is a subject for further studies.

3.2 Calculation of non-additive three body interaction for alkali halide ions

In the calculation of three body forces in alkali halides, we shall follow the work of Kim [33], who has done a similar calculation for the rare gases. We take three ions A, B and C, of electron densities ρ_A, ρ_B and ρ_C respectively. The electron density of the combined ions is assumed to be equal to the sum of the electron densities of the separate ions:

$$\begin{aligned} \rho_{AB}(\vec{r}_A, \vec{r}_B) &= \rho_A(\vec{r}_A) + \rho_B(\vec{r}_B) \\ \rho_{BC}(\vec{r}_B, \vec{r}_C) &= \rho_B(\vec{r}_B) + \rho_C(\vec{r}_C) \\ \rho_{CA}(\vec{r}_C, \vec{r}_A) &= \rho_C(\vec{r}_C) + \rho_A(\vec{r}_A) \end{aligned} \tag{3.4}$$

and

$$\rho_{ABC}(\vec{r}_A, \vec{r}_B, \vec{r}_C) = \rho_A(\vec{r}_A) + \rho_B(\vec{r}_B) + \rho_C(\vec{r}_C) \tag{3.5}$$

where ρ_{AB}, for example, is the electron density of the combined ion pair AB and ρ_{ABC} that of the total system of three ions A, B and C. Here $\vec{r}_A$, $\vec{r}_B$ and $\vec{r}_C$ are the distance vectors from the centres of the ions A, B and C respectively.

The Coulomb interaction for fixed separate charge distributions is pair-wise additive. Since we assume no re-arrangement of the separate ionic charge densities when the three ions are brought together, the Coulombic interaction energy of the three ions is the sum of the three pair-wise Coulombic interaction energies and there is no Coulombic energy contribution to the non-additve three body forces. Therefore we need only consider the remaining contributions to the energy in the present work.

The total non-Coulombic energy of the three ion system is approximated by

$$E_{G,ABC} = \int \rho_{ABC}(\vec{r}_A, \vec{r}_B, \vec{r}_C)\, E_G(\rho_{ABC})\, d\vec{r} \qquad (3.6)$$

where $E_G(\rho)$ is the energy density of the electron gas with uniform density ρ. It is given by eq. (2.29)-(2.31).

In order to get the non-additive three body interaction we substracted from eq. (3.6) the sum of three pair interaction and the sum of the non-Coulombic energies of the three ions. Therefore the non-additive three body interaction is

$$\begin{aligned}\Delta V_{ABC} = \int [\, & \rho_{ABC}(\vec{r}_A, \vec{r}_B, \vec{r}_C)\, E_G(\rho_{ABC}) - \rho_{AB}(\vec{r}_A, \vec{r}_B) E_G(\rho_{AB}) \\ & - \rho_{BC}(\vec{r}_B, \vec{r}_C) E_G(\rho_{BC}) - \rho_{CA}(\vec{r}_C, \vec{r}_A)\, E_G(\rho_{CA}) \\ & + \rho_A(\vec{r}_A)\, E_G(\rho_A) + \rho_B(\vec{r}_B)\, E_G(\rho_B) + \rho_C(\vec{r}_C)\, E_G(\rho_C)]\, d\vec{r}\end{aligned} \qquad (3.7)$$

For the evaluation of the volume integral in eq. (3.7) we used a spheroidal coordinate system [89] in which

$$\lambda = (r_A + r_B)/R_{AB}\,, \qquad \mu = (r_A - r_B)/R_{AB} \qquad (3.8)$$

and φ is the azimathal angle around axis along R_{AB}. The volume integral is expressed in terms of three new coordinates as

$$\int d\vec{r} = (R_{AB}/2)^3 \int_1^\infty d\lambda \int_{-1}^{1} d\mu \int_0^{2\pi} d\varphi\, (\lambda^2 - \mu^2) \qquad (3.9)$$

Since the electron densities of the alkali and hilegon ions are spherical, they depend only on the magnitude of the distance r_A, r_B and r_C, and not on the full distance vectors $\vec{r}_A$, $\vec{r}_B$ and $\vec{r}_C$. Thus,

$$\Delta V_{ABC} = (R_{AB}/2)^3 \int_1^\infty d\lambda \int_{-1}^{1} d\mu \int_0^{2\pi} d\varphi\, (\lambda^2 - \mu^2)\, [\rho_{ABC}(r_A, r_B, r_C) \cdot$$

$$\cdot E_G(\rho_{ABC}) - \rho_{AB}(r_A, r_B) E_G(\rho_{AB}) - \rho_{BC}(r_B, r_C) E_G(\rho_{BC})$$
$$- \rho_{CA}(r_C, r_A) E_G(\rho_{CA}) + \rho_A(r_A) E_G(\rho_A)$$
$$+ \rho_B(r_B) E_G(\rho_B) + \rho_C(r_C) E_G(\rho_C)] \qquad (3.10)$$

A geometry of the system of the three ion A, B and C is given in Fig. 3.1, where P represents a typical point in the volume over which the integration is carried out; r_A, r_B and r_C are readily expressed in terms of λ and μ from eq. (3.8) and fig. 3.1 [33]. For the ionic electron densities ρ_A, ρ_B and ρ_C in eq. (3.10), we used the ones obtained from Clementi analytical Hartree-Fock wave functions [55]. We calculated these densities at an appropriate set of grid points at the beginning and tabulated them. These tabulated densities were then used with a simple exponential interpolation to get the densities at arbitrary points. We have checked this procedure by evaluating these densities at each point directly from the analytical wave functions until the relative differences between the two procedures for the given values of densities were less than 10^{-6}. We found that resulting values of TBI were the same in the first four figures between two procedures. The integration in (3.10) was carried out numerically [90]. The φ integration was done first by introducing a new coordinate

$$x = \cos\varphi, \quad dx = -\sin\varphi\, d\varphi \qquad (3.11)$$

and then using the quadrature formula [91]

$$\int_{-1}^{1} \frac{f(x)}{(1-x^2)^{1/2}}\, dx \simeq \frac{\pi}{n} \sum_{K=1}^{n} f\left(\cos\frac{2K-1}{2n}\pi\right) \qquad (3.12)$$

The integrations over λ and μ were then carried out using Gauss-Laguerre and Gauss-Legendre numerical quadratures [92] respectively. We found that

a numerical integration with a grid of 24(μ)x16(λ)x16(φ) points leads to a numerical accuracy of 1%, which we found good enough for our present purposes. In a few cases we have checked the convergences by increasing the number of points in the grid to 48(μ)x32(λ)x32(φ). We found that the first two figures of the results were not affected by this change.

Following the above procedures the TBI potentials were calculated for NaCl, NaBr, NaI, KCl, KBr, KI, RbCl, RbBr and RbI crystals. For each crystal the total TBI potential of the B1 and B2 structure were expressed as a sum of TBI potentials of the relevant triplets ions in the B1 and B2 structures respectively. We denote an anion by X and a cation by M. Each configuration of triplet ions A,B and C can be defined by (CAB; R_{CA}, R_{CB}, γ), where a triangle formed by the triplet ions is specified by R_{CA}, R_{CB} and γ, as shown in Fig. 3.1, with a central ion assumed to be placed at point C. Three characters CAB indicate the type of ions, each character can be either X or M, to specify which ion is placed at point C, A and B respectively. For example, the configuration (XMM, R_{CA}, R_{CB}, γ) is illustrated in Fig. 3.2. In table 3.1 and 3.2 the type of energetically more relevant configurations and their number per ion are given for the B1 and B2 structures, with the value of R_{CA} and R_{CB} in units of the nearest neighbour distance R. For the sake of convenience we divided all listed configurations into three parts: 1) configurations in which $R_{CA} = R_{CB} = 1$, denoted as (1.n.n); 2) all the other isosceles triangles, i.e. in which $R_{CA} = R_{CB} \neq 1$, denoted as (ISO); 3) remaining configurations denoted as (REM).

We used n(CAB; R_{CA}, R_{CB}, γ) to denote the number of configuration (CAB; R_{CA}, R_{CB}, γ) per ion that appear in the given crystal structure (B1 or B2), and V_3(CAB; R_{CA}, R_{CB}, γ) to denote the TBI energy contributed by configuration (CAB; R_{CA}, R_{CB}, γ). Note that V_3(CAB; R_{CA}, R_{CB}, γ) is a function of the nearest neighbour distance R only. Using the notation the total TBI energy for a given crystal and structure at an assumed nearest neighbour distance R can be written as

$$V_3^{total}(R) = \sum V_3(CAB; R_{CA}, R_{CB}, \gamma)\, n(CAB; R_{CA}, R_{CB}, \gamma) \qquad (3.13)$$

where $V_3^{total}(R)$ depends only on R. Here the summation on the r.h.s. of the eq. (3.13) is over all relevant configurations as listed in table 3.1 and 3.2 for the B1 and B2 structures respectively. The contributions form the other configurations are negligible.

In order to investigate the effects of TBI on the cohesive properties, we need to know the value of $V_3^{total}(R)$ at any value of R around an equilibrium nearest neighbour distance $\bar{R}$. We first calculated the value of $V_3^{total}(R)$ for several assumed R (with spacing 0.1 a.u.), tabulated the obtained values and then use this table to calculate $V_3^{total}(R)$ at any value of R by means of a simple exponential interpolation. Using the above procedure, we calculated the total TBI energy as a function of the nearest neighbour distance. We used this in the lattice energy expression and calculated for different structure and chemical compositions.

3.3 Properties of TBI

The TBI forces in the GK model arise from the triplet overlap of the three charge distributions, which is due to the nonlinear form of the electron gas functionals. Before looking at the numerical results we shall quantitatively discuss the contribution of each electron gas functional term to the TBI. The kinetic term depends on the density whose form is $\rho^{5/3}$ with positive coefficient; notice that [33]

$$(\rho_A+\rho_B+\rho_C)^{5/3}-(\rho_A+\rho_B)^{5/3}-(\rho_B+\rho_C)^{5/3} \\ -(\rho_C+\rho_A)^{5/3}+\rho_A^{5/3}+\rho_B^{5/3}+\rho_C^{5/3}\leqslant 0 \tag{3.14}$$

where the equality sign holds in the case that any of the ρ is equal to zero. So we conclude that the kinetic term contributes an attractive energy to the TBI. With similar arguments one can conclude that the exchange and correlation terms give repulsive contributions to the TBI energy. One can easily find that the introduction of scaled factors in the MEG theory [27] leads to a reduction of repulsive force in the TBI.

First we shall take KCl as an example to see how the value of TBI depends on the configuration of the triplet of ions and how it varies with the geometrical parameters R_{CA}, R_{CB} and γ. We consider the cases of R_{CA} = R_{CB} = R. This is shown in Fig. 3.3; Fig. 3.3 (a) shows how V_3(MXX; R,R, γ) varies with R; Fig. 3.3(b) shows how V_3 (XMM; R,R, γ) varies with R, for the cases of γ = 90°, 70.5° and 109.5°. In all these cases the value of TBI starts with a negative value at very small R, increases rapidly with R to reach a certain positive value, and remains approximately constant over a certain range of R. At still larger R, TBI decays exponentially. It is of interest to point out the following properties of TBI:

1) Around the equilibrium nearest neighbour distance, for example, at R = 5.7 a.u. for the B1 structure of KCl crystal, the values of TBI are positive. This implies that each TBI gives an additional repulsion to the

to the lattice energy. We will see later that this is a common feature for all crystal of interest. Table 3.3 shows that the exponential-decay behaviour of TBI with respect to R can be roughly represented by the function $A\exp(-\beta R)$. In table 3.3 the first line gives the calculation TBI values, the second line gives the values calculated from an exponential function with A = 800 and $\beta = 1.30$. This also implies that the TBI is a short range force.

2) The magnitude of the TBI at fixed value of R, near the equilibrium, decreases considerably with the increase of the triangular opening angle γ, as shown in table 2.4 for the distance R = 5.7 a.u.

3) From table 3.4 one can also find that for a fixed geometry, i.e. the same set of values of R and γ, the magnitude of TBI is strongly dependent on the type of ions. In general $V_3(MXX; R, R, \gamma) > V_3(XMM; R, R, \gamma)$, because the anion charge distribution is more extended. This conclusion can be generalized as follows: for a fixed geometry, the configuration having more anions has a larger TBI value, i.e. $V_3(XXX; R, R, \gamma) > V_3(MXX; R, R, \gamma) > V_3(XMM; R, R, \gamma) > V_3(MMM; R, R, \gamma)$. This can be seen in table 3.5 in which the geometry was fixed at R = 7.071 a.u. and $\gamma = 90°$ for KCl. The above discussion is valid for the other eight crystals of interest.

The calculated results of total TBI energy, as a function of nearest neighbour distance, are presented in table 3.6 for nine crystals. In addition the contributions from different parts of configurations to the total TBI energy are also given.

From table 3.6.3 for NaI one can see that the contribution of TBI from the ISO part is much larger than the (1.n.n) contribution. This is due to the large dissimilarity of anion and cation in NaI crystal. On the other hand from table 3.6.7 for RbCl, one can see that the contribution from the ISO part is considerably smaller than the (1.n.n) contribution; this can be ascribed to the similarity of the anion and cation in the RbCl crystal. In general, for crystals composed of less dissimilar ions, the ISO contribution is less important.

3.4 Effects of non-additive three body interaction on polymorphic transition in alkali halides

The results of the previous sections will now be applied to the polymorphic transitions in alkali halides for which the TBI has been calculated. The total static lattice energy, including the TBI interaction, can be written as a function of the first nearest neighbour distance R. The short range ion pair potential for all M^+X^-, M^+M^+, X^-X^- ion pairs in alkali halides MX are represented by paramerized original GK potential recalculated by Boyer [29]. The total TBI as a function of R can be taken from our numerical results as listed in table 3.6. We write the total static lattice energy E(R) as

$$E_{B1}(R) = W_{B1}(R) + V_3^{total}(R) \tag{3.15}$$

for the B1 structure and

$$E_{B2}(R') = W_{B2}(R') + V_3^{total}(R') \tag{3.16}$$

for the B2 structure. Here W_{B1} and W_{B2} are pair static lattice energies for the B1 and B2 structures respectively. They can be written as

$$W_{B1}(R) = -1.7476/R + 6V_S(R)_{M^+X^-} + 6V_S(\sqrt{2}R)_{M^+M^+} + 6V_S(\sqrt{2}R)_{X^-X^-} \tag{3.17}$$

and

$$W_{B2}(R') = -1.7627/R' + 8V_S(R')_{M^+X^-} + 3V_S(2R'/\sqrt{3})_{M^+M^+} + 3V_S(2R'/\sqrt{3})_{X^-X^-} + 6V_S(2\sqrt{2}R'/\sqrt{3})_{M^+M^+} + 6V_S(2\sqrt{2}R'/\sqrt{3})_{X^-X^-} \tag{3.18}$$

where the short range pair interaction for the B1 and B2 structure are summed

up to second and third nearest neighbour respectively. The Gibbs free energies of the two phases are

$$G_{B1}(R) = E_{B1}(R) + 2R^3P \tag{3.19}$$

and

$$G_{B2}(R') = E_{B2}(R') + \frac{8}{3\sqrt{3}}R'^3P \tag{3.20}$$

where P is the externally applied pressure. The phase transition is marked by eq. (1.5).

The equilibrium lattice constants and lattice energies are determined by minimizing the lattice energy expression with respect to the nearest neighbour distance. The B1 to B2 transition pressure and relative volume changes at transitions are calculated from eq. (3.19), (3.20) and (1.5). The results are listed in table 3.7, 3.8 and 3.9. In these tables we list three sets of results and the corresponding experimental data. The results denoted by PC1 are based on pair potential approximation, i.e. used eq. (3.17) and (3.18) as the static lattice energy expression. The results PC3 are obtained by using eq. (3.15) and (3.16) as static lattice energy expression, i.e. incorporating the total TBI energy. The results PC2 incorporate the TBI energy only partially, i.e. it only includes the 1.n.n. contribution for the B1 and B2 structures respectively. Table 3.10 gives the calculated TBI energies at the predicted equilibrium distance for the B1 and B2 structures and for different crystals.

1) From the results shown in the tables 3.7-3.8, one can see that incorporating TBI gives a modest improvement for the equilibrium properties and a correct prediction of relative stability of the B1 and B2 phase for all the crystals of present interest. The PC1 results show that the GK model in terms of PPA generally over-estimates the lattice energy of the B1 phase by about 10% and the predicted equilibrium lattice constant is too

small. The non-additive three body interaction provides a supplement of repulsive forces, which leads to an increase of the equilibrium lattice constant and a decrease of the lattice energy of the B1 structure. This brings the theoretical values closer to the experimental ones. The errors in lattice energy has been reduced to less than 4%. This minor error may be attributed to the GK model itself. In the GK model the correlation energy contribution does not contain the long range vander Waals dispersion force, so that dispersion effects have not been accounted for in our calculations, which also neglected the zero-point energy, as shown by Boyer [29] these have only minor effects.

In the description of the relative stabilities of the B1 and B2 structures the TBI plays a very important role. As mentioned before, that based on pair potential approximation, the GK model predicts wrong structures for all iodide compounds and for RbBr. (see table 3.8, PC1 result). In table 3.8 positive value of ΔW_1 means that the B1 structure is more stable. Among the calculated nine crystals PC1 results gave four negative values of ΔW_1. The PC3 result gave all positive values of ΔW_1. It predicts correct structure for all nine calculated crystals. This is because even though the value of TBI itself is rather small compared with the lattice energy, it is structure sensitive and it gives relatively large repulsive force to the B2 structure, thus increases the differences of lattice energy between the two phases and makes the B1 structure more table.

2) The GK model based on PPA predicts the transition pressures which are too low for all chemical compounds, as shown in table 3.9, PC1 results. By incorporating TBI the PC3 result corrects this systematic descrepancy, increases the predicted transition pressure for all crystals of interest. The PC3 result brings theoretical value of transition pressure much closer to experimental ones for NaCl, NaBr, NaI, KI and RbI, which are composed of ions dissimilar in size. For these crystals, including ISO and REM, contributions to TBI are important. While the PC3 result over-estimates the relative stability of the B1 structure for KCl, KBr, RbCl and RbBr, hence leads to a theoretical transition pressure which is too high. For these

crystals the effects of TBI are dominated by 1.n.n. constributions. This can be seen from a comparison of PC2 and PC3 results that the predicted transition pressures have less differences in the two cases. For these crystals the rather small energy difference between the two phases generally leads to uncertainties in the prediction of theoretical transition pressure. Similar results can be found from the modified electron gas theory [27], Löwdin's approach [8] and also from Born-Mayer semi-empirical calculations [3]. An exception is the detailed semi-empirical work of Tosi and Fumi [5], where high pressure parameters were used and which showed good agreement with the experiments. We have also calculated the relative volume changes at the theoretical transition pressure, as shown in table 3.9. The significant improvement has also been achieved by incorporating TBI for NaCl, NaBr, NaI, KI and RbI (see PC3 result).

In this chapter we have shown that the original GK model can be improved by consideration of non-additive three body interactions, which give a more complete description of the overlap of charge density distributions and leads to theoretical results closer to the experiment for the cohesive and structural properties in alkali halides. The remaining descrepancies between theory and experiment may be attributed to the GK model itself and our simplified treatment in which the long range vander Waals energy, zero point energy and the long range three body forces were neglected. We also did not take account of the effect of changes of ionic charge densities from that of free ions.

CHAPTER IV - MICROSCOPIC MECHANISM OF THE B1 TO B2 TRANSITION IN ALKALI HALIDES

4.1 Introduction

As discussed in previous chapters, many theoretical attempts have been made to understand the polymorphic transition in alkali halides. However these calculations are restricted to establishing which phase has the lower free energy and hence is themodynamically stable under a given set of conditions. Thus these calculations cannot tell us the detailed microscopic mechanism of the B1 to B2 transition. Experimental and theoretical progress has been made in this direction only recently.

Two models of the transition mechanism were reported. One of them is Buerger's model [35]. Buerger conjectured that the change of the B1 to B2 structure can be achieved by the contraction along the [111] axis of the B1 structure and by the expansion at right angles with this axis. Buerger's model implies the orientation relation of B1 [111] // B2 [111] during the transition, which has not so far been observed by experiment. The other model has recently been proposed by Blaschko et al. [41]. This model is based on their neutron scattering studies of the B1 to B2 transformation in RbI. They found a strong orientation relation between the two phases, i.e. B1 [100] // B2 [011], during the transiton and observed occurence of phonon frequency anomalies for transverse accoustic phonons mainly for the TA [ζ00] branch. They described the B1 to B2 transition as a re-arrangement of ions in (100) planes of B1 structure followed by shifting ions in alternate (100) planes by a vector of [0,½, ½] in the B1 structure. This mechanism is essentially the same as that earlier proposed by Watanabe et al. [37], for the thermal transition of CsCl from the B2 to B1 structure. Watanabe described the combination of intralayer re-arrangement and interlayer transition of ions in a continuous way.

Theoretical prediction of the microscopic mechanism of the transition has not been found until a new MD method is proposed by Parrinello and Rahman [42]. In the new MD method a Lagrangian formulation is introduced which allows the shape and size of the MD cell to change according to the dynamical

equations which follow from this new Lagrangian. It has been proved that this new MD technique is well suited to the study of structural transformations in solids under external stress and at finite temperature [93, 94] . It should be remarked here that the traditional MD technique for solids has been confined to perfect and prefixed crystalline arrangement of the constituents. This has severely restricted the applicability of the method to problems involving crystal structure transformations. In order to overcome this difficulty Anderson [95] has presented a method allowing for changes in the volume of the MD cell but not the shape. Thus crystal structure transformations are still inhibited in Anderson's method.

Parrinello and Rahman have applied their new MD method to the study of the B1 to B2 transition in KC1 [43]; they showed that this transition is a first order and reversible, occuring at pressure of 44 Kbar and temperature of 925°K with a rapid density change from 2.6g.cm^{-3} to 2.85g.cm^{-3}. The calculation was described in detail to show the dynamical history of the occurrence of a B1 to B2 transition. Fig. 4.1 shows the B1 to B2 transition is accomplished by the following two operations:

Operation #1: Uniform dilatation of amount $\sqrt{2}$ in the direction of $\vec{a}$ as indicated by the thick arrow in Fig. 4.1.A. The result is shown in Fig. 4.1.B, $\vec{a}$, $\vec{b}$, $\vec{c}$ become $\vec{a}'$, $\vec{b}$, $\vec{c}$.

Operation #2: A move of ions in alternative planes in the $\vec{c}$ direction as indicated by the fine arrows in Fig. 4.1.B; the result is shown in Fig. 4.1.C; the centre of the square face formed by $\vec{a}$, $\vec{c}$ is now occupied by ● . An atom of the same type occupies the opposite square face, it is the shadowed circle in Fig. 4.1.C which shows a simple cubic lattice of like ions, the like and unlike ions together forming a B2 structure.

The work of Parrinello and Rahman describes the path in the configuration space that the system follows in going from one phase to the other. The mechanism of the B1 to B2 transition can be described as an uniaxial [011] deformation of the B1 structure plus a softening of a transverse accoustic [100] phonon mode. However the pressure and temperature needed to accomplish

the transformation on the computer simulation were much larger than those experimentally observed one and in disagreement with the predictions made by Boyer [29] on the basis of a harmonic free energy calculation that used the same Gordon-Kim potential. This leads us to believe that a complete description of the transitions requires not only an accurate evaluation of the free energy difference between two phases but also a reasonable estimate of the energy barriers that hinder the transition.

This is the first theoretical prediction for the microscopic mechanism of the B1 to B2 transition in alkali halides. We noticed that for KCl experimental evidence is not available. It is also of interest to note that the microscopic mechanism proposed by Parrinello and Rahman coincides with that proposed by Blaschko et al. [41] for RbI transforming from the B1 to B2 structure. In their experimental studies, Blaschko et al. have also found the transition starts in regions of high dislocation densities and depends on the previous thermal and mechanical treatments of the sample. This implies an actual transition pressure different from the thermodynamic equilibrium point.

The work of Parrinello and Rahman stimulated our present study. In this chapter we shall try to achieve the uniaxial deformation by a convenient uniaxial tensile load and investigate the effect of the load on the crystal stability. We shall also estimate the lattice energy barriers between the B1 and B2 phases. The result shows that the energy barriers depend on the value of hydrostatic pressure, which somewhat explains that a higher pressure is needed in the computer simulation to make the transition possible on the very short time scale (10^{-12} sec.) of their computer experiments.

4.2 Potassium chloride crystal under uniaxial tensile loading

As discussed in section 4.1, a microscopic mechanism of KCl transforming from the B1 to B2 structure has recently been presented by Parrinello and Rahman [43]. The process of the transformation consists of two steps. During the first step the B1(f c c) lattice is subject to two types of shear deformation* : a) A C_{44} type shear deformation in the (100) plane described by an increasing of $\cos\varphi$ from zero; and b) A $C_{11}-C_{12}$ type shear deformation in (010) and (001) planes described by $\eta_1 < 1$ and $\eta_2 > 1$ from $\eta_1 = \eta_2 = 1$, as shown in Fig. 4.2. Modifying its configuration continuously, the distorted system finally reaches a deformed face central tetragonal (f.c.t) lattice (see Appendix A) characterized by parameters $\eta_2 = 1.2247\,\eta_1$, $\cos\varphi = 0.3333$, i.e. $\varphi = 70.53°$. The second step was completed by collective ion jumps, i.e. ions of alternate planes in the [100] direction collectively jump along the [0, -1, 1] direction. Note that the discontinuous way of ion movements may mean that at the end of the first step the system reaches an unstable point. As pointed out by Parrinello and Rahman, this instability would be characterized by the softening of a transverse accoustic, [1.0.0] , zone boundary phonon with polarization vector in the [0, -1, 1] direction.

In this section we shall try to achieve the deformation by a convenient uniaxial load. We start from the B1 equilibrium configuration and apply an uniaxial tensile load along [0, 1, 1] direction to the KCl crystal to see how the system modifies its configuration to reach an unstable point. In addition we apply an isotropic pressure to investigate the effects of the pressure on the height of the energy barrier and on the stability of the crystal. First, we shall neglect the zero point motion and the harmonic vibrations. In the next section this study will then be extended to include the zero point motions.

(A) Formulation

Our study is based on the Gibbs free energy calculation for KCl crystal under a generally applied stress, i.e. a combination of hydrostatic pressure

---

* A detailed description of distorted fcc lattice is given in Appendix A.

and uniaxial tensile load. In writing static lattice energy the short range ionic interactions are represented by parametrized GK potentials [29], and the three body interactions are neglected. The Gibbs free energy per unit cell can be written as

$$G = W_l + V_{el} \tag{4.1}$$

where W_l and V_{el} are the lattice energy and the elastic energy per unit cell respectively.

When a general external stress is applied, the lattice energy, elastic energy and hence the Gibbs free energy will be functions of the configurational parameters $\{\lambda_1, \lambda_2$ and $\cos\varphi\}$; the latter two terms are also functions of the external stress. Let us apply an uniaxial stress S along the [0, 1, 1] direction in addition to a hydrostatic pressure P. We assume that a perfect B1 structure with lattice constant a = 5.99Å and configurational parameter $\lambda_1 = \lambda_2 = 1$, $\cos\varphi = 0$ is distorted to a deformed tetragonal lattice of configurational parameters $\{\lambda_1, \lambda_2, \cos\varphi\}$. Thus the lattice energy per unit cell can be written as follows

$$W(\lambda_1, \lambda_2, \cos\varphi; a) = V_s(\lambda_1, \lambda_2, \cos\varphi; a) - \frac{\alpha(\lambda_1, \lambda_2, \cos\varphi)}{a} \tag{4.2}$$

where V_s is the short range part of the lattice energy and is given by

$$\begin{aligned} V_s(\lambda_1, \lambda_2, \cos\varphi; a) = {} & 2V_s(\lambda_1 a/2)_{MX} + 4V_s(\lambda_2 a/2)_{MX} + V_s(\lambda_2 a \cos\tfrac{\varphi}{2})_{MM} \\ & + V_s(\lambda_2 a \sin\tfrac{\varphi}{2})_{MM} + 4V_s(\tfrac{1}{2}\sqrt{\lambda_1^2 + \lambda_2^2}\, a)_{MM} \\ & + V_s(\lambda_2 a \cos\tfrac{\varphi}{2})_{XX} + V_s(\lambda_2 a \sin\tfrac{\varphi}{2})_{XX} \\ & + 4V_s(\tfrac{1}{2}\sqrt{\lambda_1^2 + \lambda_2^2}\, a)_{XX} \end{aligned} \tag{4.3}$$

The second term on the r.h.s. of eq. (4.2) is the Madlung energy per unit cell; the $\alpha(\lambda_1, \lambda_2, \cos\varphi)$ is Madlung constant for the lattice of configuration $\{\lambda_1, \lambda_2, \cos\varphi\}$ with respect to a. We use the Ewald method [64] to express α as follows

$$\begin{aligned}\alpha(\lambda_1,\lambda_2,\cos\varphi) &= 2\left(\frac{\eta}{\pi}\right)^{\frac{1}{2}} \\ &+ \sum_{l_1 l_2 l_3} (-1)^{l_1+l_2+l_3} R(l_1,l_2,l_3)^{-1} F(\eta^{\frac{1}{2}} R(l_1,l_2,l_3)) \\ &- \frac{8}{\lambda_1 \pi \sin\varphi} \sum_{m_1,m_2,m_3}{}' G(m_1,m_2,m_3)^{-1} \exp\left(-\frac{\pi^2}{\lambda_3^2 \eta} G(m_1,m_2,m_3)\right)\end{aligned} \qquad (4.4)_1$$

where

$$G(m_1,m_2,m_3) = \left(\frac{\lambda_2}{\lambda_1}\right)^2 (-m_1+m_2+m_3)^2 + \frac{m_1^2}{\cos^2\frac{1}{2}\varphi} + \frac{(-m_2+m_3)^2}{\sin^2\frac{\varphi}{2}} \qquad (4.4)_2$$

$$R(l_1,l_2,l_3) = \frac{1}{2}\left(l_1^2\lambda_1^2 + \lambda_2^2(l_2^2+l_3^2+2l_2l_3\cos\varphi)\right)^{\frac{1}{2}} \qquad (4.4)_3$$

and

$$F(x) = \frac{2}{\sqrt{\pi}} \int_x^\infty \exp(-s^2)\,ds \qquad (4.4)_4$$

is the complementary error function. Here η is a dimensionaless parameter, whose value can be chosen so as to ensure rapid convergence of both real and reciprocal space sums. The prime in the sum of m_1, m_2 and m_3 indicates that the sum runs over those integers where $m_1 + m_2 + m_3$ = odd integers, as appropriate to our structure which is derived from an fcc lattice. The sum over l_1, l_2, l_3 run over all integers with the exception that l_1, l_2, l_3 simultaneously take zero values.

When a general stress is applied, the elastic energy V_{el} in eq. (4.1) can be written in the following form, which is given by Parrinello and Rahman [93]

$$V_{el} = P(\Omega - \Omega_0) + \Omega_0 Tr(S - P)\epsilon \tag{4.5}$$

where S is the external stress and P the hydrostatic pressure; ϵ is the strain tensor with respect to a reference configuration. Ω_0 and Ω are the volume of unit cell of reference and distorted configuration respectively. It is convenient to take the equilibrium configuration under the hydrostatic pressure as a reference state, which is an fcc lattice with a shorter lattice constant a. Note that Eq. (4.5) reduces to

$$V_{el} = P(\Omega - \Omega_0) \tag{4.6}$$

when $S_{ij} = +P\delta_{ij}$ is a pure hydrostatic pressure. Eq. (4.6) differs only by an immaterial constant with the usual P term appropriate to the hydrostatic case. When an uniaxial load is applied, crystal is forced to be a deformed fct lattice, with configuration parameters $\{\eta_1, \eta_2, \cos\varphi\}$. The elastic energy per unit cell V_{el} is thus given by

$$V_{el} = \Omega_0 (S(\cos^2\tfrac{\varphi}{2}\lambda_1^2 - 0.5) + P(\lambda_1\lambda_2^2 \sin\varphi - 1)) \tag{4.7}$$

where $\Omega_0 = \frac{1}{4} a^3$. The above equation can be obtained from eq. (4.5) by noticing that the strain tensor is written in terms of the deformations $\{\eta_1, \eta_2, \cos\varphi\}$ considered here:

$$\underline{\epsilon} = \begin{pmatrix} \frac{\lambda_1^2-1}{2} & 0 & 0 \\ 0 & \frac{\lambda_2^2-1}{2} & \lambda_3^2\left(\cos^2\frac{\varphi}{2}-\frac{1}{2}\right) \\ 0 & \lambda_3^2\left(\cos^2\frac{\varphi}{2}-\frac{1}{2}\right) & \frac{\lambda_2^2-1}{2} \end{pmatrix} \qquad (4.8)$$

While an external stress of intensity S in the [011] direction leads to a stress tensor of the form

$$\underline{S} = \begin{pmatrix} 0 & 0 & 0 \\ 0 & \frac{1}{2}S & \frac{1}{2}S \\ 0 & \frac{1}{2}S & \frac{1}{2}S \end{pmatrix} \qquad (4.9)$$

For a fixed external stress, we minimize the G in eq. (4.1) with respect to the configuration parameters $\{\pi_1, \pi_2, \cos\varphi\}$, we find the local minimum of G and the corresponding relative stable configuration $\{\bar{\pi}_1, \bar{\pi}_2, \overline{\cos\varphi}\}$ under the given stress. Substituting the configuration parameter $\{\bar{\pi}_1, \bar{\pi}_2, \overline{\cos\varphi}\}$ into the lattice energy expression (4.2) we got the corresponding lattice energy. Changing the external stress step by step and repeating the above procedures we can follow the evolution of the system.

In order to monitor the stability of each configuration generated, we set up a dynamical matrix which depends on the configuration parameter $\{\bar{\pi}_1, \bar{\pi}_2, \overline{\cos\varphi}\}$. The general expression for the dynamical matrix of an ionic crystal with pairwise short range forces is given by Maradudin et al.

[96] . Diagonalizing the dynamical matrix for a wave vector q, we got the phonon frequency for that $\vec{q}$. We use the rigid ion model [71] so that no empirical parameters are introduced. The main effect of non rigid-ion type behaviour on the lattice dynamics of alkali halides is known from other model calculations [97] to be mostly of quantitative relevance.

For the microscopic stability of the system the phonon frequencies ω_q must be real:

$$\omega_q^2 > 0 \qquad (q = 1, 2, \ldots\ldots, 6N) \tag{4.10}$$

In fact an imaginary frequency of vibrations implies the normal mode of vibrations which grow exponentially with time, thus leading to the disruption of the system.

(B) Numerical method and results

Obviously the minimization of eq. (4.1) relative to the parameters $\{\pi_1, \pi_2, \cos\varphi\}$ cannot be done analytically. Thus for a fixed value of S we calculated G on a suitable grid of points and looked for those parameters $\{\pi_1, \pi_2, \cos\varphi\}$ that minimize G. In order to minimize computer time we centre this grid of parameters around an estimated equilibrium configuration. This estimated $\{\pi_1, \pi_2, \cos\varphi\}$ is obtained by linear elasticity theory at low values of S and by appropriate extrapolations at larger stresses. The grid of values over which G is calculated is such that different values of π_1, π_2 and $\cos\varphi$ differ by 2×10^{-4}, 4×10^{-4} and 4×10^{-3} respectively. The stress is increased by steps of S = 2.94Kbar until an instability point at

which some ω_q^2 becomes negative is found. The maximum value of S for which the system is found to be stable is called S_{max}. This kind of calculation has been performed for P = 0, 12 and 44 Kbar.

The results are summarized in the following tables and figures. Table 4. (1), (2) and (3) give the configurations created by the uniaxial tensile loads for cases of hydrostatic pressure P = 0, 12 and 44 Kbar respectively. $\bar{\pi}_1$, $\bar{\pi}_2$ and $\overline{\cos\varphi}$ in these tables are configurational parameters which are measured relative to the equilibrium lattice constant at the relevant hydrostatic pressure. The equilibrium lattice parameters are found to be a = 5.99, 5.910, and 5.742 Å at the pressures of P = 0, 12 and 44 Kbar respectively. We also give the calculated corresponding lattice energy W_1, which is the sum of the Madlung energy E_{Mad} and the short range part energy V_s as defined in eq. (4.2).

Fig. 4.3 (A), (B) and (C) give the phonon dispersion curves along the [100], [011] and [111] directions for P = 0, 12 and 44 Kbar respectively. The solid lines are for the case of S = 0. Note that in the case of P = 0, i.e. in Fig. 4.3 (A), the solid lines give the phonon dispersion curves for KCl in the equilibrium B1 structure. The dashed lines in these Figs. give the phonon dispersion curves for the crystal under uniaxial tensile load, whose value is equal to S_{max}, and a hydrostatic pressure P, as indicated in each Figure. We add subscripts 1 and 2 to Ta and To to indicate the directions of the polarization vectors, subscript 1 denotes [0, -1, 1] direction and 2 [0, 1, 1] direction. Fig. 4.4 gives the variation of the frequency of Ta1 mode of [100] zone boundary phonon with uniaxial tensile load S for the cases of P = 0, 12 and 44 Kbar.

From the above numerical results we observe that:

1) The numerical results agree well with linear elastic theory at small stresses. This we have proved as follows.

We first calculated the elastic constants by the formulas [29]:

$$C_{11} = -1.2780\frac{e^2}{r_1^4} + \frac{1}{r_1}(V''_{HX} + V''_{HH} + V''_{XX} + \frac{1}{r_2}(V'_{HH} + V'_{XX})) \qquad (4.11)_1$$

$$C_{12} = 0.0565\,\frac{e^2}{r_1^4} + \frac{1}{r_1}\left(-\frac{1}{r_1}V'_{MX} + \frac{1}{2}\left(V''_{MM} + V''_{XX}\right) - \frac{5}{2r_2}\left(V'_{MM} + V'_{XX}\right)\right) \qquad (4.11)_2$$

$$C_{44} = 0.0390\,\frac{e^2}{r_1^4} + \frac{1}{r_1}\left(\frac{1}{r_1}V'_{MX} + \frac{1}{2}\left(V''_{MM} + V''_{XX}\right) + \frac{3}{2r_2}\left(V'_{MM} + V'_{XX}\right)\right) \qquad (4.11)_3$$

These equations can be obtained by comparing the long wave length limit of the dynamical matrix with corresponding results from the elastic theory [2]. In these expressions, the derivatives of the V_{MX} potential are evaluated at $r_1 = \frac{1}{2}a$ (a is the lattice constant of B1 structure) and the derivative of V_{MM} and V_{XX} at $r_2 = \frac{\sqrt{2}}{2}a$. Note that eq. (4.11) expresses the elastic constants as functions of the equilibrium lattice constant, which depends on the pressure. The results for the elastic constants are given in table 4.2 for the cases of P = 0, 12 and 44 Kbar.

Inserting then the values of C_{ij} thus obtained, we can make use of the lienar elasticity relation between the stress and strain

$$\underset{\sim}{\epsilon} = \underset{\approx}{C}^{-1}\,\underset{\sim}{S} \qquad (4.12)$$

where $\underset{\approx}{C}$ is the elastic constant matrix. In the present case of cubic symmetry and with our applied external stress of the type described in eq. (4.9), we find the following relations

$$\varepsilon_{yy} = \frac{1}{2}S/(C_{11} + C_{12} - 2C_{12}^2/C_{11}) \qquad (4.13)_1$$

$$\varepsilon_{xx} = -2C_{12}\,\varepsilon_{yy}/C_{11} \qquad (4.13)_2$$

and

$$\cos\varphi = \frac{1}{2}S/C_{44} \qquad (4.13)_3$$

To linear order the relation between our parameters and the usual definition of the strain becomes:

$$\bar{\varepsilon}_{yy} = \bar{\lambda}_2 - 1 \qquad (4.14)_1$$

and

$$\bar{\varepsilon}_{xx} = \bar{\lambda}_1 - 1 \qquad (4.14)_2$$

where values of $\bar{\lambda}_1$, $\bar{\lambda}_2$ and $\overline{\cos\varphi}$ can be found in table 4.1. Table 4.3 gives a comparison of the results calculated from eq. (4.13) with that from eq. (4.14). As can be seen that the agreement is rather good for S = 2.94 Kbar, but already at S = 5.88 Kbar nonlinearities become significant.

2) Comparing values of S in the last rows of tables 4.1(1) and 4.1(3), one can find that the higher hydrostatic pressure the less S_{max} system is needed to reach an unstable point. Fig. 4.5 shows the variation of lattice energy with the uniaxial tensile load. One can see that the hydrostatic pressure decreases the lattice energy barrier, which may be defined as the differences between the lattice energies in cases of S = 0 and S = S_{max}, i.e. the difference of lattice energy between the values given by the first and last rows in tables 4.1(1)-(3). We denote the energy barier by ΔW_1, as shown in table 4.4. We note that Parrinello and Rahman have observed the transition at pressure of 44 Kbar and temperature of 925°K. This temperature corresponds to an energy 1.88 Kcal/mole. If we take this as a very rough measure of the energy barrier we find that the energy scale of the barrier is reasonably well described by the theory developed here. The lowering of the energy barrier as a function of the pressure explain also why they had to go to 44 Kbar before observing the transition.

It is of interest to observe the phonon dispersion curves presented in Fig. 4.3(A)-(C). From the study of the effect of the uniaxial stress on the phonon dispersion curves we see that at P = 0 all the phonon frequencies are changed by the application of the stress. In particular, the [100] Ta branch is split by the reduction of the symmetry induced by the external stress into a Ta1 mode polarized in the [0, -1, 1] direction and a Ta2 mode polarized in the [0, 1, 1] direction. This Ta1 mode is lower in energy and is the

mode that eventually does go soft. However at P = 44 Kbar the phonon frequencies are only marginally changed by external stress with the exception of the [1 0 0] Ta mode, which is split and softened in its Ta1 component. This peculiar behaviour strengthens the conclusion of Parrinello and Rahman that in their MD experiment the B1 to B2 transition can be described as a combination of [0 1 1] uniaxial deformation of the B1 structure and a softening of [100] transverse accoustic phonon mode with polarization vector in [0, -1, 1] direction.

4.3 Including zero point motion

In this section we shall extend the results of the previous section to include the effects of zero point motion. The determination of the zero point energy of the crystal requires integration of periodic functions over the Brillouin Zone. The calculations are ususally very complicated and time consuming. To speed up calculations the recently developed Baldereschi point [98, 99] and many specail point scheme [100, 101] will be used. This reduces the integration over the B.Z. to a sum over a few points with an enormous gain in computational efficiency. However for the deformed fct lattice, special points are not available and will be calculated in the Appendix A.

(A) Effect of harmonic vibrations on the equilibrium lattice constants

In the case that the harmonic vibrations at finite temperature are included the Gibbs free energy expression in eq. (4.1) should be replaced by

$$G = F + V_{el} \tag{4.15}$$

where F is the Halmholz free energy and can be written in harmonic approximation:

$$F = W_1 + \frac{1}{2N}\sum_i h\nu_i + \frac{KT}{N}\sum_i \ln\{1-\exp(h\nu_i/KT)\} \tag{4.16}$$

where N is the number of the unit cell and the i summation runs over all phonon modes; the second and third terms on the r.h.s of eq. (4.16) are the zero point energy W_{zero} and the thermal vibration energy W_T respectively.

Using Baldereschi mean value point for fcc lattice eq. (4.16) can be approximately written as follows:

$$F = W_1 + \frac{1}{2}\sum_{r=1}^{6} h\nu_r(\vec{k}_0) + KT\sum_{r=1}^{6}\ln\{1-\exp(-h\nu_r(\vec{k}_0)/KT)\} \tag{4.17}$$

where $\vec{K}_\bullet$ is Baldereschi point [99], r sum ranges over the six branches of phonon mode of $\vec{K}_\bullet$.

If we know a set of many special points $\left\{ \vec{K}_i, \alpha_i ; i = 1, 2 \ldots . n \right\}$ the eq. (4.16) becomes

$$F = W_1 + \frac{\hbar}{2} \sum_{r=1}^{6} \sum_{i=1}^{n} \alpha_i \nu_r(\vec{K}_i) + KT \sum_{r=1}^{6} \sum_{i=1}^{n} \alpha_i \ln\left\{1 - \exp\left(\frac{-h\nu_r(\vec{K}_i)}{KT}\right)\right\} \qquad (4.18)$$

The Halmholz free energy F in eq. (4.17) and (4.18) is a function of the lattice constant a, configuration parameter $\left\{ \lambda_1, \lambda_2 \text{ and } \cos\varphi \right\}$ and temperature T as well. For a perfect fcc lattice it is a function of a and T only. Minimizing eq. (4.17) or (4.18) with respect to the lattice constant a, we got the equilibrium lattice constant at temperature T. The results are summarized in table 4.5 at T = 0,300°, 500° and 800° K. For comparison the last row of the table gives the results of Boyer [29], who used a brute force method for the numerical integration over the B.Z. with a mesh of $\sim$1000 points.

It is of interest to note that at T = 0 the net effect of zero point motion is to increase the equilibrium lattice constant value from 5.990 to 6.017 Å. Table 4.6 also gives detailed comparison between various schemes for the different energy terms entering in the eq. (4.17) and (4.18). It is shown that if we are interested only in the properties of perfect crystal configuration, it is often sufficient to use a single Baldereschi point. The accuracy in the prediction of the lattice constant is of 0.02%. We have also calculated the effect of the harmonic vibration on the transition pressure at T = 0 and T = 300°K. The transition pressure is found to depend only slightly on T and is 11.8 at T = 0 and 12.2 Kbar at T = 300°K, in good agreement with Boyer's calculation. Note also that at T = 0 the static calculation of section 3.4 gives P_c = 11.5 Kbar, only slight different from the value P_c = 11.8 Kbar obtained with the inclusion of quantum effects due to the zero point motion vibration.

(B) Effects of zero point motion

In order to include the effect of zero point motion and thermal vibration on the energy barrier calculation presented in section 4.2, it is useful to extend the special point scheme to the case of a deformed fct lattice. This we have done for the first time here and the results are presented in Appendix A. At T = 0 there are no thermal vibrations and the only modification to the scheme described above in section 4.2 is the addition to the calculation of the energy of zero point motion

$$W_{zero} = \frac{1}{2} \sum_{\substack{i \\ B.Z}} h\nu_i \qquad (4.19)$$

where the integration over the B.Z. is approximated by a sum over the 8 special points described in the eq. (A.25) of Appendix A. The convergency of the scheme has been checked in a few cases comparing the results obtained with 8 special points with those obtained with 32 and 128 points (which are given in eqs. (A.26) and (A.27) of Appendix A respectively). It is shown that the use of 8 special points is sufficient for the present purpose. Note that the symmetry lowering induced by the external stress increases the number of special points needed to achieve a satisfactory degree of accuracy.

The results are summarized in table 4.7. The results show that as was to be expected that the effect of zero point motion is rather small. It only slightly reduces the energy barrier from 5.5 to 4.5 Kcal/mole in the case of P = 0, from 0.68 to 0.64 Kcal/mole in case of P = 44 Kbar respectively.

We have tried to extend our study to include the effects of the thermal vibrations at finite temperatures. The convergency of using special points in evaluation of thermal vibration energy was checked by using 2, 8, 32 and 128 special points (see eqs.(A.24)-(A.27) of Appendix A) for some configurations, as shown in Table 4.8 for T = 300° and T = 925°K. From these tables one can see that using 8 or 32 special points can only ensure the accuracy in thermal vibration energy which is of order of 10^{-4} a.u. (while the accuracy in zero point energy is of the order of 10^{-6} a.u.) Thus the accuracy in Gibbs free

energy is also of the order of 10^{-4} a.u. The reduced accuracy in calculation of thermal vibration energy by the special point scheme can be ascribed to the exponential dependence of functions on phonon frequencies in B.Z. sum. This makes results more sensitive to the choice of the special points and requires the use of more special points. On the other hand we found that if thermal vibrations were included, the dependence of Gibbs free energy on configurational parameters is very flat near the equilibrium configuration. Thus, in order to ensure the accuracy in configurational parameter of equilibrium, say 0.0004 for η_1 and η_2, 0.004 for $\cos\varphi$, the accuracy in Gibbs free energy is required to be of $10^{-5} \sim 10^{-6}$ a.u. This can be seen from table 4.9. For this reason, the extension of our study to include thermal vibrations at finite temperature has not been completed. To do this would require a greater computational effort.

4.4 Effect of different choices of potential on energy barrier

For comparison we have also used the Tosi Fumi potential [19] to estimate the lattice energy barrier. Following the procedures described in section 4.2, we obtained the lattice energy barrier for P = 0 and P = 44 Kbar, which are 4.28 Kcal/mole and 1.59 Kcal/mole respectively. It is of interest to note that 1) the obtained values of lattice energy barriers are of the same order for two potentials; 2) the higher applied hydrostatic pressure decreases the height of the barriers; 3) for the case of P = 44 Kbar, the barrier evaluated from the Tosi Fumi potential, which is 1.59 Kcal/mole, is larger than that from GK potential, which is 0.684 Kcal/mole. This may be attributed to the fact that the predicted transition pressure by the Tosi Fumi potential is 64 Kbar, which is larger than 44 Kbar, as predicted by Gk potential.

Conclusions and discussions

In this thesis we have discussed the development of the theory of polymorphic transition in alkali halides, mainly concerning two aspects: prediction of the transition and microscopic mechanism of the transition. In particular, we have calculated the nonadditive three body interaction for some alkali halides and displayed its effects on the B1 to B2 transition. We have also studied the microscopic mechanism of the B1 to B2 transition proposed by Parrinello and Rahman [43] and the effects of uniaxial tensile load on the configurational deformation and of the microscopic instabilities of the crystal. In some of the calculations sums over the Brillouin Zone were needed. These were performed by means of an appropriate generalization of the Baldereschi point technique [99]. To our knowledge it is the first time that these special points have been evaluated and used for the deformed crystal structure of interest in the present context.

In our study of the polymorphic transition in alkali halides we have examined the GK potentials. We have shown that the pair potential approximation needed to be improved. We have tried to achieve this improvement by incorporating the nonadditive three body interaction (TBI). This gives a more complete description of the overlap of ionic charge densities and supplies more repulsive forces to the ionic interactions. The most significant effect of TBI is its structural sensitivity, which is expected to play an important role in problems of relative stability of crystal structure. We have noticed that the effects of TBI depend on the dissimilarity of the ions composing the crystal. No attempt has been made to improve the GK scheme, so our three body forces show all the defects of the original GK model. For instance, we have not allowed the charge densities to deform nor have we properly accounted for the vander Waals forces. These are of course a subject for further studies.

Recent progress in the study of the kinetics of the transition from the B1 to B2 structure have stimulated our interest in this direction. In fact in the study of kinetics of the transition there are still many open questions, such as the nature of the nucleation process, the role of the

defects on the transition and the temperature dependence of the hysteresis phenomenon etc. In their MD studies Parrinello and Rahman have described the B1 to B2 transition of KCl as an uniform uniaxial deformation of the B1 phase along the [011] direction plus a softening of the transverse [100], zone boundary phonon with polarization vector along [0, -1, 1] direction (Ta1 mode). In this thesis we have achieved this deformation by a convenient [011] uniaxial tensile load, and have shown that its main effect is the softening of the Ta1 mode as expected from the Parrinello and Rahman studies. By calculating the lattice energies of deformed crystal along the path in which crystal modifies its configurations, we calculated the energy barriers which hinder the transition. It is shown that appropriately applied hydrostatic pressure reduces the barrier. Our result has also agreed with that predicted by Parrinello and Rahman. Our study has quantitatively indicated that uniaxial stress, either externally applied or locally induced may create favourable deformation and thus trigger the transition.

In view of the above discussions we suggest some topics for further studies:

1) More refined theories for the calculation of many body forces that go beyond the simple GK scheme are needed. In particular the assumption of a rigid free-ion like charge density has to be abandoned as suggested by Andreoni et al. [32].

2) As to the kinetic of the transition it would be of interest to see the role played by the defects in nucleating the transition. Also the many body forces in the nucleation of the transition is a subject of interest.

ACKNOWLEDGEMENTS

The work presented in this thesis was carried out at the SCUOLA INTERNAZIONALE SUPERIORE DI STUDI AVANZATI (SISSA),Trieste, Italy, in the period November 1981 - July 1983, under the supervision of Prof. M. Parrinello, to whom I am deeply indebted for his earnest, tireless and helpful instructions and for his invaluable encouragement during the course of the work. I would like to emphasize that the work included in this thesis originated with him and was done in collaboration with him.

The help of Prof. R. Resta is much acknowledged for his several, enlightening discussions on lattice dynamics. I also thank Prof. E. Tosatti for his constant encouragement and helpful advices on my studies.

I am grateful to Prof. P. Budinich, L. Fonda for the fellowship grant and for their hospitality at SISSA.

I wish to thank Miss L. Bogo and Mrs. A. Mehan for their patient and energetic assistance in typing all the manuscript.

REFERENCES

(1) J.C. Slater, Phys. Rev. 23, 488 (1924).

(2) M. Born and K. Huang "Dynamical Theory of Crystal Lattice" (Oxford 1954).

(3) M.P. Tosi in "Solid State Physics", 16, 1 (1964).

(4) M.P. Tosi and T. Arai, in "Advances in High Pressure Research" Ed. by R.S. Bradicy, Vol. I (1966).

(5) M.P. Tosi and F.G. Fumi, Int.J. Phys. Chem.Sol. 23, 359 (1962).

(6) A. Hylleraas, Z. Phys., 63, 771 (1930).

(7) R. Landshoff, Z. Phys., 102, 120 (1936).

(8) P.O. Löwdin, Adv.Phys., 5, 1(1956).

(9) P. Hohenberg and W. Kohn, Phys. Rev., 136, B864 (1964).

(10) W. Kohn and L.J. Sham, Phys. Rev., 140, A1133 (1965).

(11) A. Zunger and M.L. Cohen, Phys.Rev. B18, 5449 (1979); D.R. Hamman M. Schlüter and C. Chiang, Phys. Rev.Lett. 43, 1494 (1979).

(12) J. Ihm and M.L. Cohen, Phys.Rev. B21, 1527 (1980); M.T. Yin and M.L. Cohen, Phys.Rev.Lett. 45, 1004 (1980); J. Ihm and J.D. Joannopoulos, Phys.Rev. B24, 4191 (1981); G.B. Bachelet, H.S. Greenside, G.A. Baraff and M. Schluter, ibid., 24, 4745 (1981).

(13) P.K. Lam and M.L. Cohen, Phys.Rev. B 24, 4224 (1981).

(14) W. Andreoni and K. Maschke, Phys.Rev. B 22, 4816 (1980).

(15) W. Andreoni, K. Maschke and M. Schlüter, Phys.Rev. B26, 2314 (1982).

(16) E. Madelung, Phys. Z. 11, 898 (1910).

(17) M. Born, Atomtheorie des festen Zustandes (Teubner, Leiprig and Berlin, 1923).

(18) M. Born and J.E. Mayer, Z. Phys. 75, 1 (1932).

(19) M.P. Tosi and F.G. Fumi, J.Phys.Chem.Solids 25, 45 (1964).

(20) F.G. Fumi and M.P. Tosi, J.Phys.Chem.Solids 25, 31 (1964).

(21) R. Narayan and R. Ramasesshan, J.Phys.Chem.Solids 37, 395 (1976); R. Narayan and R. Ramasesshan, Phys.Rev. Lett. 42, 992 (1979).

(22) R. Eggenhoffner, F.G. Fumi and C.S.N. Murthy, J.Phys.Chem.Solids. 43, 583 (1982).

(23) R. Eggenhoffner, C.S.N. Murthy and F.G. Fumi, J.Phys.Chem.Solids 39, 1295 (1978).

(24) R.G. Gordon and Y.S. Kim, J.Chem.Phys. 56, 3122 (1972).

(25) Y.S. Kim and R.G. Gordon, J. Chem.Phys. 60, 4332 (1974).

(26) Y.S. Kim and R.G. Gordon, Phys.Rev. B9, 3548 (1974).

(27) A.J. Cohen and R.G. Gordon, Phys.Rev. B12, 3228 (1975).

(28) A.J. Cohen and R.G. Gordon, Phys.Rev. B14, 4593 (1976).

(29) L.L. Boyer, Phys.Rev. B23, 3673 (1981).

(30) For a review see, M.J. Clugston, Adv.Phys. 27, 893 (1978).

(31) J.N. Murrel, Rare Gas Solids (Edited by M.L. Klein and J.A. Venables), Vol. I, Chap. 3, Section 2. Academic Press, New York (1976).

(32) F. Gygi, K. Maschke and W. Andreoni, 3rd European Phys.Soc. (C.D.M.) Lausanne (1983).

(33) Y.S. Kim, Phys.Rev. A11, 796 (1975).

(34) H. Shoji, Z. Kristallogr, Kristallogeorn, Kristallchem, 77, 381 (1937).

(35) M.J. Buerger in "Phase Transformation in Solids" Edited by R. Smoluchowski, J.E. Mayer and W.A. Weyl (Wiley, New York, 1951).

(36) W.L. Fraser and S. W. Kennedy, Acta Crystallogr. Soc. A30, 13 (1951).

(37) M. Watanabe, M. Tokonami and N. Rimoto, Acta Crystallogr Sec. A33, 294 (1977).

(38) O. Blaschko et al., J.Phys. (Paris) 38, 407 (1977).

(39) O. Blaschko et al., Rev.Sci.Instrum. 45, 256 (1974).

(40) O. Blaschko et al., Phys. Rev. B11, 3960 (1975).

(41) O. Blaschko et al., Phys.Rev. B23, 3017 (1981).

(42) M. Parrinello and A. Rahman, Phys.Rev.Lett. 45, 1196 (1980).

(43) M. Parrinello and A. Rahman, J.De.Phys. C6, 511 (1981).

(44) Chen Chuan hong, SISSA Internal Report, 21/83/C.M., to appear in Solid State Commun., Vol. 48, No.3, pp 235-237 (1983).

(45) L.P. Bonckaerdt, R. Smoluchowski and E. Wigner, Phys.Rev. 50, 58 (1936).

(46) P.W. Bridgman, Pro.Amer.Acad.Arts.Sci. 76, 1(1945); Phys.Rev. 72, 533 (1947); Proc.Amer. Acad.Arts and Sci. 76, 55 (1948).

(47) M.H. Rice, R.G. McQueen and J.M. Walsh, Solid State Phys. 6, 1(1958).

(48) W.A. Bassett, T. Takahashi, H.K. Mao and J.S. Weaver, J.Appl.Phys. 39, 319 (1968).

(49) P.W. Bridgman, in "Phys.of High Pressure" Chap. VIII, G. Bell, London (1949); C.E. Weir and G.J. Piermarini, J.Res.Nat.Bur.Stand. 68a, 105 (1964); V.V. Evdokimova and L.F. Vereshchagin, Soviet Phys. J. E.T.P. 16, 855 (1963).

(50) J.N. Fritz, S.P. Marsh , W.J. Carter and R.G. McQueen, Natl.Bur.Stand. Publ.No. 326 (U.S. GPO, Washington, D.C., 1971), p.201, and ref.(48).

(51) A. Lacam and J. Peyronneau, Rev.Phys.Appl., 10, 293(1975).

(52) R.B. Jacobs, Phys.Rev. 54, 468 (1938).

(53) P.O. Löwdin, "A Theoretical Investigation into Some Properties of Ionic Crystals" Almquist, Uppsala, and Ref (8).

(54) R. Landshoff, Phys.Rev. 52, 246 (1937); L.P. Howland, Phys.Rev. 109, 1927 (1958); J. Yamashita, J.Phys.Soc.Jap. 7, 284 (1952); S.O. Lundqvist, Ark.Fys, 8, 177 (1954); A. Froman and P.O. Löwdin, J. Phys. Chem. Solids 23, 75 (1962); K. Mansikka and F. Bystrand, J.Phys.Chem. Solids 27, 1073 (1966); J.L. Culais and K. Mansikka, Ark.Fys. 34, 361 (1967); J. Uallin, G. Petersson, J.L. Culais and K. Mansikka, Ark.Fys., 34, 371(1967); ibid. 37, 267 (1968).

(55) E. Clementi and C. Roetti, Atomic Data and Nuclear Tables (Academic, New York, 1974).

(56) D. Pines, "Elementary Excitations in Solids", Chap. 3, Benjamin, New York (1963).

(57) W.J. Carr, Jr.R.A. Calrwell-Horsfall and A.E. Fein, Phys.Rev. 124, 747 (1961); W.J. Carr, Jr. R.A. Caldwell-Horsfall and A.A. Maradudin, Phys.Rev. 133, A376 (1964).

(58) D.W. Sidn , Phil.Mag. 2 , 761 (1957); P.T. Wedepohl, Proc.Phys.Soc. 92, 79 (1976); V.I. Gayduenko and V. Nikulin, Chem.Phys.Lett. 7, 360 (1970); A.A. Abrahamson, Phys.Rev. 178, 76 (1969).

(59) M. Waldman and R.G. Gordon, J.Chem.Phys. 71, 1340(1979).

(60) M. Waldman and R.G. Gordon, J.Chem.Phys. 71, 1325 (1979).

(61) P.K.L. Drude, The Theory of Optics (Longmans, London, 1933).

(62) W.P. Wang, R.G. Parr, D.R. Murphy and G.A. Henderson, Chem.Phys. Lett. 43, 409 (1976); K.A. Buechner, Adv.Chem.Phys. 14, 215 (1969); J.C. Slater and K.H. Johnson, Phys.Rev. B5, 844 (1972).

(63) C. Muhlhausen and R.G. Gordon, Phys.Rev.B23, 900 (1981); ibid B24, 2147 (1981).

(64) P.P. Ewald, Ann.Physik (4), 64, 253 (1921); C. Kittle, "An introduction to Solid State Physics", Appendix A,2nd edition, Wiley, Inc.(1956).

(65) R.E. Watson, Phys.Rev. 111, 1108 (1958).

(66) M.T. Yin and M.L. Cohen, Phys.Rev. B26, 3259 (1982); K. Kune and R.M. Martin, Phys.Rev.Lett. 48, 406(1982).

(67) M. Dixon and C.S.N. Murthy, Phys.Chem.Liq.12, 83 (1982).

(68) J.H. Hildebrand, Z.Phys. 67, 127 (1931).

(69) M.L. Huggins and J.E. Mayer, J.Chem.Phys. 1, 643 (1933).

(70) J.E. Mayer, J. Chem.Phys. 1, 270 (1933).

(71) E.W. Kellermann, Phil. Trans. R.SOc. A238, 513 (1940)

(72) see e.g. K.P. Thakur, Acta. Crystallogr. A31, 540 (1975).

(73) C.R.A. Catlow, K.M. Diller and M.J. Norgett, J.Phys.C10, 1395 (1977).

(74) J. Corish, B.M.C. Parker and P.W. Jacobs, Can.J.Chem. 54, 3839(1976).

(75) M.J.L. Sangster, U. Schroder and R.M. Atwood, J.Phys.C11, 1523 (1978). M.J.L. Sangster and R.M. Atwood, J.Phys. C11, 1541 (1978).

(76) R.J. Hardy, S. Bijanski and A.M. Karo, Phys.Rev. B13, 900 (1976);

R.J. Hardy and A.M. Karo, J.Phys.Chem.Solids 38, 335 (1977); ibid 38, 905 (1977).

(77) For a review, see H. Margenau and N.R. Kestner, Theory of Intermolecular Forces (Pergamon, New York, 1969).

(78) B.M. Axilrod and E. Teller, J.Chem.Phys. 11, 299 (1943).

(79) P. Rosen, J.Chem.Phys. 21, 1007 (1953); A. Shostak, ibid. 23, 1808 (1955); R.F.W. Bader, O.A. Novaro and V. Beltran-Lopez, Chem.Phys.Lett. 8, 568 (1971); W. Kolow and A. Les, ibid 14, 167 (1973).

(80) R.D. Present, J.Chem.Phys. 47, 1793 (1967).

(81) L. Jansen, Adv. Quantum Chem. 2, 119(1966).

(82) B.G. Dick, Jr. And A.W. Overhauser, Phys.Rev. 112, 90 (1958).

(83) For a review, see A.N. Basu, U. Roy and S. Sengupta, Phys.Stat.Sol. (a) 23, 11 (1974); Ref.(67).

(84) A.K. Sarker and S. Sengupta, Solid State Commun. 7, 135 (1969); D. Roy, A.N. Basu and S. Sengupta, Phys.Stat.Sol., 35, 3499 (1969); A.N. Basu ans S. Sengupta, J.Phys. C5, 1158 (1972); ibid., Phys.Rev. B8, 2932 (1973).

(85) G. Jaccuci, I.R. McDonald and R. Rahman, Phys.Rev. 13, 1581 (1976).

(86) L. Jansen and E. Lombardi, Chem.Phys.Lett., 1, 417(1967); E. Lombardi and L. Jansen, Phys.Rev. 167, 822 (1968); E. Lombardi, L. Jansen and R. Ritter, ibid. 185, 1150(1969); 185, 1158 (1969); E. Lombardi, R. Ritter and L. Jansen, Int.Quantum Chem. 7, 155 (1973).

(87) Ref.(77), pp. 171-174.

(88) C.S. Barrett and L. Meyer, J.Chem.Phys. 42, 107 (1965); H.W. Graben, R.D. Present and M.D. McCulloch, Phys.Rev. 144, 140 (1066); C.E.

Swenberg, Phys.Lett. A24, 163 (1967).

(89) See, e.g., D.R. Bates, K. Ledsham and A. Stewart, Philos.Trans. R.Soc. Lond. 246, 215 (1953).

(90) V.I. Krylov, Approximate Calculation of Integrals (McMillan, New York, 1962).

(91) Ref. (90), Eq. (7.3.6).

(92) Ref. (90), Appendices A and C.

(93) M. Parrinello and A. Rahman, J. Appl.Phys. 52, 7182 (1981).

(94) M. Parrinello and A. Rahman, J.Chem.Phys. 76, 2662 (1982).

(95) H.C. Andersen , J. Chem.Phys. 72, 2384 (1980).

(96) A.A. Maradudin, E.W. Montroll and G.H. Weiss,in "Theory of Lattice Dynamics in the Harmonic Approximation" edited by F. Seitz and D. Turnbuld (Academic New York).

(97) J.R. Hardy and A.M. karo, lattice Dynamics and Statics of Alkali Halide Crystals (Plenum, New York, 1979).

(98) A. Baldereschi, Bull.Am.Phys.Soc. 17, 237 (1972).

(99) A. Baldereschi, Phys.Rev. B7, 5212 (1973).

(100) D.J. Chadi and M.L. Cohen, Phys.Rev. B8, 5747 (1973).

(101) H.J. Monkhort and J.D. Pack, Phys.Rev. B13, 5188 (1975).

(102) P.J. Lin-Chung, Phys.Stat.Sol. (b), 85, 743 (1978).

APPENDICES

Appendix A. Distorted FCC lattice under uniaxial tensile load and its special points

I. Introduction

When a f.c.c. lattice is subjected by a uniaxial loading along (1,0,0) direction, it would become a face central tetragonal lattice (f.c.t. lattice). While if a uniaxial loading along (0,1,1) direction is applied, f.c.t. lattice would be further deformed so that two axes of the crystallgraphic unit cell will not cross at right angle. We call this lattice as deformed face centered tetragonal lattice (d.f.c.t. lattice). The determiantion of the total energy of the distorted and undistorted crystals requires integrations of periodic functions over the Brillouin zone. Such calculations are often complicated and time consuming. The recently developed techniques known as the "special point method" [99, 100] enables us to reduce the B.Z. sums to sums only over a few points and it is accurate enough to calculate the small energy difference between distorted and undistorted crystals.

In the special point method once a set of special points $\vec{K}_i$ each with a weighting factor α_i , i = 1,2,... n, is found, the integration of a periodic funcitons $f(\vec{k})$ over the B.Z.

$$I = \frac{\Omega}{(2\pi)^3} \int_{B.Z} f(\vec{K})\, d\vec{K} \tag{A.1}$$

can be approximately written as

$$I = \sum_{i=1}^{n} \alpha_i f(\vec{K}_i) \tag{A.2}$$

provided $\vec{k}_i$ satisfy

$$\sum_{i=1}^{n} \alpha_i A_m(\vec{K}_i) = 0 \quad \text{for } m = 1, 2, \ldots\ldots \qquad \text{(A.3)}$$

where

$$A_m(\vec{K}_i) = \sum_{|\vec{R}_m| = d_m} \exp(i\vec{K}_i \cdot \vec{R}_m), \quad m = 1, 2, \ldots\ldots \qquad \text{(A.4)}$$

dm is the mth nearest neighbour distance. Eq.(A.2) becomes an excellent approximation if Eq.(A.3) is satisfied for m covering a large number of neighbours.

The procedures of finding a set of special points can be found in Ref. (100). The many special points for some cubic and non cubic lattice have been presented [99,100,102]. We present here for the first time several sets of special points for the f.c.t. and d.f.t.c. lattices.

II. Special Points for f.t.c. Lattice

The crystallographic unit cell of f.c.t. lattice is a simple tetragonal (s.t.) spanned by three mutually perpendicular vectors $\vec{b}_1$, $\vec{b}_2$, $\vec{b}_3$ with $\vec{b}_1 \perp \vec{b}_2 \perp \vec{b}_3$ and $|\vec{b}_1| = n_1 a$, $|\vec{b}_2| = |\vec{b}_3| = n_2 a$, $n_1 \neq n_2$. In rectangular coordinate the basic vector for the direct and reciprocal lattice of s.c. lattice are given by

$$\vec{b}_1 = a(n_1, 0, 0), \quad \vec{b}_2 = a(0, n_2, 0), \quad \vec{b}_3 = a(0, 0, n_2) \qquad \text{(A.5)}$$

$$\vec{b}_1^* = \frac{2\pi}{a}\left(\frac{1}{n_1}, 0, 0\right), \quad \vec{b}_2^* = \frac{2\pi}{a}\left(0, \frac{1}{n_2}, 0\right), \quad \vec{b}_3^* = \frac{2\pi}{a}\left(0, 0, \frac{1}{n_2}\right) \qquad \text{(A.6)}$$

with $\vec{b}_i \cdot \vec{b}_j^* = 2\pi \delta_{ij}$.

In the rectangular coordinate systems the basis vectors for the direct and reciprocal f.c.t. lattices are as follows:

$$\vec{B}_1=\frac{a}{2}(0,\,n_2,\,n_2)\,,\ \vec{B}_2=\frac{a}{2}(n_1,0,n_2)\,,\ \vec{B}_3=\frac{a}{2}(n_1,n_2,0) \qquad (A.7)$$

$$\vec{B}_1^*=\frac{2\pi}{a}(-\frac{1}{n_1},\frac{1}{n_2},\frac{1}{n_2})\,,\ \vec{B}_2^*=\frac{2\pi}{a}(\frac{1}{n_1},-\frac{1}{n_2},\frac{1}{n_2}),\ \vec{B}_3^*=\frac{2\pi}{a}(\frac{1}{n_1},\frac{1}{n_2},-\frac{1}{n_3}) \qquad (A.8)$$

with $\vec{B}_i\cdot\vec{B}_j^*=2\pi\delta_{ij}$. However it is convenient to express the direct and reciprocal lattice vector of f.c.t. in terms of the basis vectors in s.t. This gives $\vec{R}_m=M_1\vec{B}_1+M_2\vec{B}_2+M\vec{B}_3=m_1\vec{b}_1+m_2\vec{b}_2+m_3\vec{b}_3\equiv[m_1,m_2,m_3]$ with m_1, m_2, m_3, any integers simultaneously or one is an integer and the other two are odd integers divided by two. A general point in the B.Z. is $\vec{K}=U\vec{B}_1^*+V\vec{B}_2^*+W\vec{B}_3^*=u\vec{b}_1^*+v\vec{b}_2^*+w\vec{b}_3^*=[u,v,w]$. $\vec{k}$ becomes a reciprocal lattice vector when u,v,w are simultaneously even integers or simultaneously odd integers.

. Notice that when f.c.c. lattice is deformes to a f.c.t. lattice, the lattice point group is reduced from O_h to D_{4h}, which transforms a point [x,y,z] in both direct and reciprocal space to $[\pm x,\pm y,\pm z]$, $[\pm x,\mp z,\pm y]$, $[\pm x,\mp y,\mp z]$, $[\pm x,\mp z,\mp y]$, $[\mp x,\pm y,\mp z]$, $[\mp x,\mp y,\pm z]$, $[\mp x,\mp z,\pm y]$, $[\mp x,\mp z,\mp y]$. We have the following expressions:

$$\vec{R}_m\equiv[m_1,m_2,m_3]=a(m_1n_1,\,m_2n_2,\,m_3n_2) \qquad (A.9)$$

$$\vec{K}_i\equiv[u,v,w]=\frac{2\pi}{a}(\frac{u}{n_1},\frac{v}{n_2},\frac{w}{n_2}) \qquad (A.10)$$

$$\vec{R}_m\cdot\vec{K}_i=2\pi(m_1u+m_2v+m_3w) \qquad (A.11)$$

For $\vec{K}_i=[u,v,w]$, the Eq. $Am(\vec{k}_i)=0$ corresponding to mth shell characterized by lattice vector $\vec{R}_m=[m_1,\,m_2,\,m_3]$ would take the following form:

$$\cos 2m_1 u\pi \left(\cos 2m_2 v\pi \cdot \cos 2m_3 w\pi + \cos 2m_2 w\pi \cdot \cos 2m_3 v\pi \right) = 0 \qquad \text{(A.12)}$$

Following the procedure of finding special points [100] , we present the following sets of points:

Set I: Starting from points $\vec{k}_1 = [\frac{1}{2},\frac{1}{2},\frac{1}{2}]$ and $k_2 = [\frac{1}{4},\frac{1}{4},\frac{1}{4}]$ we generate the following three points

$$\begin{aligned} \vec{K}_1 &= [\tfrac{1}{4},\tfrac{1}{4},\tfrac{1}{4}] \ , \quad \alpha_1 = \tfrac{1}{4} \\ \vec{K}_2 &= [\tfrac{3}{4},\tfrac{1}{4},\tfrac{3}{4}] \ , \quad \alpha_2 = \tfrac{1}{2} \\ \vec{K}_3 &= [\tfrac{3}{4},\tfrac{1}{4},\tfrac{1}{4}] \ , \quad \alpha_3 = \tfrac{1}{4} \end{aligned} \qquad \text{(A.13)}$$

These three points satisfy Eq. (A.3) for $\vec{R}_m$ up to $[2,0,0]$. $\vec{R}_m$ will include neighbours up to the 6th n.n.s. for the case $1 < \frac{n_2}{n_1} < \sqrt{2}$.

Set II: Adding a point $\vec{k}_3 = [\frac{1}{8},\frac{1}{8},\frac{1}{8}]$ to Set I, we generate the following twenty points:

$$\begin{aligned} &\vec{K}_1 = [\tfrac{3}{8},\tfrac{3}{8},\tfrac{3}{8}] \ , \ \vec{K}_2 = [\tfrac{1}{8},\tfrac{1}{8},\tfrac{1}{8}] \ , \ \vec{K}_3 = [\tfrac{3}{8},\tfrac{1}{8},\tfrac{1}{8}] \ , \\ &\vec{K}_4 = [\tfrac{1}{8},\tfrac{3}{8},\tfrac{3}{8}] \ , \ \vec{K}_5 = [\tfrac{7}{8},\tfrac{3}{8},\tfrac{3}{8}] \ , \ \vec{K}_6 = [\tfrac{5}{8},\tfrac{1}{8},\tfrac{1}{8}] \ , \\ &\vec{K}_7 = [\tfrac{7}{8},\tfrac{1}{8},\tfrac{1}{8}] \ , \ \vec{K}_8 = [\tfrac{5}{8},\tfrac{3}{8},\tfrac{3}{8}] \ , \ \vec{K}_9 = [\tfrac{7}{8},\tfrac{3}{8},\tfrac{7}{8}] \ , \\ &\vec{K}_{10} = [\tfrac{7}{8},\tfrac{1}{8},\tfrac{5}{8}] \ , \ \vec{K}_{11} = [\tfrac{5}{8},\tfrac{3}{8},\tfrac{5}{8}] \ , \ \vec{K}_{12} = [\tfrac{5}{8},\tfrac{3}{8},\tfrac{7}{8}] \ , \\ &\vec{K}_{13} = [\tfrac{7}{8},\tfrac{1}{8},\tfrac{3}{8}] \ , \ \vec{K}_{14} = [\tfrac{5}{8},\tfrac{3}{8},\tfrac{1}{8}] \ , \ \vec{K}_{15} = [\tfrac{7}{8},\tfrac{1}{8},\tfrac{7}{8}] \ , \\ &\vec{K}_{16} = [\tfrac{7}{8},\tfrac{3}{8},\tfrac{5}{8}] \ , \ \vec{K}_{17} = [\tfrac{5}{8},\tfrac{1}{8},\tfrac{7}{8}] \ , \ \vec{K}_{18} = [\tfrac{5}{8},\tfrac{1}{8},\tfrac{5}{8}] \ , \\ &\vec{K}_{19} = [\tfrac{1}{8},\tfrac{1}{8},\tfrac{3}{8}] \ , \ \vec{K}_{20} = [\tfrac{3}{8},\tfrac{1}{8},\tfrac{1}{8}] \ . \end{aligned} \qquad \text{(A.14)}$$

with the weighting factors $\alpha_i = \frac{1}{32}$ for i = 1,2,...,8 and $\alpha_i = \frac{1}{16}$ for i = 9,10,...,20. These twenty points satisfy Eq.(A.3) for $\vec{R}_m$ up to $\vec{R}_m = [4,0,0]$. $\vec{R}_m$ will include neighbours up to 37th n.n.s. for the case $1 < \frac{n_2}{n_1} < \sqrt{2}$. Returning to the cubic coordinate system the $\vec{K} = [K_1, K_2, K_3]$ should be understood as $\frac{2\pi}{a}\left(\frac{K_1}{n_1}, \frac{K_2}{n_2}, \frac{K_3}{n_2}\right)$.

Notice that if $n_1 = n_2$, f.c.t. lattice becomesf.c.c. lattice. The above two sets of special points in Eq.(A.13) and (A.14) will be reduced to be two special points and ten special points for f.c.c. lattice respectively. This can be seen by noticing that some of the points in Set I (or Set II) can be transformed into each other by adding a reciprocal lattice vector and applying a symmetry operation of group O_h. We regroup these points together and sum up their weighting factors to give a single special point of f.c.c. lattice with a correct weighting factor as presented in ref.(100).

For an even higher degree of accuracy, one can progressively include more points $\vec{K} = \frac{1}{8}[2^{-n}, 2^{-n}, 2^{-n}]$, n = 1,2,3,... to generate more new sets of points.

III. Special points for d.f.c.t. lattice

The crystallographic unit cell of a d.f.c.t. lattice is spanned by three vectors $\vec{c}_1$, $\vec{c}_2$, $\vec{c}_3$, with $\vec{c}_1 \perp \vec{c}_2$, $\vec{c}_1 \perp \vec{c}_3$ and $\vec{c}_2 \cdot \vec{c}_3 = |\vec{c}_2| \cdot |\vec{c}_3| \cos\varphi \neq 0$; and with $|\vec{c}_1| = n_1 a$, $|\vec{c}_2| = |\vec{c}_3| = n_2 a$, $n_1 \neq n_2$. We call a lattice having $\vec{c}_1$, $\vec{c}_2$, $\vec{c}_3$ as the basis vectors as a deformed simple cubic lattice (d.s.c. lattice). In rectangulas coordiante the basis vector for direct and reciprocal lattice of d.s.c. lattice are given by

$$\begin{aligned}
\vec{c}_1 &= (n_1 a, 0, 0) \\
\vec{c}_2 &= \left(0, n_2 a \tfrac{\sqrt{2}}{2}(\cos\tfrac{\varphi}{2} + \sin\tfrac{\varphi}{2}), n_2 a \tfrac{\sqrt{2}}{2}(\cos\tfrac{\varphi}{2} - \sin\tfrac{\varphi}{2})\right) \\
\vec{c}_3 &= \left(0, n_2 a \tfrac{\sqrt{2}}{2}(\cos\tfrac{\varphi}{2} - \sin\tfrac{\varphi}{2}), n_2 a \tfrac{\sqrt{2}}{2}(\cos\tfrac{\varphi}{2} + \sin\tfrac{\varphi}{2})\right)
\end{aligned} \qquad (A.15)$$

and

$$\vec{C}_1^* = \frac{2\pi}{a}\left(\frac{1}{n_1},\ 0,\ 0\right)$$
$$\vec{C}_2^* = \frac{2\pi\sqrt{2}}{a\,2\sin\varphi}\left(0,\ \frac{1}{n_2}\left(\cos\frac{\varphi}{2}+\sin\frac{\varphi}{2}\right),\ \frac{1}{n_2}\left(\sin\frac{\varphi}{2}-\cos\frac{\varphi}{2}\right)\right)$$
$$\vec{C}_3^* = \frac{2\pi\sqrt{2}}{a\,2\sin\varphi}\left(0,\ \frac{1}{n_3}\left(\sin\frac{\varphi}{2}-\cos\frac{\varphi}{2}\right),\ \frac{1}{n_3}\left(\cos\frac{\varphi}{2}+\sin\frac{\varphi}{2}\right)\right) \qquad \text{(A.16)}$$

with $\vec{C}_i \cdot \vec{C}_j^* = 2\pi \cdot \delta_{ij}$. In rectangular coordinate systems the basis vector for the direct and reciprocal lattice of d.c.t. lattive are given by

$$\vec{A}_1 = \frac{\sqrt{2}}{2} n_2 a \cos\frac{\varphi}{2}\,(0,\ 1,\ 1)$$
$$\vec{A}_2 = \frac{a}{2}\left(n_1,\ \frac{n_2}{\sqrt{2}}\left(\cos\frac{\varphi}{2}-\sin\frac{\varphi}{2}\right),\ \frac{n_2}{\sqrt{2}}\left(\cos\frac{\varphi}{2}+\sin\frac{\varphi}{2}\right)\right) \qquad \text{(A.17)}$$
$$\vec{A}_3 = \frac{a}{2}\left(n_1,\ \frac{n_3}{\sqrt{2}}\left(\cos\frac{\varphi}{2}+\sin\frac{\varphi}{2}\right),\ \frac{n_3}{\sqrt{2}}\left(\cos\frac{\varphi}{2}-\sin\frac{\varphi}{2}\right)\right)$$

and

$$\vec{A}_1^* = \frac{2\pi}{a}\left(-\frac{1}{n_1},\ \frac{\sqrt{2}}{2}\frac{1}{n_2\cos\frac{\varphi}{2}},\ \frac{\sqrt{2}}{2}\frac{1}{n_2\cos\frac{\varphi}{2}}\right)$$
$$\vec{A}_2^* = \frac{2\pi}{a}\left(\frac{1}{n_1},\ -\frac{\sqrt{2}}{2}\frac{1}{n_2\sin\frac{\varphi}{2}},\ \frac{\sqrt{2}}{2}\frac{1}{n_2\sin\frac{\varphi}{2}}\right) \qquad \text{(A.18)}$$
$$\vec{A}_3^* = \frac{2\pi}{a}\left(\frac{1}{n_1},\ \frac{\sqrt{2}}{2}\frac{1}{n_2\sin\frac{\varphi}{2}},\ -\frac{\sqrt{2}}{2}\frac{1}{n_2\sin\frac{\varphi}{2}}\right)$$

with $\vec{A}_i \cdot \vec{A}_j^* = 2\pi\,\delta_{ij}$. It is convenient to express the direct and reciprocal lattice vectors of the d.f.c.t. in terms od the basis vector of d.s.c. This gives $\vec{R}_m = M_1\vec{A}_1 + M_2\vec{A}_2 + M_3\vec{A}_3 = m_1\vec{C}_1 + m_2\vec{C}_2 + m_3\vec{C}_3 \equiv \{m_1, m_2, m_3\}$ with m_1, m_2, m_3 are simultaneously integers divided by two. A general point in the B.Z. is $\vec{K} = U\vec{A}_1^* + V\vec{A}_2^* + W\vec{A}_3^* = u\vec{C}_1^* + v\vec{C}_2^* + w\vec{C}_3^* \equiv \{u, v, w\}$ If u,v,w are simultaneously even or simultaneously odd integers then $\vec{k}$ is a reciprocal vector.

The lattice point group of d.f.c.t. is D_{2h} which transforms a point $\{x,y,z\}$ in both direct and reciprocal space to $\{\pm x, \pm y, \pm z\}$, $\{\pm x, \mp y, \mp z\}$, $\{\mp x, \pm z, \pm y\}$, $\{\mp x, \mp z, \mp y\}$. Notice that

$$\vec{R}_m \equiv \{m_1, m_2, m_3\}$$
$$= a\Big(m_1 n_1,\ \frac{\sqrt{2}}{2} n_2 (m_2+m_3)\cos\frac{\varphi}{2} + \frac{\sqrt{2}}{2} n_2 (m_2-m_3)\sin\frac{\varphi}{2},\ \qquad \text{(A.19)}$$
$$\frac{\sqrt{2}}{2} n_2 (m_2+m_3)\cos\frac{\varphi}{2} + \frac{\sqrt{2}}{2} n_2 (m_3-m_2)\sin\frac{\varphi}{2}\Big)$$

$$\vec{K}_i \equiv \{u, v, w\}$$
$$= \frac{2\pi}{a}\left(\frac{u}{n_1}, \frac{\sqrt{2}}{4}\left(\frac{v-w}{\sin\frac{\varphi}{2}} + \frac{v+w}{\cos\frac{\varphi}{2}}\right), \frac{\sqrt{2}}{4}\left(\frac{w-v}{\sin\frac{\varphi}{2}} + \frac{v+w}{\cos\frac{\varphi}{2}}\right)\right) \tag{A.20}$$

and $\vec{R}_m . \vec{K}_i$ takes the following simple form:

$$\vec{R}_m \cdot \vec{K}_i = 2\pi(m_1 u + m_2 v + m_3 w) \tag{A.21}$$

The Eq. $A_m(\vec{K}_i) = 0$ can be expressed as follows

$$\cos 2\pi m_1 u \cdot \left(\cos 2\pi(m_2 v + m_3 w) + \cos 2\pi(m_2 w + m_3 v)\right) = 0 \tag{A.22}$$

In the case of v = w Eq.(A.22) becomes

$$\cos 2\pi m_1 u \cdot \cos 2\pi(m_2 + m_3)\cdot v = 0 \tag{A.23}$$

Now we present two sets of special points for d.f.c.t. lattice as follows:

Set I: Starting from two points $\vec{K}_1 = \{\frac{1}{2}, \frac{1}{2}, \frac{1}{2}\}$ and $\vec{K}_2 = \{\frac{1}{4}, \frac{1}{4}, \frac{1}{4}\}$ we generate the following two points

$$\vec{K}_1 = \{\tfrac{1}{4}, \tfrac{1}{4}, \tfrac{1}{4}\} \quad , \quad \alpha_1 = \tfrac{1}{2}$$
$$\vec{K}_2 = \{\tfrac{3}{4}, \tfrac{1}{4}, \tfrac{1}{4}\} \quad , \quad \alpha_2 = \tfrac{1}{2} \tag{A.24}$$

The two points satisfy Eq.(A.3) for $\vec{R}_m$ up to $\vec{R}_m = \{0, \frac{1}{2}, \frac{3}{2}\}$, $\vec{R}_m$ will include neighbours up 5th n.n.s. for the case $1 < \frac{n_2}{n_1} < \sqrt{2}$ and $0 < \cos\varphi < \frac{1}{3}$.

Set II: Adding a new point $\vec{K}_3 = \{\frac{1}{8}, \frac{1}{8}, \frac{1}{8}\}$, we generate the following eight points:

$$\vec{K}_1=\{\tfrac{3}{8},\tfrac{3}{8},\tfrac{3}{8}\}\ ,\quad \vec{K}_2=\{\tfrac{1}{8},\tfrac{1}{8},\tfrac{3}{8}\}\ ,$$
$$\vec{K}_3=\{\tfrac{3}{8},\tfrac{1}{8},\tfrac{1}{8}\}\ ,\quad \vec{K}_4=\{\tfrac{1}{8},\tfrac{3}{8},\tfrac{3}{8}\}\ ,\qquad (A.25)$$
$$\vec{K}_5=\{\tfrac{7}{8},\tfrac{3}{8},\tfrac{3}{8}\}\ ,\quad \vec{K}_6=\{\tfrac{7}{8},\tfrac{1}{8},\tfrac{1}{8}\}\ ,$$
$$\vec{K}_7=\{\tfrac{5}{8},\tfrac{3}{8},\tfrac{3}{8}\}\ ,\quad \vec{K}_8=\{\tfrac{5}{8},\tfrac{1}{8},\tfrac{1}{8}\}\ .$$

with equal weighting factor $\alpha_i=\frac{1}{8}$, i = 1,2,...,8. These eight points satisfy Eq.(A.3) for $\vec{R}_m$ up to $\vec{R}_m=\{0,\frac{3}{2},\frac{5}{2}\}$, R_m will include neighbours up to 17th n.n.s. for the case $1<\frac{n_2}{n_1}<\sqrt{2}$ and $0<\cos\varphi<\frac{1}{3}$. Returning to the cubic coordinate system the $\vec{K}=\{K_1, K_2, K_3\}$ in Eq.(A.24) and Eq. (A.25) should be understood as $\frac{2\pi}{a}\left(\frac{K_1}{n_1},\frac{K_2 h}{n_2},\frac{K_3 h}{n_2}\right)$ with $h=\frac{1}{\sqrt{2}\cos\frac{\varphi}{2}}$ This can be done by substituting K_1, K_2, K_3 into Eq. (A.20) and noticing that in our cases $K_2 = K_3$. Notice that special points in Eq.(A.24) and Eq.(A.25) satisfy Eq. (A.3) for less neighbours because d.f.c.t. lattice has lower symmetry.

For an even higher degree of accuracy, one can progressively include more points $\vec{K}=\frac{1}{8}\{2^n,2^n,2^n\}$, n = 1,2,3,.... to generate more new sets of points. In the cases of n=1 and n=2 we generated the following two new sets of special points.

Set III: 32 special points with equal weighting factor $\alpha_i=\frac{1}{32}$, i = 1,2,...32. For the representation of those special points , a special point $\{\frac{x}{16},\frac{y}{16},\frac{z}{16}\}$ will be abbreviated to $\{x,y,z\}$. These 32 points are:

$$\{7,7,7\}\ ,\{5,5,5\}\ ,\{7,5,5\}\ ,\{5,7,7\}$$
$$\{3,3,3\}\ ,\{1,1,1\}\ ,\{3,1,1\}\ ,\{1,3,3\}$$
$$\{7,3,3\}\ ,\{5,1,1\}\ ,\{7,1,1\}\ ,\{5,3,3\}$$
$$\{3,7,7\}\ ,\{1,5,5\}\ ,\{3,5,5\}\ ,\{1,7,7\}$$
$$\{15,7,7\}\ ,\{13,5,5\}\ ,\{15,5,5\}\ ,\{13,7,7\} \qquad (A.26)$$

$\{11,3,3\}$, $\{9,1,1\}$, $\{11,1,1\}$, $\{9,3,3\}$
$\{15,3,3\}$, $\{13,1,1\}$, $\{15,1,1\}$, $\{13,3,3\}$
$\{11,7,7\}$, $\{9,5,5\}$, $\{11,5,5\}$, $\{9,7,7\}$ (A.26)

Set IV: 128 special points with equal weighting factor $\alpha_i = \frac{1}{128}$, $i = 1,2,\cdots,128$

Here a special point $\{\frac{x}{32}, \frac{y}{32}, \frac{z}{32}\}$ will be abbreviated to $\{x,y,z\}$

These 128 points are:

$\{15,15,15\}$, $\{13,13,13\}$, $\{15,13,13\}$, $\{13,15,15\}$
$\{11,11,11\}$, $\{9,9,9\}$, $\{11,9,9\}$, $\{9,11,11\}$
$\{15,11,11\}$, $\{13,9,9\}$, $\{15,9,9\}$, $\{13,11,11\}$
$\{11,15,15\}$, $\{9,13,13\}$, $\{11,13,13\}$, $\{9,15,15\}$
$\{7,7,7\}$, $\{5,5,5\}$, $\{5,7,7\}$, $\{7,5,5\}$
$\{3,3,3\}$, $\{1,1,1\}$, $\{3,1,1\}$, $\{1,3,3\}$
$\{7,3,3\}$, $\{5,1,1\}$, $\{7,1,1\}$, $\{5,3,3\}$
$\{3,7,7\}$, $\{1,5,5\}$, $\{3,5,5\}$, $\{1,7,7\}$
$\{15,7,7\}$, $\{13,5,5\}$, $\{13,7,7\}$, $\{15,5,5\}$
$\{11,3,3\}$, $\{9,1,1\}$, $\{11,1,1\}$, $\{9,3,3\}$ (A.27)
$\{15,3,3\}$, $\{13,1,1\}$, $\{15,1,1\}$, $\{13,3,3\}$
$\{11,7,7\}$, $\{9,5,5\}$, $\{11,5,5\}$, $\{9,7,7\}$
$\{7,15,15\}$, $\{5,13,13\}$, $\{7,13,13\}$, $\{5,15,15\}$
$\{3,11,11\}$, $\{1,9,9\}$, $\{1,11,11\}$, $\{3,9,9\}$
$\{7,11,11\}$, $\{5,9,9\}$, $\{5,11,11\}$, $\{7,9,9\}$
$\{3,15,15\}$, $\{1,13,13\}$, $\{3,13,13\}$, $\{1,15,15\}$
$\{31,15,15\}$, $\{29,13,13\}$, $\{31,13,13\}$, $\{29,15,15\}$
$\{27,11,11\}$, $\{25,9,9\}$, $\{27,9,9\}$, $\{25,11,11\}$
$\{31,11,11\}$, $\{29,9,9\}$, $\{31,9,9\}$, $\{29,11,11\}$
$\{27,15,15\}$, $\{25,13,13\}$, $\{27,13,13\}$, $\{25,15,15\}$
$\{23,7,7\}$, $\{21,5,5\}$, $\{23,5,5\}$, $\{21,7,7\}$

$$
\begin{array}{llll}
\{19,\ 3,\ 3\} & \{17,\ 1,\ 1\} & \{19,\ 1,\ 1\} & \{17,\ 3,\ 3\} \\
\{23,\ 3,\ 3\} & \{21,\ 1,\ 1\} & \{23,\ 1,\ 1\} & \{21,\ 3,\ 3\} \\
\{19,\ 7,\ 7\} & \{17,\ 5,\ 5\} & \{19,\ 5,\ 5\} & \{17,\ 7,\ 7\} \\
\{31,\ 7,\ 7\} & \{29,\ 5,\ 5\} & \{31,\ 5,\ 5\} & \{29,\ 7,\ 7\} \\
\{27,\ 3,\ 3\} & \{25,\ 1,\ 1\} & \{27,\ 1,\ 1\} & \{25,\ 3,\ 3\} \\
\{31,\ 3,\ 3\} & \{29,\ 1,\ 1\} & \{31,\ 1,\ 1\} & \{29,\ 3,\ 3\} \\
\{27,\ 7,\ 7\} & \{25,\ 5,\ 5\} & \{25,\ 7,\ 7\} & \{23,15,15\} \\
\{27,\ 5,\ 5\} & \{21,13,13\} & \{23,13,13\} & \{21,15,15\} \\
\{19,11,11\} & \{17,\ 9,\ 9\} & \{19,\ 9,\ 9\} & \{17,11,11\} \\
\{23,11,11\} & \{21,\ 9,\ 9\} & \{23,\ 9,\ 9\} & \{21,11,11\} \\
\{19,15,15\} & \{17,13,13\} & \{17,15,15\} & \{19,13,13\}
\end{array}
\qquad (A.27)
$$

TABLE CAPTIONS AND TABLES

Table Captions:

Table 2.1 Observed B1 to B2 transition pressures (in Kbar), lattice energy differences (in Kcal/mole) between B1 and B2 phases and relative volume changes at transition pressure of some alkali halides.

Table 2.2 Equilibrium properties of some alkali halide crystals in B1 phase and the B1 to B2 transition pressure in Löwdin's theory. Large errors of theoretical values for Li compounds may be due to inaccurate HF wave function used for Li^+ ion (Ref.(26)).

Table 2.3 Equilibrium nearest neighbour distance R and lattice energy D of LiF and NaF in the B1 phase, predicted by MEG theories (ref.(63)).

Table 2.4 Structure dependent constants entering the lattice energy; M and M' are number of the first and second neighbour respectively; a is the ration of the second neighbour and the first neighbour distances.

Table 2.5 The contribution of the second nearest neighbour interaction to lattice energy in terms of the original GK model in B1 phase for some alkali halides (energy in units of Kcal/mole).

Table 2.6 Equilibrium lattice constants, lattice energies of some alkali halides in the B1 phase and the B1 to B2 transition pressure for some alkali halides, calculated from various GK models. Experimental data are taken from Ref. (29); values in bracket are measured at temperature of 298°K, at 0°K otherwise.

Table 2.7 Comparison of the calculated and measured thermal-expansion

coefficients for zero pressure and room temperature (in units of $10^{-6}K^{-1}$). The calculation has been performed in Ref.(29) by using a parametrized version of the original GK model.

Table 2.8 Comparison of calculated and measured transition pressure (in units of Kbar). The calculation has been performed in Ref.(29) by using a parametrized version of the original GK model.

Table 3.1 Relevant configurations of triplet ions and their number per ion in the B1 structure.

Table 3.2 Relevant configurations of triplet ions and their number per ion in the B2 structure.

Table 3.3 Comparison of V_3(MXX; R,R,90°) and an exponential fit to its dependence on R. The units of energy are 10^{-3} a.u.

Table 3.4 The magnitude of TBI (in a.u.) at different triangular opening angles.

Table 3.5 Dependence of values of TBI on the type of ions for the geometry $R_{CA} = R_{CB} = R = 7.071$ a.u. and $\gamma = 90°$.

Table 3.6 Calculated nonadditive three body interactions per ion pair (in units of 10^{-2} a.u.) varying with nearest neighbour distance R (in a.u.)

Table 3.6(1) NaCl.

Table 3.6(2) NaBr.

Table 3.6(3) NaI.

Table 3.6(4) KCl.

Table 3.6(5) KBr.

Table 3.6(6) KI.

Table 3.6(7) RbCl.

Table 3.6(8) RbBr.

Table 3.6(9) RbI.

Table 3.7 The equilibrium lattice constant of B1 structure for some alkali halides (in units of $\mathring{A}$).

Table 3.8 The equilibrium lattice energy W_1 of B1 structure and lattice energy differences ΔW_1 between the B1 and B2 structure at zero temperature (in units of Kcal/mole).

Table 3.9 Critical pressure for the B1 to B2 structure transition (in units of Kbar) and relative volume changes at transition pressure in some alkali halides. Experimental data are taken from Ref.(29). The missing enties mean either that the wrong structure is predicted or that no experimental data exist.

Table 3.10 The calcualted total TBI energies and contributions from various parts to the total TBI at equilibrium predicted by PC3 for B1 and B2 structures of some alkali halides. (The column indicated by " % " gives the percentage of total TBI energy to the lattice energy of the corresponding structure).

Table 4.1 Configuration parameters and values of corresponding Madlung energy E_{Mad}, short range interaction energy V_s and the lattice energy W_1 (in units of Kcal/mole) for KCl under uniaxial tensile loads S (in units of Kbar) and hydrostatic pressure P = 0,12 and 44 Kbar.

Table 4.1(1) P = 0.

Table 4.1(2) P = 12 Kbar.

Table 4.1(3) P = 44 Kbar.

Table 4.2 The elastic constants C_{11}, C_{12} and C_{44} (in units of Kbar) for KCL in the B1 structure at pressure P = 0,12 and 44 Kbar. The experimental values are given in brackets (from Ref.(29)).

Table 4.3 Comparison of present results with linear elastic theory. A indicates the present results, values are obtained from eq.(4.14), where λ_1, λ_2 and $\cos\varphi$ are taken from tables 4.1(1)-(3); B gives the values obtained from eq.(4.13), where elastic cosntants are taken from table 4.2.

Table 4.4 The maximum allowed uniaxial stress S_{max} and lattice energy barrier ΔW_1 for varying hydrostatic pressure.

Table 4.5 The equilibrium lattice constant (in units of $\mathring{A}$) of KCl crystal in B1 phase at finite temperature, is calculated by using differnet special point schemes and compared with results obtained by a standard numerical integration over the B.Z.

Table 4.6 Calculated values of zero point energy W_{zero}, thermal vibration energy W_T and Helmholtz free energy F (in a.u.) of KCl crystal in B1 structure at equilibrium in different approximations to the B.Z. sum.

Table 4.7 Configuration parameters and values of corresponding zero point energy W_{zero}, thermal vibration energy W_T and Helmhotz free energy F (units of Kcal/mole) for KCl under uniaxial tensile load S (in units of Kbar) and hydrostatic pressure P = 0 and 44 Kbar.

Table 4.7(1) P = 0.

Table 4.7(2) P = 44 Kbar

Table 4.8 Test of convergency of use of special points for the evaluation of zero point energy W_{zero} and the thermal vibration energy W_T (in a.u.)

at temperature T = 300° K and T = 925° K. The corresponding Helmhotz free energy F and Gibbs free energy G are also given.

Table 4.8(1) P = 0 and T = 300°K.

Table 4.8(2) P = 0 and T = 925°K.

Table 4.9 Dependence of Gibbs free energy G (in a.u.) on configuration parameters π_1, π_2 and $\cos\varphi$ at finite temperature:

Table 4.9(1) P = 0., S = 8.82 Kbar and T = 300°K.

Table 4.9(2) P = 0., S = 2.92 Kbar and T = 925°K.

TABLES:

Table 2.1

	P_c (a)	ΔW_L (b)	V_{B1}/V_{O1} (a)	$\Delta V_{B2}/V_{O1}$ (a)	$\Delta V_t/V_{O1}$ (a)
KCl	20	2.2	0.085	0.197	0.112
KBr	19	2.0	0.088	0.193	0.105
KI	17.8	2.0	0.105	0.190	0.085
RbCl	5.5	0.9	0.030	0.170	0.140
RbBr	5.0	0.8	0.033	0.166	0.133
RbI	4.0	0.9	0.030	0.158	0.128
NaCl	300	7.2 (c)	0.357	0.394	0.037

(a) Ref 27. (b) Ref 4.

(c) Calculated from experimental transition pressure, $\Delta V_t/V_{O1}$ and equilibrium lattice parameter for NaCl.

Table 2.2

	lattice constant R(Å) Theor.	Expt[a]	cohesive energy W (Kcal/mole) Theor.	Expt	Bulk modulus B(10^{11}dyne/cm^2) Theor.	Expt	B1 to B2 transition Pressure P_t (Kbar) Theor.	Expt
LiF	4.4	4.028	199.5	246.8	2.5	7.2		
LiCl	5.38	5.140	187.7	198.9	2.38	5.17		
NaF	4.58	4.634	205.1	217.9	2.70	2.74		
NaCl	5.50	5.640	183.2	185.3	2.17	1.97	103	300
KCl	6.18	6.596	166.9	169.5	1.67	1.79	31.4	20

(a) Expt. data compiled by Kim and Gordon, Ref.(26).

Table 2.3

	LiF				NaF			
	MEG[a]	MG1[b]	MGSS[c]	expt	MEG	MG1	MGSS	expt
R(a.u)	4.03	4.071	3.854	3.806	4.61	4.638	4.490	4.378
D(a.u)	.3833	.3774	.3979	.3933	.3377	.3353	.3842	.3472

(a) Using MEG potentials in pair potential approximations.

(b) Using eq.(2-35) and (2-36) in caloulation of binding energy.

(c) As b , but using ss density.

Table 2.4

	M	M'	a	α_R	$S_1(6)$	$S_2(6)$	$S_1(8)$	$S_2(8)$
B1	6	12	2	1.74756	6.5952	1.8067	6.1457	0.8001
B2	8	6	$2/\sqrt{3}$	1.76267	8.7088	3.5446	8.1575	2.1977

Table 2.5

	NaCl	NaBr	NaI	KCl	KBr	KI	RbCl	RbBr	RbI
V_s(1.n.n)	24.8	24.3	26.8	17.5	18.6	20.0	16.1	15.8	16.7
V_s(2.n.n)	-7.21	-6.34	-13.5	-5.45	-7.01	-10.5	-4.61	-5.75	-8.52
V_s^{tot}	17.61	15.67	13.26	12.03	11.57	9.44	11.46	10.03	8.22
$\frac{V_s(2.n.n)}{V_s^{tot}}$ %	-40.9	40.5	-101	-45.3	-60.6	-89.9	-40.2	-57.3	-103

Table. 2.6

	lattice constant (Å)					lattice energy (Kcal/mole)				B1 to B2 transirion pressure(Kbar)				
	CK	CG	Present	CK(B)	Expt.	CK	CG	Present	Expt.	CK	CG	Present	CK(B)	Expt.
LiF	3.86	4.26	4.011	4.036	4.008	260.2	240.5	258.11	246.8	550	2900	>200	>200	>100
LiCl	4.94	5.20	4.900	4.938	5.106	206.1	202.0	215.71	201.8	160	980	162	>200	>100
LiBr	5.32	5.46	5.223	5.266	5.460	192.3	194.9	224.61	189.8	110	924	94	96	>100
LiI		5.80	5.535	5.545	5.946		186.4	195.16	177.7		184	-22	-27	>100
NaF	4.62	4.88	4.657	4.680	4.609	222.3	211.9	220.84	217.9	142	326	238	> 200	>200
NaCl	5.72	5.86	5.604	5.628	5.597	182.7	179.9	189.49	185.3	49	107	46	46	300
NaBr	6.08	6.10	5.958	5.985	5.939	172.6	173.8	179.11	174.3	35	79	29.5	30	>100
NaI		6.50	6.329	6.338	6.411		164.9	170.12	162.3		23	-12	-7	>100
KF	5.20	5.42	5.175	5.197	5.322	204.1	194.4	206.16	194.5	51	85	7.4	7.5	>100
KCl	6.10	6.28	5.990	6.020	6.247	175.3	170.1	180.12	169.5	21	34	11.5	12	20
KBr	6.40	6.50	6.281	6.297	6.541	167.2	165.4	173.20	159.3	17	23	5.6	7	19
KI		6.88	6.670	6.670	7.003		158.0	164.49	151.1		3.6	-9.7	-10	19
RbF	5.54	5.66	5.488	5.500		194.0	188.1	196.10	(181.4)	30	65	61	61	>100
RbCl	6.38	6.52	6.287	6.303	6.531	169.4	165.0	173.15	(159.3)	14	17.1	4	4	5
RbBr	6.64	6.78	6.567	6.576	6.831	161.9	159.8	166.70	(152.6)	12.4	9.7	-1.2	0	5
RbI		7.16	6.954	6.954	7.231		152.7	158.56	(144.9)			-9	-9	4

Table 2.7

	LiF	LiCl	LiBr	LiI	NaF	NaCl	NaBr	NaI
Calc.	40.5	31.1	31.2	26.8	31.4	34.5	34.7	31.7
Expt.	33.2	43.2	49.8	59.4	31.7	39.7	42.3	45.5
%dev	22	-28	-37	-55	-1	-13	-18	-30
	KF	KCl	KBr	KI	RbF	RbCl	RbBr	RbI
Calc.	30.1	32.2	33.1	31.3	30.9	32.8	34.0	32.5
Expt.	31.7	37.1	38.7	40.8	34.0	36.1	37.8	38.0
% dev	-5	-13	-14	-23	-9	-9	-10	-15

Table 2.8

	NaCl	KCl	KBr	KI	RbCl	RbBr	RbI
Calc.	46	12	7	-10	4	0	-9
Expt.	300	20	19	19	5	5	4
% dev.	-85	-40	-63	-100	-20	-100	-100

Table 3.6 (1) NaCl

PHASE	R / V_3	4.7	4.8	4.9	5.0	5.1	5.2	5.3	5.4	5.5	5.6	5.7	5.8
B1	1.n.n	.964	.834	.774	.690	.612	.540	.476	.416	.364	.318	.280	.244
	I S O	1.456	1.260	1.086	.934	.802	.686	.586	.500	.428	.366	.314	.270
	R E M	.268	.216	.176	.142	.112	.092	.074	.060	.048	.038	.030	.024
	TOTAL	2.68	2.34	2.04	1.766	1.526	1.318	1.136	.976	.840	.722	.624	.538
B2	1.n.n	2.06	1.876	1.692	1.518	1.360	1.214	1.080	.958	.848	.664	.662	.586
	I S O	1.988	1.654	1.460	1.342	1.156	1.024	.896	.782	.682	.516	.516	.448
	R E M	1.064	.890	.744	.620	.514	.422	.346	.290	.242	.166	.166	.134
	TOTAL	5.12	4.42	3.90	3.48	3.04	2.66	2.32	2.04	1.774	1.544	1.346	1.168

Table 3.6 (2) NaBr

PHASE	V_3 \ R	5.0	5.1	5.2	5.3	5.4	5.5	5.6	5.7	5.8	5.9	6.0	6.1
B1	l.n.n	.948	.850	.758	.674	.598	.528	.464	.406	.354	.308	.270	.235
	I S O	1.580	1.364	1.178	1.016	.874	.746	.640	.548	.468	.402	.346	.293
	R E M	.230	.184	.150	.122	.100	.082	.066	.054	.044	.036	.028	.023
	TOTAL	2.76	2.40	2.08	1.812	1.572	1.356	1.170	1.008	.866	.746	.642	.555
B2	l.n.n	1.872	1.706	1.548	1.400	1.264	1.138	1.022	.916	.822	.732	.650	.514
	I S O	2.40	2.10	1.760	1.620	1.424	1.248	1.092	.958	.838	.730	.636	.571
	R E M	1.122	.946	.796	.668	.558	.458	.384	.322	.272	.228	.190	.160
	TOTAL	5.40	4.76	4.10	3.70	3.24	2.84	2.50	2.20	1.932	1.690	1.476	1.292

Table 3.6 (3) NaI

PHASE	V_3 \ R	5.4	5.5	5.6	5.7	5.8	5.9	6.0	6.1	6.2	6.3	6.4	6.5
B1	1.n.n	.946	.848	.752	.674	.598	.530	.466	.410	.358	.314	.276	.244
	I S O	2.04	1.782	1.558	1.364	1.190	1.036	.896	.782	.680	.592	.514	.448
	R E M	.312	.254	.210	.172	.140	.114	.094	.076	.062	.050	.042	.036
	TOTAL	3.30	2.88	2.52	2.22	1.928	1.680	1.458	1.268	1.100	.956	.832	.728
B2	1.n.n	2.00	1.840	1.684	1.560	1.396	1.266	1.148	1.038	.936	.844	.758	.682
	I S O	3.08	2.74	2.44	2.16	1.914	1.696	1.508	1.334	1.182	1.046	.922	.812
	R E M	1.436	1.234	1.056	.906	.774	.652	.550	.474	.408	.348	.298	.254
	TOTAL	6.52	5.82	5.18	4.62	4.08	3.62	3.20	2.84	2.52	2.24	1.978	1.748

Table 3.6 (4) KCl

PHASE	V_3 \ R	5.1	5.2	5.3	5.4	5.5	5.6	5.7	5.8	5.9	6.0	6.1	6.2
l.n.n	l.n.n	1.284	1.150	1.026	.912	.810	.722	.644	.572	.506	.448	.396	.357
B1	I S O	.804	.686	.588	.502	.428	.368	.320	.272	.234	.198	.170	.145
	R E M	.440	.356	.290	.236	.192	.156	.124	.102	.082	.066	.060	.048
	TOTAL	2.52	2.20	1.904	1.650	1.430	1.246	1.108	.946	.822	.712	.626	.553
B2	l.n.n	2.42	2.52	2.26	2.02	1.798	1.594	1.416	1.244	1.096	.960	.840	.734
	I S O	1.178	1.030	.900	.786	.686	.596	.516	.448	.388	.336	.292	.252
	R E M	.694	.564	.460	.398	.314	.258	.214	.176	.144	.118	.096	.079
	TOTAL	4.70	4.12	3.62	3.18	2.80	2.44	2.14	1.868	1.628	1.414	1.228	1.109

Table 3.6 (5) KBr

PHASE	V_3 \ R	5.3	5.4	5.5	5.6	5.7	5.8	5.9	6.0	6.1	6.2	6.3	6.4
B1	l.n.n	1.432	1.292	1.166	1.048	.936	.838	.750	.670	.598	.532	.474	.420
	I S O	1.016	.874	.748	.642	.558	.468	.402	.344	.296	.250	.214	.184
	R E M	.444	.362	.300	.244	.196	.162	.132	.114	.088	.072	.060	.048
	TOTAL	2.90	2.52	2.22	1.934	1.680	1.468	1.284	1.128	.982	.854	.748	.652
B2	l.n.n	3.02	2.72	2.46	2.20	1.972	1.760	1.562	1.386	1.226	1.086	.956	.841
	I S O	1.618	1.342	1.180	1.036	.912	.802	.700	.610	.526	.458	.400	.360
	R E M	.838	.696	.570	.474	.362	.330	.274	.228	.190	.156	.130	.108
	TOTAL	5.48	4.76	4.22	3.72	3.24	2.90	2.54	2.22	1.942	1.70	1.486	1.309

Table 3.6 (6) K1

PHASE	V_3 \ R	5.8	5.9	6.0	6.1	6.2	6.3	6.4	6.5	6.6	6.7	6.8	6.9
B1	l.n.n	1.398	1.268	1.148	1.034	.930	.836	.754	.678	.610	.544	.488	.446
	I S O	1.192	1.036	.850	.782	.680	.592	.514	.448	.390	.336	.294	.256
	R E M	.342	.288	.240	.200	.168	.140	.116	.096	.080	.066	.056	.046
	TOTAL	2.94	2.60	2.24	2.02	1.778	1.568	1.384	1.222	1.080	.946	.836	.748
B2	l.n.n	2.78	2.52	2.28	2.06	1.852	1.626	1.488	1.330	1.188	1.062	.946	.840
	I S O	1.788	1.592	1.422	1.258	1.118	.994	.876	.776	.686	.606	.536	.472
	R E M	.850	.712	.604	.516	.442	.378	.324	.374	.236	.198	.170	.146
	TOTAL	5.42	4.82	4.30	3.834	3.42	3.00	2.68	2.38	2.12	1.866	1.652	1.522

Table 3.6 (7) RbCl

PHASE	V_3 \ R	5.3	5.4	5.5	5.6	5.7	5.8	5.9	6.0	6.1	6.2	6.3	6.4
B1	l.n.n	1.382	1.226	1.086	.964	.854	.756	.666	.588	.522	.462	.408	.360
	I S O	.594	.506	.432	.370	.318	.272	.230	.198	.178	.140	.120	.106
	R E M	.518	.420	.376	.278	.228	.186	.152	.122	.100	.082	.066	.054
	TOTAL	2.50	2.16	1.874	1.612	1.400	1.214	1.048	.910	.800	.684	.594	.520
B2	l.n.n	3.20	2.88	2.58	2.32	2.06	1.828	1.622	1.434	1.264	1.114	.978	.854
	I S O	..926	.798	.698	.604	.524	.458	.392	.340	.294	.254	.216	.184
	R E M	.566	.486	.400	.330	.268	.220	.188	.148	.124	.100	.082	.066
	TOTAL	4.70	4.16	3.68	3.26	2.86	2.50	2.20	1.922	1.682	1.468	1.276	1.104

Table 3.6 (8) RbBr

PHASE	V_3 \ R	5.8	5.9	6.0	6.1	6.2	6.3	6.4	6.5	6.6	6.7	6.8	6.9
B1	l.n.n	1.070	.968	.866	.774	.688	.614	.546	.486	.432	.384	.342	.298
	I S O	.470	.404	.346	.296	.252	.216	.184	.158	.136	.116	.098	.082
	R E M	.284	.236	.194	.158	.130	.106	.088	.072	.058	.048	.040	.032
	TOTAL	1.824	1.608	1.406	1.228	1.070	.936	.818	.716	.626	.548	.480	.412
B2	l.n.n	2.48	2.24	1.990	1.772	1.574	1.394	1.232	1.086	.954	.836	.732	.626
	I S O	.806	.704	.612	.534	.468	.406	.354	.308	.266	.228	.196	.162
	R E M	.396	.308	.272	.226	.186	.156	.132	.106	.088	.070	.066	.050
	TOTAL	3.86	3.26	2.88	2.54	2.22	1.956	1.718	1.500	1.308	1.134	.988	.838

Table 3.6 (9) Rb1

PHASE	V_3^R	6.0	6.1	6.2	6.3	6.4	6.5	6.6	6.7	6.8	6.9	7.0	7.1
B1	l.n.n	1.460	1.318	1.188	1.074	.970	.876	.788	.706	.636	.572	.514	.462
	I S O	.900	.784	.680	.628	.516	.448	.374	.324	.284	.248	.216	.186
	R E M	.396	.332	.278	.228	.192	.162	.136	.114	.094	.078	.066	.054
	TOTAL	2.76	2.44	2.14	1.930	1.678	1.786	1.298	1.144	1.014	.898	.796	.546
B2	l.n.n	3.10	2.82	2.54	2.30	2.06	1.842	1.644	1.468	1.308	1.164	1.036	.928
	I S O	1.416	1.252	1.114	.994	.878	.776	.686	.606	.536	.474	.414	.366
	R E M	.702	.612	.520	.442	.376	.318	.272	.228	.194	.164	.140	.120
	TOTAL	5.22	4.68	4.18	3.74	3.32	2.94	2.60	2.30	2.04	1.802	1.590	1.414

Table 3.7

	PC1	PC2	PC3	Expt.[a]
NaCl	5.604	5.673	5.784	5.597
NaBr	5.958	6.038	6.154	5.939
NaI	6.329	6.424	6.609	6.411
KCl	5.990	6.091	6.181	6.247
KBr	6.281	6.392	6.493	6.541
KI	6.670	6.805	7.080	7.003
RbCl	6.287	6.387	6.482	6.531
RbBr	6.567	6.678	6.758	6.831
RbI	6.954	7.102	7.213	7.231

(a) Experimental data are taken from Ref.(29)

Table 3.8

	W_L				W_L		
	PC1	PC2	PC3	Expt.[a]	PC1	PC2	PC3
NaCl	189.5	186.2	187.2	185.3	3.31	4.93	5.44
NaBr	179.1	176.4	173.0	174.3	2.60	4.41	5.91
NaI	170.1	167.3	162.3	162.3	-.35	1.85	4.56
KCl	180.1	176.4	174.0	169.5	1.16	3.70	3.90
KBr	173.2	168.9	166.4	159.3	.71	3.00	3.68
KI	164.5	159.6	156.4	156.1	-1.87	0.91	2.33
RbCl	173.2	169.4	167.6	(159.3)	.38	3.43	3.33
RbBr	166.7	162.7	160.8	(152.6)	-.15	2.64	2.84
RbI	158.6	153.8	151.3	(144.9)	-2.18	.82	1.80

(a) data taken from Ref.(29), values in brackets are measured at 298° K, otherwise at 0° K.

Table 3.9

	transition pressure P_c				relative volume change at P_c			
	PC1	PC2	PC3	Expt.[a]	PC1	PC2	PC3	Expt.[a]
NaCl	46	80.6	104.7	300	.100	.079	.068	.037
NaBr	29.5	58.8	91.1	>100	.106	.083	.064	
NaI	-12	16.2	46.2	>100		.110	.083	
KCl	11.5	45.8	47.0	20	.108	.088	.083	.113
KBr	56	31.2	36.5	19	.141	.092	.087	.105
KI	-9.7	5.9	15.9	19		.125	.098	.085
RbCl	4	34.7	32.9	5	.132	.091	.096	.140
RbBr	-1.2	22.3	24.1	5		.100	.095	.133
RbI	-9	4.7	10.0	4		.126	.112	.126

Table 3.10

structure	B1						B2					
	nearest neighbour distance (Å)	lnn	ISO	REM	TOTAL	%	nearest neighbour distance (Å)	lnn	ISO	REM	TOTAL	%
			(Kcal/mole)						(Kcal/mole)			
NaCl	2.892	2.40	2.84	0.33	5.57	3.0	3.048	3.87	2.98	0.93	7.78	4.4
NaBr	3.077	2.18	2.87	0.27	5.32	3.1	3.202	3.65	3.79	1.76	9.20	5.5
NaI	3.305	2.12	4.02	0.31	6.45	4.0	3.413	4.52	5.44	1.64	11.60	7.4
KCl	3.094	3.42	1.61	0.52	5.55	3.2	3.228	5.27	1.83	0.61	7.71	4.5
KBr	3.247	3.61	1.76	0.51	5.88	3.5	3.360	5.64	2.38	0.75	8.77	5.4
KI	3.540	3.46	2.14	0.34	5.94	3.8	3.625	5.60	3.58	0.78	9.96	6.5
RbCl	3.241	3.18	1.06	0.60	4.84	2.9	3.321	6.35	1.42	0.54	8.31	5.0
RbBr	3.389	3.42	1.15	0.56	5.13	3.2	3.540	5.33	1.45	0.45	7.23	4.6
RbI	3.607	3.93	1.75	0.55	6.23	4.1	3.704	6.50	2.60	0.88	9.88	6.7

Table 4.1(1)

S	$\bar{n}_1$	$\bar{n}_2$	$\overline{\cos\varphi}$	E_{Mad}	V_s	W_1
0.000	1.0000	1.0000	0.000	-193.550	13.169	-180.381
2.94	.9992	1.0025	.016	-193.271	12.901	-180.370
5.88	.9983	1.0051	.033	-192.968	12.636	-180.332
8.82	.9970	1.0085	.053	-192.561	12.308	-180.253
11.76	.9956	1.0115	.070	-192.206	12.049	-180.157
14.70	.9940	1.0155	.088	-191.721	11.703	-180.018
17.64	.9920	1.0200	.110	-191.161	11.350	-179.811
20.58	.9898	1.0250	.130	-190.557	10.988	-179.569
23.52	.9876	1.0305	.148	-189.907	10.612	-179.295
26.46	.9846	1.0370	.170	-189.147	10.224	-178.910
29.40	.9812	1.0455	.194	-188.202	9.788	-178.414
32.34	.9768	1.0565	.224	-186.993	9.313	-177.680
35.28	.9713	1.0716	.254	-185.521	8.815	-176.706
38.22	.9624	1.0988	.298	-183.177	8.298	-174.879
38.51	.9608	1.1050	.306	-182.482	8.413	-174.069

Table 4.1(2)

S	$\bar{n}_1$	$\bar{n}_2$	$\overline{\cos\varphi}$	E_{Mad}	V_s	W_1
0.000	1.0000	1.0000	0.000	-196.366	16.174	-180.192
2.94	.9994	1.0018	.016	-196.161	15.953	-180.208
5.88	.9986	1.0044	.036	-195.851	15.650	-180.200
8.82	.9976	1.0066	.056	-195.552	15.396	-180.156
11.76	.9964	1.0096	.076	-195.152	15.070	-180.082
14.70	.9950	1.0126	.096	-194.743	14.770	-179.973
17.64	.9935	1.0160	.112	-194.296	14.436	-179.860
20.58	.9916	1.0200	.136	-193.730	14.085	-179.645
23.52	.9896	1.0244	.156	-193.134	13.714	-179.420
26.46	.9874	1.0294	.176	-192.471	13.321	-179.150
29.40	.9846	1.0356	.200	-191.650	12.884	-178.766
32.34	.9820	1.0420	.220	-190.846	12.463	-178.383
35.28	.9786	1.0500	.244	-189.870	12.021	-177.849
36.46	.9744	1.0604	.272	-188.653	11.536	-177.117

Table 4.1(3)

S	$\bar{n}_1$	$\bar{n}_2$	$\overline{\cos\varphi}$	E_{Mad}	V_s	W_1
0.000	1.0000	1.0000	0.000	-202.112	23.573	-178.539
2.94	.9994	1.0016	.024	-201.915	23.321	-178.594
5.88	.9988	1.0032	.046	-201.680	23.071	-178.609
8.82	.9980	1.0048	.070	-201.412	22.843	-178.569
11.76	.9972	1.0070	.094	-201.022	22.507	-178.515
14.70	.9960	1.0096	.116	-200.585	22.149	-178.436
17.64	.9946	1.0122	.140	-200.106	21.821	-178.285
20.58	.9932	1.0154	.162	-199.538	21.404	-178.134
23.52	.9916	1.0186	.182	-198.983	21.128	-177.855

Table 4.2

P	C_{11}	C_{12}	C_{44}
0	571.4 (408)	89.14 (69)	89.14 (63)
12	700.2	107.2	83.38
44	924.2	154.0	65.41

Table 4.3

	S (Kbar)	ε_{YY} A	ε_{YY} B	ε_{XX} A	ε_{XX} B	Cosφ A	Cosφ B
P=0	2.94	0.0025	0.0024	-0.0008	-0.0008	0.016	0.016
	5.88	0.0051	0.0048	-0.0017	-0.00016	0.033	0.032
P=12Kbar	2.94	0.0018	0.0019	-0.0006	-0.0006	0.016	0.017
	5.88	0.0044	0.0038	-0.0014	-0.00012	0.036	0.034
P=44Kbar	2.94	0.0016	0.0014	-0.0006	-0.0005	0.024	0.023
	5.88	0.0032	0.0028	-0.0012	-0.0010	0.048	0.046

Table 4.4

P(Kbar)	S_{max}(Kbar)	ΔW_L(KCal/mole)
0	~ 38.51	5.512
12	~ 36.46	3.075
44	~ 23.52	0.684

Table 4.5

scheme	lattice constant at T			
	T=0°K	T=300°K	T=500°K	T=800°K
Baldereschi point	6.017	6.054	6.090	6.174
two special points	6.017	6.054	6.103	6.190
ten special points	6.017	6.054	6.096	6.182
Standard numerical method[a]	6.02	6.06	6.10	6.18

(a) Ref.(29).

Table 4.6

		Baldereshi point	two special points	ten special points
T=0°K	W_{zero}	0.00185254	0.00184802	0.00184951
	W_T	0	0	0
	F	-.28559794	-.28560246	-.28560097
T=300°K	W_{zero}	0.00180283	0.00179737	0.00179910
	W_T	-.00457860	-.00461829	-.00463003
	F	-.29011892	-.29016408	-.29017408
T=500°K	W_{zero}	.00175382	.00173346	.00174246
	W_T	-.01159161	-.01174218	-.01172230
	F	-.29697846	-.29707497	-.29708419
T=800°K	W_{zero}	.00165100	.00162297	.00163203
	W_T	-.02547657	-.02584701	-.02578900
	F	-.31024188	-.31045192	-.31044918

Table 4.7(1)

S	$\bar{n}_1$	$\bar{n}_2$	$\overline{\cos\varphi}$	W_1	W_{zero}	F
0.000	1.0000	1.0000	0.000	-180.371	1.127	-179.244
2.94	.9990	1.0028	.016	-180.350	1 118	-179.232
5.88	.9980	1.0054	.036	-180.297	1.108	-179.189
8.82	.9966	1.0088	.052	-180.219	1.097	-179.122
11.76	.9954	1.0122	.074	-180.086	1.085	-179.001
14.70	.9934	1.0162	.092	-179.931	1.072	-179.859
17.64	.9914	1.0210	.110	-179.730	1.057	-178.673
20.58	.9888	1.0264	.134	-179.432	1.040	-178.392
23.52	.9861	1.0326	.156	-179.083	1.021	-178.062
26.46	.9830	1.0400	.178	-178.654	.999	-177.654
29.40	.9793	1.0492	.202	-178.090	.973	-177.117
32.34	.9742	1.0616	.232	-177.266	.938	-176.327
36.46	.9678	1.0796	.268	-175.161	.921	-174.740

Table 4.7(2)

S	$\bar{n}_1$	$\bar{n}_2$	$\overline{\cos\varphi}$	W_1	W_{zero}	F
0.000	1.0000	1.0000	0.000	-178.717	1.369	-177.348
2.94	.9994	1.0016	.024	-178.768	1.363	-177.405
5.88	.9986	1.0032	.048	-178.766	1.357	-177.410
8.82	.9980	1.0052	.074	-178.735	1.348	-177.387
11.76	.9966	1.0074	.094	-178.678	1.346	-177.332
14.70	.9954	1.0098	.120	-178.549	1.331	-177.218
17.64	.9943	1.0128	.144	-178.411	1.318	-177.093
20.58	.9929	1.0154	.166	-178.221	1.309	-176.912
23.52	.9907	1.0198	.190	-177.999	1.295	-176.704

Table 4.8.1 T=300°K and P=0

Test 1 configuration parameters: η_1=0.9860, η_2=1.0290, cosφ=.1300 and s=17.64 Kbar					
number of special points	W_L	W_{zero}	W_T (a.u)	F	G
128	-.285627	.001618	-.005418	-.289427	-.291632
32	-.285627	.001618	-.005427	-.289435	-.291641
8	-.285627	.001619	-.005397	-.289405	-.291610
2	-.285627	.001627	-.005276	-.289276	-.291481

Test 2 configuration parameters: η_1=0.9740, η_2=1.0500, cosφ =.1900 and s=23.52 Kbar					
number of special points	W_L	W_{zero}	W_T (a.u)	F	G
128	-.283646	.001538	-.005780	-.287890	-.292559
32	-.283646	.001538	-.005793	-.287901	-.292570
8	-.283646	.001539	-.005765	-.287872	-.292541
2	-.283646	.001546	-.005653	-.287754	-.292422

Table 4.8.2 T=925°K and P=0.

Test 1 configuration parameter: η_1=0.9954, η_2=1.0122, cosφ=0.074 and S=11.86Kbar.					
number of special points	W_1	W_{zero}	W_T (a.u.)	F	G
128	-.284633	0.001456	-.034639	-.317816	-.318636
32	-.284633	0.001456	-.034897	-.318074	-.318894
8	-.284633	0.001457	-.034818	-.317994	-.318815
2	-.284633	0.001463	-.034489	-.316616	-.321657
Test 2 configuration parameter: η_1=0.9830, η_2=1.0400, cosφ=.178 and S=26.46 Kbar.					
number of special points	W_1	W_{zero}	W_T (a.u)	F	G
128	-.281591	0.001343	-.036423	-.316671	-.321712
32	-.281591	0.001343	-.036699	-.316947	-.321988
8	-.281591	0.001344	-.036636	-.316884	-.321925
2	-.281591	0.001348	-.036373	-.316616	-.321657

Table 4.9.1 T=300°K, P=0 and s=8.82 Kbar

λ_1	λ_2	cos φ	G
0.9955	1.0110	.048	-.290853
0.9950	1.0120	.052	-.290858
0.9945	1.0124	.056	-.290862
0.9945	1.0128	.060	-.290863

Table 4.9.2 T=925°K, P=0 and s=2.92 Kbar

λ_1	λ_2	cos φ	G
0.9954	1.0090	.024	-.318235
0.9954	1.0090	.028	-.318240
0.9950	1.0098	.032	-.318345
0.9950	1.0098	.036	-.318247

FIGURE CAPTIONS AND FIGURES

Figure captions:

Fig. 2.1 (a) Lattice cell and (b) unit cell of the B1 structure. (c) unit cell of B2 structure.

Fig. 2.2 Brillouin Zone for (a) face-centeres cubic; (b) simple cubic lattices.

Fig. 2.3 (a) B1 structure, (b) bcc lattice, (c) B2 structure.

Fig. 3.1 Geometry of the system of three ions A, B and C. P represents a point in the volume over which the integration in eq.(3.10) is carried out. P' is the projection of P onto the plane made by ABC. Both PD and P'D are perpendicular to AB. φ is the angle between PD and P'D.

Fig. 3.2 Schematical representation of the configuration (XMM; R_{CA}, R_{CB}, γ).

Fig. 3.3 (a) The variation of V_3(MXX;R,R, γ) with R for KCl, for the cases of γ = 70.5°, 90° and 109.5°. (b) The variation of V_3(XMM;R,R, γ) with R for KCl, for the cases of γ= 70.5°, 90° and 109.5°.

Fig. 4.1 Detail of the B1 to B2 transition mechanism proposed by Parrinello and Rahman. (A) shows a body-central tetragonal lattice, lattice vector $\vec{a},\vec{b};\vec{c}$; length a,a , $\sqrt{2}$a respectively. (see chapter II, Fig.2.3). The ions are indicated by • and •. This is an fcc lattice of • ions. The other species shown as ○ , two species of ions together complete the B1 structre. The thick arrow in A indicates a dilatation, resulting in B. Fine arrows in B indicate displacements of particles with a common $\vec{c}$ direction coordiante, resulting in the final structure C. A is the B1 and C a B2 structure.

Fig. 4.2 Shear deformations occurred during the first step of the B1 to B2 transition, the figures in dashed lines represent undestorted fcc lattice in which configuration parameters are $\eta_1 = \eta_2 = 1$ and $\cos\varphi = 0$. (a) C_{44} type shear deformation in the (100) plane of the B1 structure. (b) $C_{11} - C_{12}$ type shear deformation in the (010) and (001) planes of the B1 structure.

Fig. 4.3 Phonon dispersion curves of KCl crystal under an uniaxial tensile load S and hydrostatic pressures P = 0, 12 and 44 Kbar. The solid lines give the phonon dispersion curves for case of S = 0, i.e. for the case of equilibrium of the crystal under the hydrostatic pressure. The dashed lines give the phonon dispersion curves for the crystal under the uniaxial tensile load, whose value is equal to S_{max}:

Fig. 4.3(a) P = 0.

Fig. 4.3(b) P = 12 Kbar.

Fig. 4.3(c) P = 44 Kbar.

Fig. 4.4 The variation of the frequancy of Ta1 mode of [100], zone boundary phonon with uniaxial tensile load S for the cases of hydrostatic pressure P = 0, 12 and 44 Kbar.

Fig. 4.5 The variation of lattice energy W_1 with the uniaxial tensile load S for cases of hydrostatic pressure P = 0, 12 and 44 Kbar.

FIGURES:

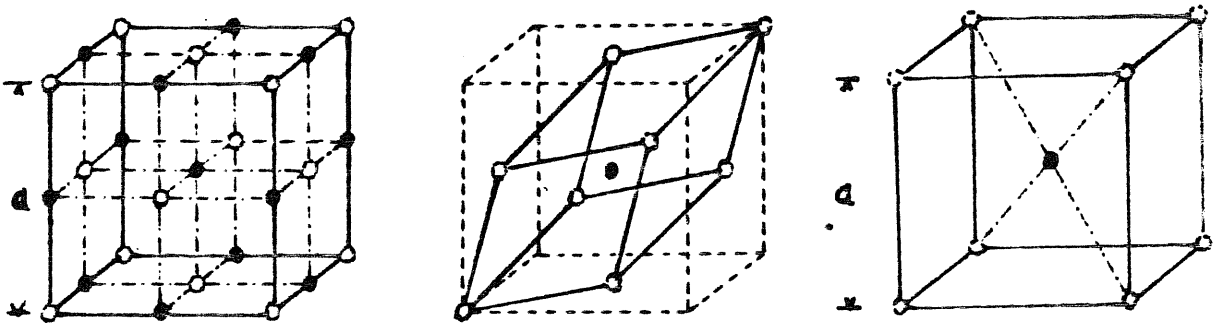

(a) (b) (c)

Fig2.1

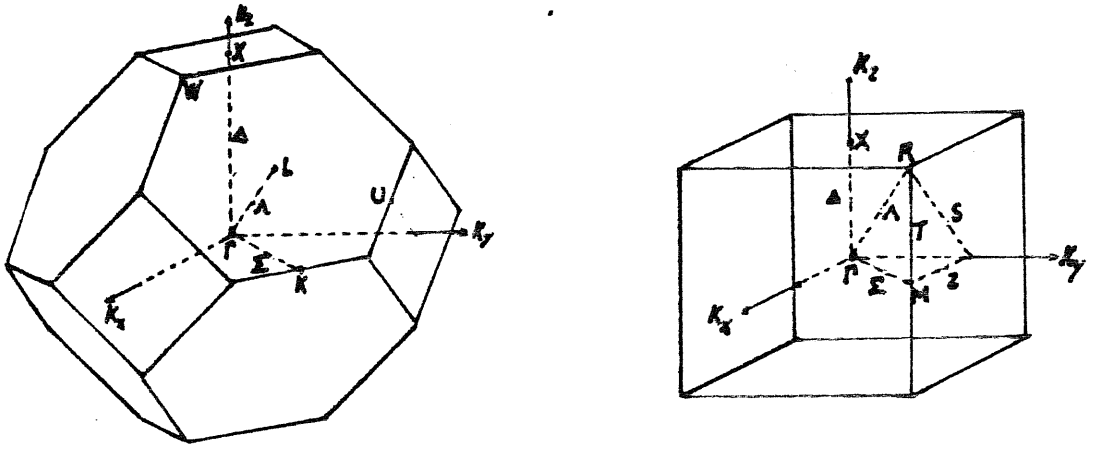

(a) (b)

Fig2.2

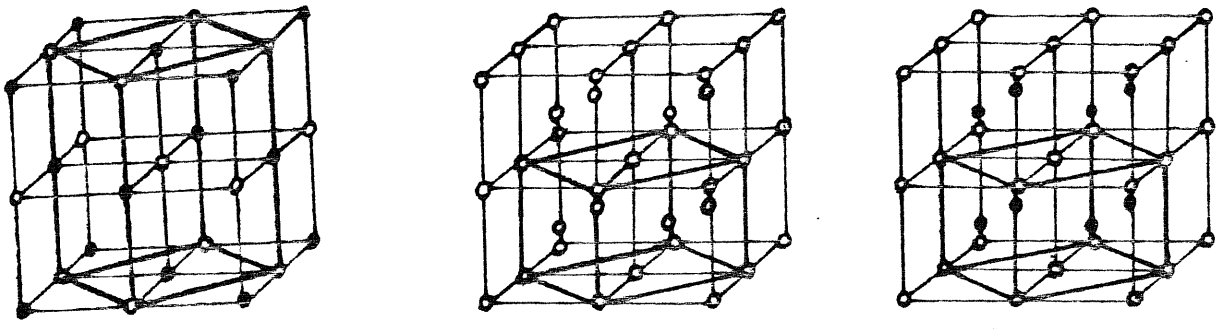

(a) (b) (c)

Fig2.3

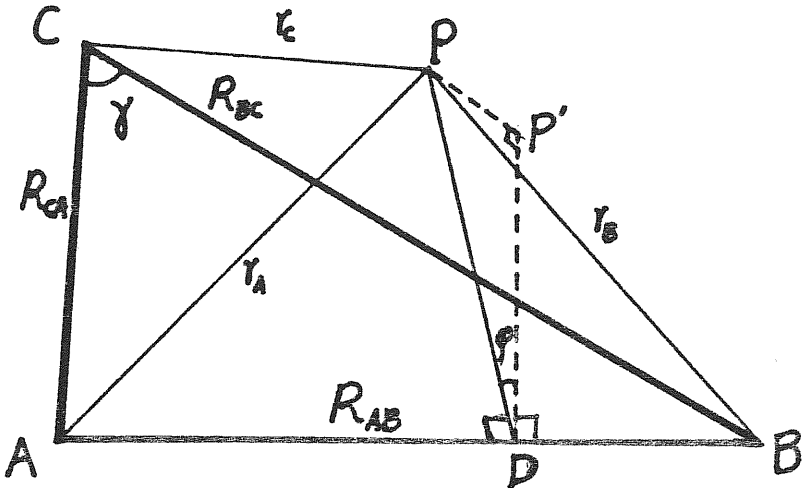

Fig.3.1

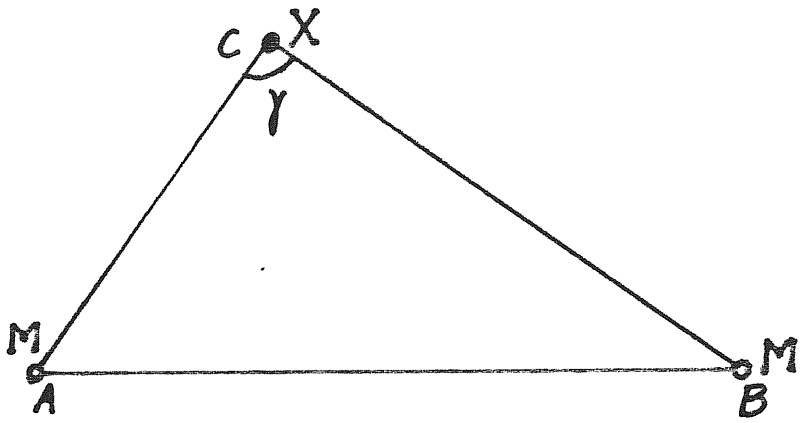

Fig.3.2

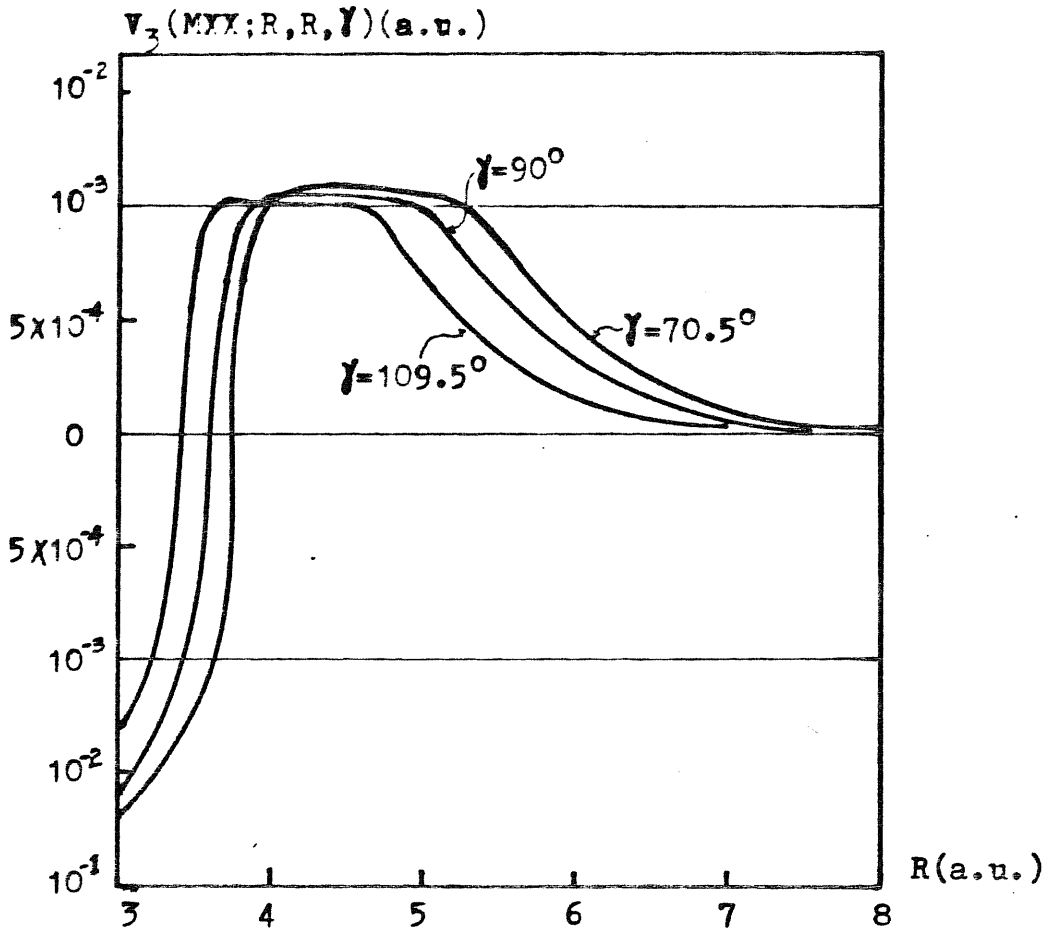

Fig. 3.3(a)

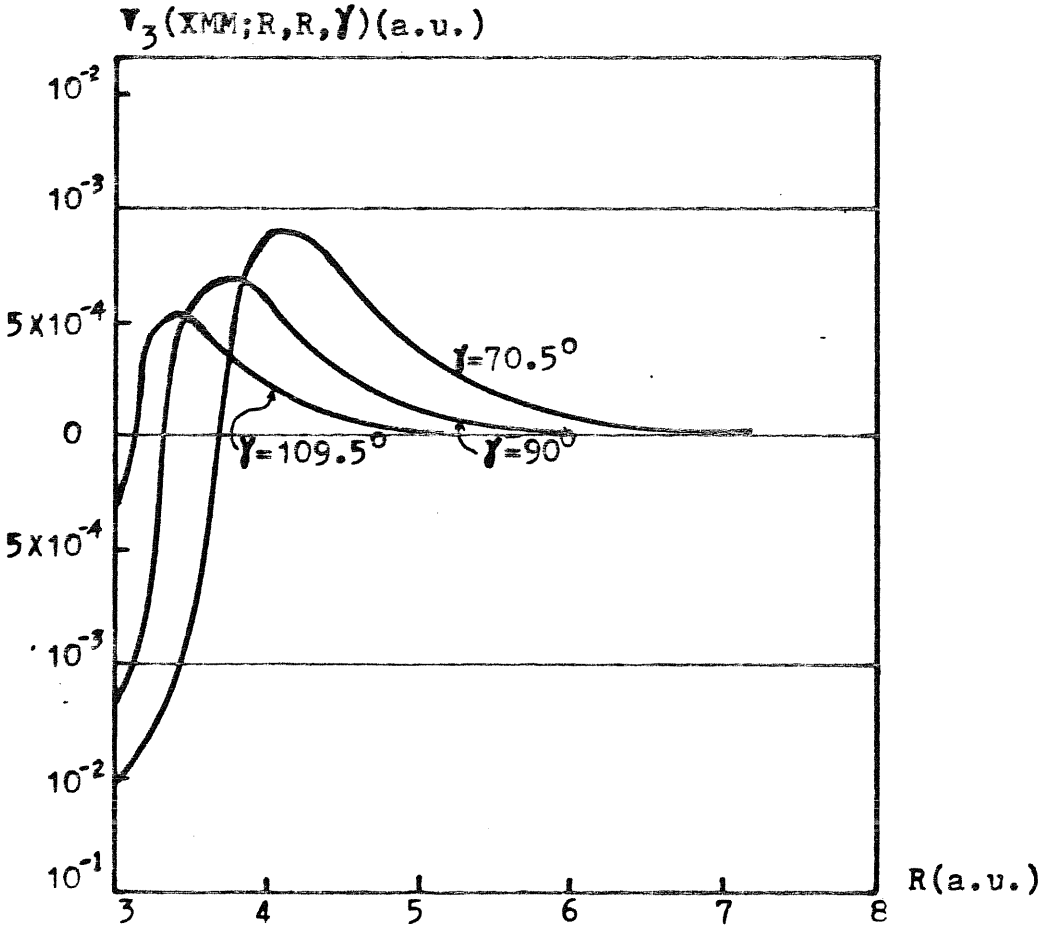

Fig.3.3(b)

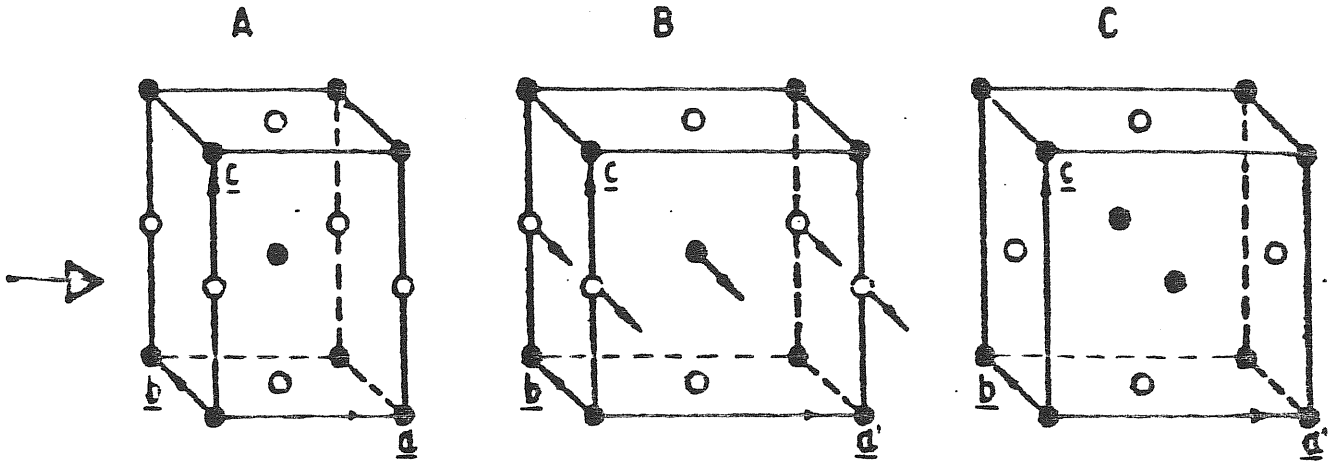

Fig.4.1

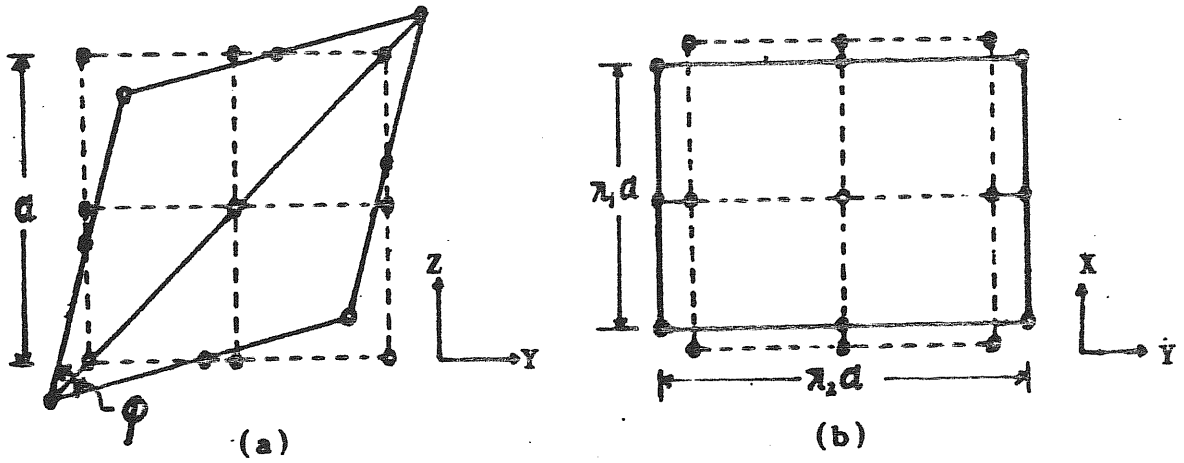

Fig.4.2

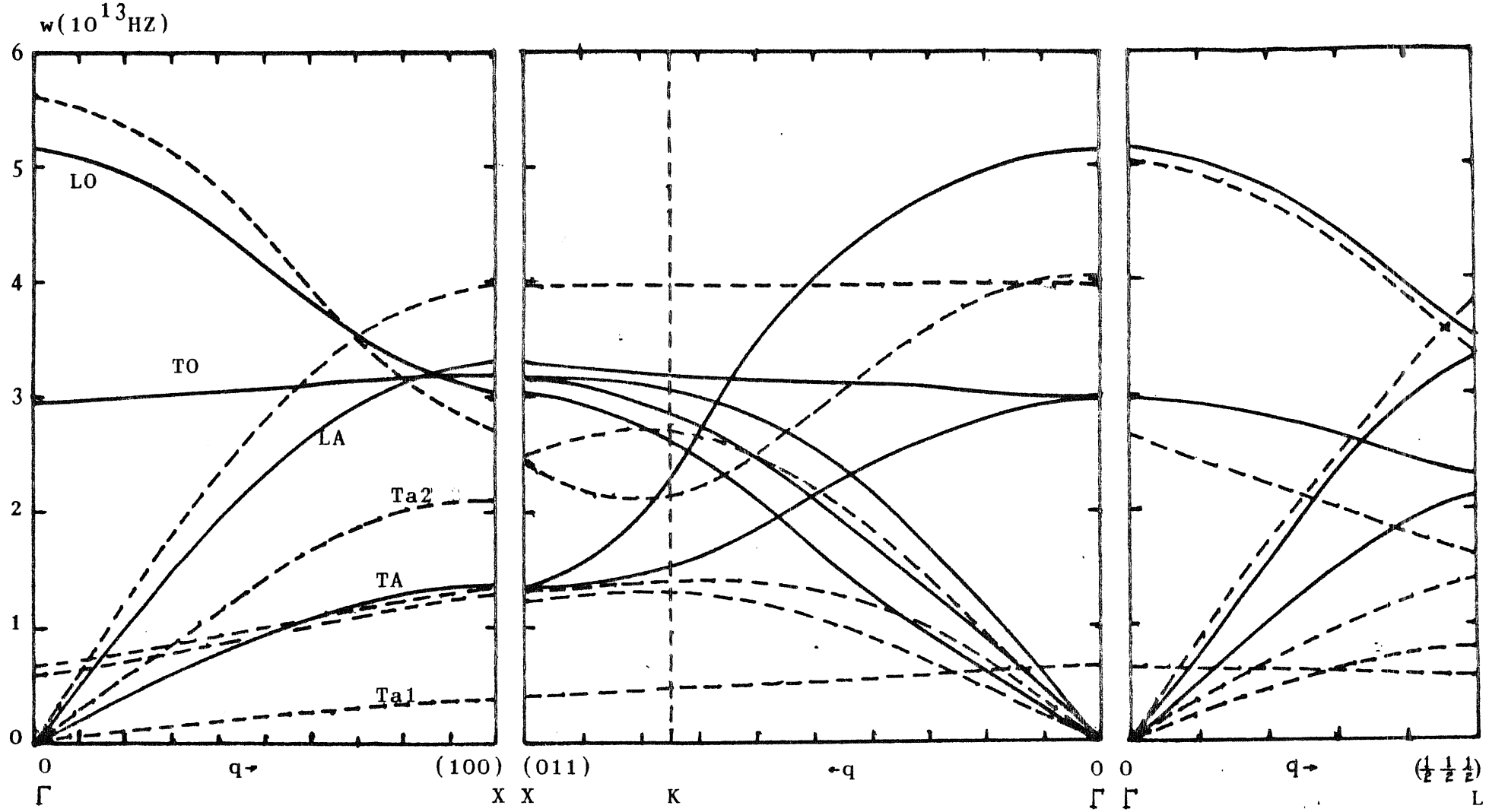

Reduced wave vector coordinate

Fig. 4.3(a)

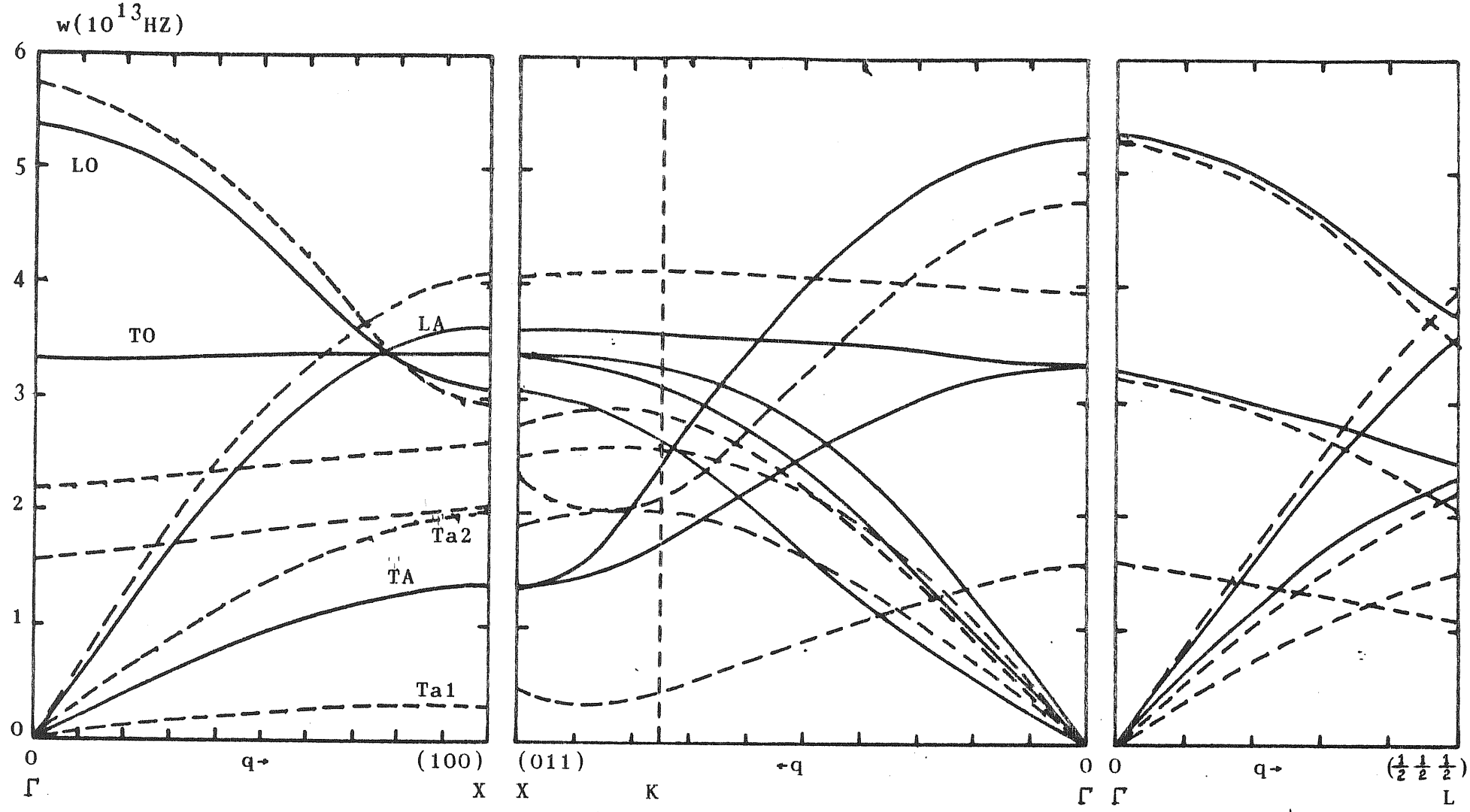

Reduced wave vector coordinate

Fig. 4.3(b)

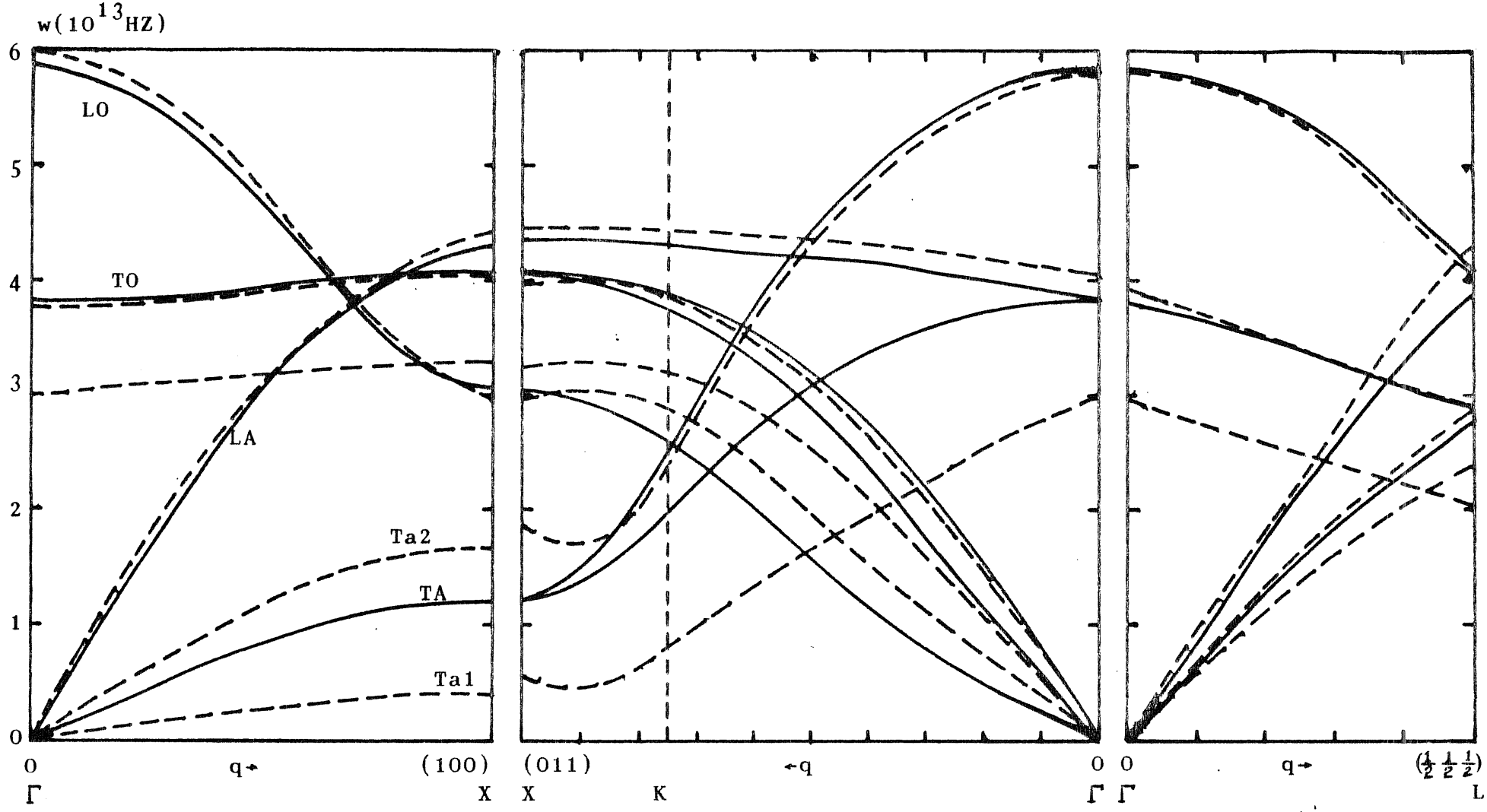

Reduced wave vector coordinate

Fig. 4.3(c)

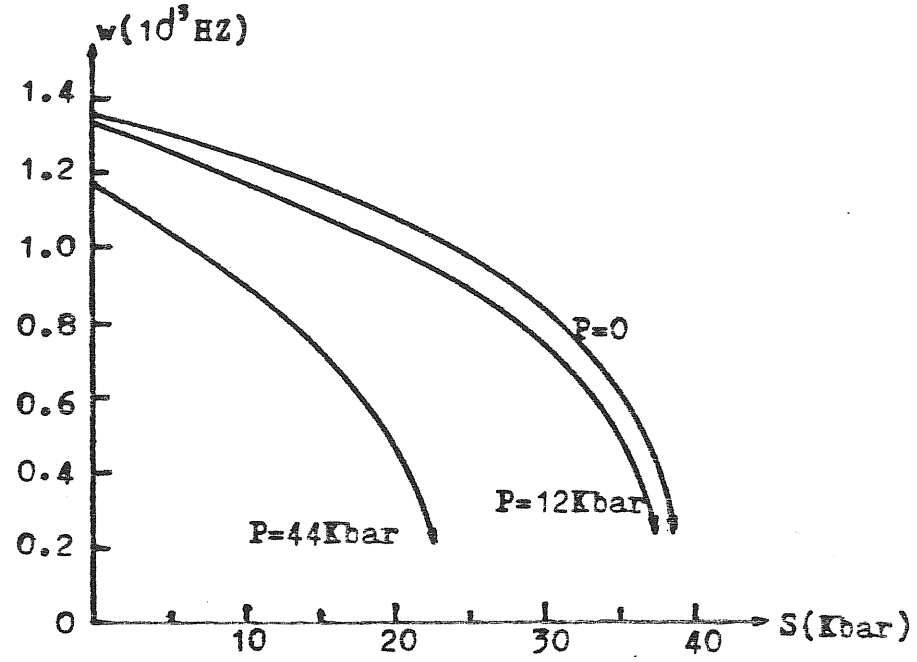
w(10³HZ)
1.4
1.2
1.0
0.8
0.6
0.4
0.2
0
P=0
P=12Kbar
P=44Kbar
10
20
30
40
S(Kbar)

Fig.4.4

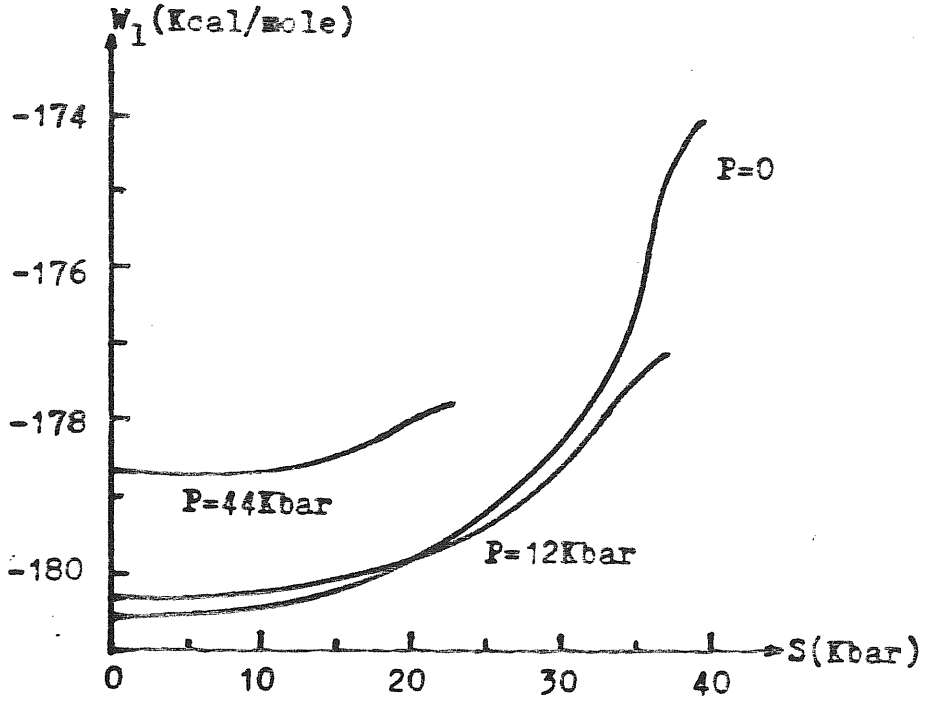
W1(Kcal/mole)
-174
-176
-178
-180
P=0
P=44Kbar
P=12Kbar
0
10
20
30
40
S(Kbar)

Fig.4.5